NASA TECHNICAL NOTE

NASA TN D-4589

NASA TN D-4589

c. 1

THE RADIATION BALANCE OF THE EARTH-ATMOSPHERE SYSTEM FROM RADIATION MEASUREMENTS OF THE NIMBUS II METEOROLOGICAL SATELLITE

by Ehrhard Raschke

Goddard Space Flight Center
Greenbelt, Md.

NATIONAL AERONAUTICS AND SPACE ADMINISTRATION • WASHINGTON, D. C. • JULY 1968

THE RADIATION BALANCE OF THE EARTH-ATMOSPHERE SYSTEM FROM RADIATION MEASUREMENTS OF THE NIMBUS II METEOROLOGICAL SATELLITE

By Ehrhard Raschke

Goddard Space Flight Center
Greenbelt, Md.

NATIONAL AERONAUTICS AND SPACE ADMINISTRATION

For sale by the Clearinghouse for Federal Scientific and Technical Information
Springfield, Virginia 22151 – CFSTI price $3.00

ABSTRACT

Measurements of the reflected solar radiation and emitted infrared radiation were obtained over the entire globe from the Nimbus II meteorological satellite during the period from 16 May 1966 to 28 July 1966. From these measurements, the outgoing long-wave radiation flux, the albedo, and the radiation balance of the earth-atmosphere system were computed for five subperiods, each of a half month's length. All results are presented here in maps.

The global albedo was found to be between 29 and 31 percent, which is less than earlier accepted values of 33 percent and more. The globally emitted long-wave radiation flux results in an equivalent black-body temperature of the planet earth of about 255°K, which is 3—4 degrees higher than was found in earlier studies. These results indicate that in earlier studies of the radiation balance the cloud cover and possibly the cloud height were slightly overestimated. The global averages of the radiation balance obtained were between 0.002 cal cm^{-2} min^{-1} of surplus and 0.007 cal cm^{-2} min^{-1} deficit.

CONTENTS

Abstract ii

INTRODUCTION 1

THE NIMBUS II MEASUREMENTS 2

THE BALANCE EQUATION 3

COMPUTATION OF THE FLUX OF OUTGOING LONG-WAVE RADIATION E 4

COMPUTATION OF THE INCIDENT (S) AND REFLECTED (R) FLUX OF SOLAR RADIATION 5

GEOGRAPHIC DISTRIBUTIONS OF RESULTS 8

GLOBAL AND HEMISPHERICAL BUDGET 10

COMPARISON OF THE RESULTS WITH DIRECT MEASUREMENTS 13

COMPARISON WITH OTHER RADIATION BALANCE STUDIES 15

CONCLUSIONS 17

ACKNOWLEDGMENT 18

References 19

Appendix A—Computation of Angles θ, ψ, ζ 25

Appendix B—Computation of Long-Wave Radiation Flux E 27

Appendix C—Relations to Determine Directional Reflectance r from Bidirectional Reflectance ρ' 29

Appendix D—Summary of Computer Program 33

Appendix E—Maps of Results 35

Appendix F—Mean Cloud Cover Over the Northern Hemisphere 77

THE RADIATION BALANCE OF THE EARTH-ATMOSPHERE SYSTEM FROM RADIATION MEASUREMENTS OF THE NIMBUS II METEOROLOGICAL SATELLITE*

by
Ehrhard Raschke†
Goddard Space Flight Center

INTRODUCTION

In studies of the heat-balance of the earth-atmosphere system, only two energy fluxes are considered: radiative energy of absorbed solar electromagnetic radiation and of re-emitted long-wave (thermal) radiation. Other possible energy sources and sinks (such as heat flow from the earth's interior and crust and solar particle radiation, as well as energy transport by waves to space) are unimportant and can be neglected here.

About 99 percent of the energy of solar electromagnetic radiation reaching the top of the atmosphere is within the spectral range between 0.2 and 4.0 microns. Its shortwave component, for wavelengths <0.3 microns (which amounts to 1.2 percent of the total flux), is almost completely absorbed in atmospheric layers 50 km above the earth's surface. Of the rest, about 60—70 percent are absorbed mainly at the ground and in tropospheric layers, while 30—40 percent are scattered and reflected from ground to space (Reference 1).

Of the flux of outgoing long-wave radiation, only about 5 percent originate in layers above the tropopause; the main part is emitted from the ground and from tropospheric layers to space. Thus, any investigations of the radiative budget or radiation balance of the earth-atmosphere system will consider mainly the radiation balance at a level less than 30 to 50 km above the surface. Results on spatial and temporal changes will be highly correlated with properties of the system beneath this level.

Our present knowledge of the radiation balance on the earth-atmosphere system was obtained from earlier investigations, whose source material was climatological data (References 1—7). These showed that at low latitudes the absorbed radiation from the sun exceeds the re-emitted thermal radiation lost to space, while over both polar regions more radiation is lost to space than is gained by absorption (References 8, 9, 10). The thermal gradient between these regions of energy surplus and deficit causes the circulation of our atmosphere. Since the earth-atmosphere mean

*Laboratory for Atmospheric and Biological Sciences Technical report.
†On leave from the University of Munich, Germany, as a National Academy of Sciences Post-Doctoral Resident Research Associate. Present Affiliation: Bereich Extraterrestrische Physik, Ruhr-Universität Bochum, Germany.

temperature did not change over periods of a few years, it was assumed to be at radiative equilibrium at these times.

The accuracy of the earlier investigations was limited by the sparse material for observation available at that time; this affected their usefulness in the study of the atmospheric circulation. Therefore, satellite experiments were designed to measure the reflected solar radiation and emitted infrared radiation continuously over the entire globe. Such experiments had already been flown aboard Explorer VII (References 11, 12, 13), and several TIROS satellites (References 14 through 18), but these satellites were not in polar orbits; their measurements covered only parts of the globe between about 60°N and 60°S. Reliable results were only obtained for the outgoing long-wave radiation. Results obtained for the reflected component of incident solar radiation showed large uncertainties. These can be partly explained by postlaunch degradation of instrumental response (Reference 14) and by the assumption of complete isotropic reflection characteristics (Lambert-surface) of the earth-atmosphere system. There is so far no report on results obtained from measurements of the Soviet COSMOS-satellites.

The meteorological satellite Nimbus II (Reference 19) was the first satellite to measure the radiation balance over the entire globe. Launched on 15 May 1966, its instrumentation made measurements from 16 May to 28 July 1966 (a period centered on the northern summer solstice). From these measurements were computed the outgoing long-wave radiation flux, the reflected solar-radiation flux, and the radiation balance. The solar constant was assumed to 2.0 cal cm^{-2} min^{-1}. The anisotropic nature of the earth-atmosphere reflection characteristic was taken into consideration, with simple models derived empirically from published data of airplane and balloon measurements. The computational procedures are discussed extensively in the next three sections of this report. Appendixes A, B, and C present some additional formulas used in the computer programs, and describe the determination of empirical models on the anisotropy of the reflection properties of the earth-atmosphere system. Appendix D summarizes the data flow in the computer program.

Results on the albedo, the outgoing long-wave radiation, and the radiation balance of the earth-atmosphere system were obtained for five semimonthly periods covering the full period of available Nimbus II measurements. Appendix E shows maps of these quantities; they are briefly described in the main text under "Geographic Distribution of Results." Geographic distributions for selected periods have received a more detailed discussion elsewhere (References 20 and 21) and will be the subject of a forthcoming paper by Raschke and Bandeen.

The global and hemispherical budget is discussed further on, while the subsequent sections make comparisons of the new results with earlier investigations and with direct measurements of emitted thermal and reflected solar radiation.

THE NIMBUS II MEASUREMENTS

Nimbus II crossed the equator on a nearly polar, sunsynchronous, circular orbit, northbound near local noon and southbound near local midnight; its mean height above the earth's surface was

about 1140 km. Because of its orbital period of 108.6 minutes, the entire globe could be observed, day and night, within a 24-hour interval. The reflected solar radiation and the outgoing long-wave radiation were measured in the spectral ranges from 0.2 to 4.0 microns and from 5.0 to 30.0 microns with a medium-resolution radiometer, which is described in detail elsewhere (Reference 22). The field of view of the scanning mean-resolution-infrared-radiometer was about 2.5 degrees. It enabled a spatial resolution of 50 km (near the subsatellite point) to about 110 km (at a nadir angle of 40 degrees). The radiometer scans were performed perpendicular to the orbital plane. The measurements of outgoing infrared radiation were continuously controlled by an onboard calibrated system; thus they are accurate within ±2 percent. The consistency of measurements of reflected solar radiation was investigated, comparing the bidirectional reflectances (Equation 3, page 6) over various cloud-free portions of the Sahara and Saudi Arabia. That is, the ratio between the measured radiance and the vertically incident irradiance of solar radiation was determined (see next section). These cloud-free portions were selected according to the equivalent black-body temperature of concurrent infrared-radiation measurements in the 10- to 11-micron range. The bidirectional reflectance over these areas varied within limits of ±5 percent of a mean value, not indicating a temporary change of instrumental response. Thus the measurements of reflected solar radiation should be fairly accurate, provided that there was no deterioration of instrumental response immediately after launch.

THE BALANCE EQUATION

The net radiation flux, Q, or radiation balance of the earth-atmosphere system at a horizontal surface element outside the atmosphere of geographic longitude, λ, and latitude, ϕ, is the sum of radiation fluxes crossing this surface:

$$Q(\lambda, \phi, d) = S(\lambda, \phi, d) - R(\lambda, \phi, d) - E(\lambda, \phi, d) , \qquad (1)$$

where S and R are the fluxes of incoming and reflected solar radiation, respectively, and E is the emitted long-wave radiation flux. The letter d designates the day of the year for which the balance computations are made. (It stands for the sun's declination, the true distance from sun to earth, and the measurements at this particular day—according to the subject under discussion.) The difference S-R determines that part of the sun's radiation which is absorbed in the earth-atmosphere system, while the ratio R/S is the albedo.

The computation of the outgoing fluxes from measured radiances requires three major steps:

1. Conversion of the measured filtered radiance N_f to unfiltered radiance N,
2. Integration over all angles of measurement, and
3. Averaging over a 24-hour interval to obtain mutually comparable values.

Since the earth-atmosphere system up to only 30 to 50 km above the surface is almost the only source of reflected and emitted outgoing radiation fluxes R and E, the second step can be simplified.

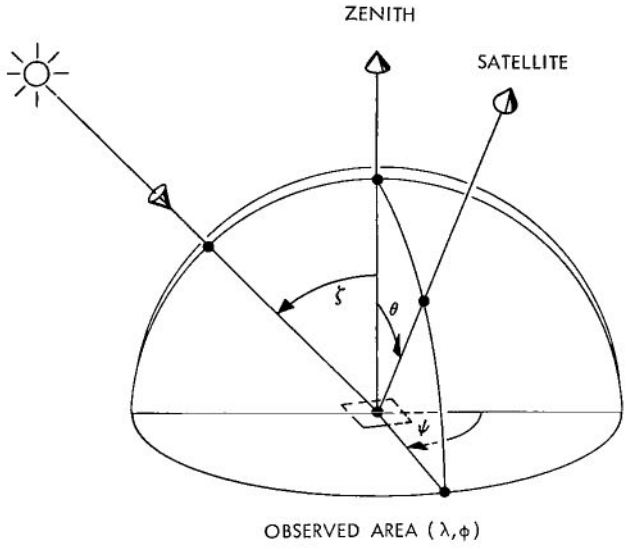

Figure 1—Geometrical configuration of earth and satellite.

The radiation from the earth-atmosphere system is considered as coming entirely from the bottom of the atmosphere, i.e., from the earth's surface (a sphere 6371 km in radius). Then, the integration of outgoing radiances N will be carried out above an observed surface element by

$$\text{Flux} = \int_0^{2\pi} \int_0^{\pi/2} N(\theta, \psi) \sin\theta \cos\theta \, d\theta \, d\psi \,, \quad (2)$$

where θ and ψ are the zenith and azimuthal angle of measurement respectively (Figure 1). Uncertainties caused by this and other simplifications will be diminished sufficiently by averaging over all single results falling within gridfields about 300 km × 300 km. This grid size has been used in mapping the results (see Appendix E).

COMPUTATION OF THE FLUX OF OUTGOING LONG-WAVE RADIATION E

The outgoing long-wave radiation E was computed as shown in Reference 23. The first step was to convert the measured filtered radiance to the unfiltered radiance (i.e., the infrared radiation emitted in the spectral range from about 4 to 50 microns); Lienesch* derived a relationship between radiances N_f and N for about 60 atmospheric profiles. Figure 2 shows his results for a vertical upward path (plain dots) and for a slant path (circled dots) with a zenith angle of $\theta = 78.5°$. These results show that the relation between N_f and N, is nearly linear and independent of the zenith angle θ, since the spectral response of the Nimbus II Medium Resolution Infrared Radiometer (MRIR) (5.0 to 30.0 microns) covers a region where 80 percent of the total radiative energy is emitted to space.

The further integration of N was accomplished assuming symmetrical radiant emittance at the viewed area. Thus, only the dependence on the zenith angle θ needs to be known. It was obtained statistically by Lienesch and Wark (Reference 24) from measurements of TIROS satellites. The formulas are presented in Appendix B.

The computation of a 24-hour average, as expressed in the third of the above steps, requires several measurements over the same area at different local times. Diurnal variation of atmospheric conditions (mainly clouds and temperature) over some areas causes diurnal variation of the outgoing

*Lienesch, J. H., private communication, 1966.

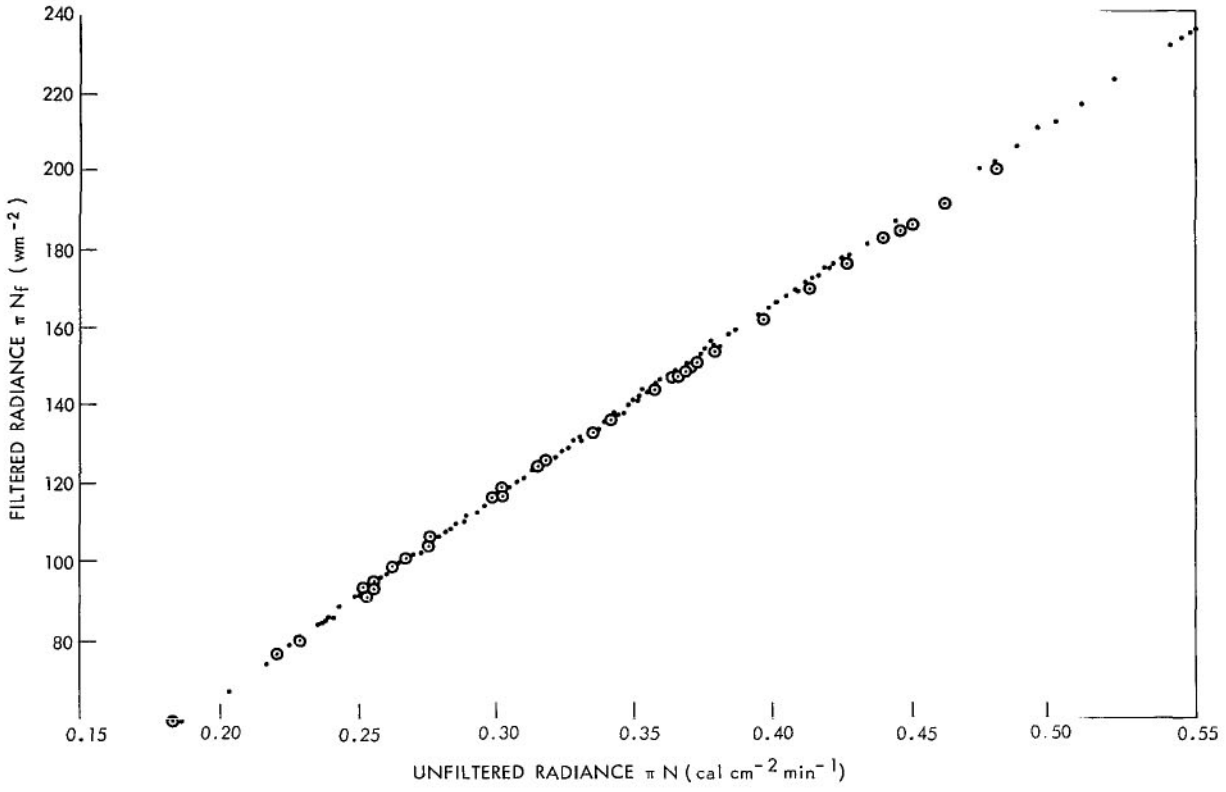

Figure 2—Relation between the filtered (5.0—30.0 microns) and the unfiltered radiance of outgoing long-wave radiation.

long-wave radiation. The Nimbus II measurements indicated that nearly all land areas were considerably "warmer" by day than at night, while over the oceans the difference between day and night measurements was in either direction.

But between 40°N and 40°S, the satellite orbit permitted only one or two measurements by day, near local noon, and one or two at night near local midnight. More measurements were obtained over both polar regions, where the suborbital paths overlapped each other. These measurements, were assumed to be representative for each condition, day and night. The 24-hour average, then, was obtained by weighting each flux value over the same gridfield with the length of day or night over this particular area. This was done with the semi-monthly averages of flux values for each gridfield. Over areas where either day or night data were missing, no values of the outgoing flux were determined. Thus there are gaps in the geographical distributions of the outgoing long-wave radiation flux. They are indicated in the maps by dashed isolines and stippled areas (Appendix E).

COMPUTATION OF THE INCIDENT (S) AND REFLECTED (R) FLUX OF SOLAR RADIATION

Theoretical (References 25 through 29) and experimental (References 30 –32) studies of the reflection characteristics of the earth-atmosphere system showed a strong dependence on θ, ψ,

and ζ (Figure 1). This was confirmed by statistical analyses of satellite measurements of reflected solar radiation Levine* and References 33 through 35. Viezee et al. (Reference 36) and Råbbe (Reference 37) demonstrated the angular dependence of reflected solar radiation, with examples of satellite measurements.

Thus, the bidirectional reflectance ρ_f' of an observed area λ, ϕ (as obtained from N_f, the measured radiance of reflected solar radiation) must be considered dependent on θ, ψ, and ζ'

$$\rho_f'(\theta, \psi, \zeta'; \lambda, \phi) = \frac{N_f(\lambda, \phi)}{\cos \zeta' \cdot S_f'} \text{ steradian}^{-1} , \tag{3}$$

where S_f' is the incident solar irradiance at the moment of measurement and within the filter range of the instrument. It is obtained by integrating over all wavelengths the product of the spectral response of the instrument (Reference 22) with Johnson's data (Reference 38) on the extraterrestrial spectral solar irradiance. The latter are based on the solar constant $S_0 = 2.0$ cal cm^{-2} min^{-1}. Then, the solar irradiance on the day of measurement was determined by

$$S' = S_0 \left(\ell_1^2 / \ell^2 \right) \tag{4}$$

where ℓ_1 and ℓ are the mean and the true distance from sun to earth, respectively.

The response of the instrument covers a spectral range, within which about 99 percent of the energy of solar electromagnetic radiation enters the atmosphere. Therefore, it is assumed in all further steps that ρ_f' is a mean value for the entire solar spectrum $(\rho_f' = \rho')$. As for outgoing flux of emitted long-wave radiation, the computation of the reflected flux of solar radiation requires measurements under various values of θ, ψ, and ζ'. However, over most areas of the globe only one measurement was obtained in 24 hours. Thus, it was required to determine the outgoing flux from a single radiance measurement. The steps in this process are discussed below.

We compute the directional reflectance r (the ratio between the solar radiation reflected into the upper hemisphere and the incoming solar radiation) from the bidirectional reflectance (Equation 3), using empirically determined relations. These relations were derived from airplane and balloon measurements of reflected solar radiation with different values of θ and ψ (References 30 – 32). Figure 3 shows one of three diagrams in which isolines $X = r/\rho$ (where $\rho = \pi \cdot \rho'$) are drawn vs θ and ψ. This figure was used to convert all ρ' from measurements at solar zenith angles ζ', such that $60° < \zeta' \leq 80°$, to r. Two other diagrams were constructed for $0 < \zeta' \leq 35°$ and $35° < \zeta' \leq 60°$ (see Appendix C). The patterns of the isolines $X = r/\rho$ in Figure 3 shows that at low sun an observed area appears much brighter near the horizon than it would be at the subobserved point. The integral of r/ρ over the hemisphere is π. The outgoing flux R' of solar radiation reflected from a

*Levine, J. S., "The Planetary Albedo Based on Satellite Measurements Taking into Account the Anisotropic Nature of the Reflected and Backscattered Solar Radiation," Master's Thesis, New York Univ., Graduate School of Arts and Science (private communication).

surface element to space between sunrise t_r and sunset t_s is then obtained from

$$R'(\lambda, \phi) = \frac{1}{t_s - t_r} \int_{t_r}^{t_s} r\left(\zeta(t); \lambda, \phi\right) \cdot S' \cos \zeta(t)\, dt \ , \quad (5)$$

where $t_s - t_r$ is the daylight period in hours of an observed area (λ, ϕ). Here a general relation $r(\zeta)$ was required, which describes the change of the directional reflectance r with the sun's zenith angle; this relation was derived from the above measurements and from results of statistical analyses of satellites measurements (References 33 and Levine*). Figure 4 shows a normalized plot $r(\zeta)/r(\zeta = 0)$ vs ζ of this relation and compares it with the statistical results of other authors. The directional reflectance of a surface element was found to increase with increase of the sun's zenith angle. The 24-hour average of the outgoing flux of reflected solar radiation is:

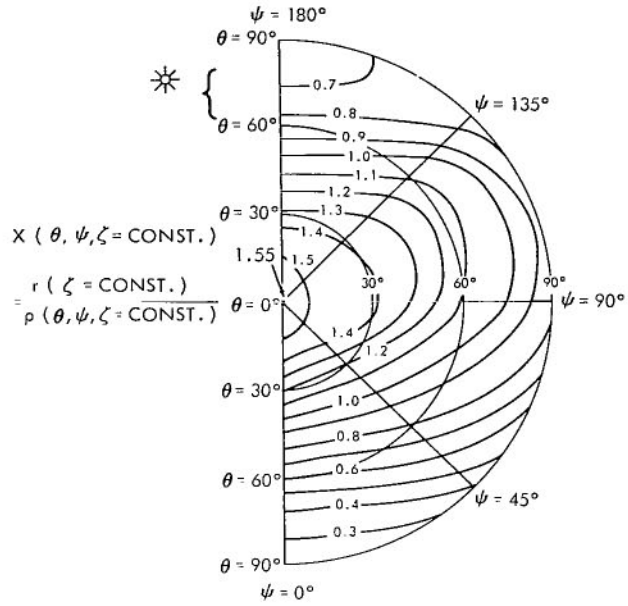

Figure 3—Dependence of the ratio $X = r/\rho$ on the angles θ and ψ of measurement, at very low sun $(60° < \zeta \leq 80°)$.

$$R = (t_s - t_r) \cdot R'/24 \ . \quad (6)$$

Appendix C explains the determination of the above-mentioned models in greater detail.

Using the relation of $r(\zeta)/r(\zeta = 0)$ to ζ in Figure 4 to compute the flux of solar radiation reflected from an area to space between sunrise and sunset implies this assumption: that the physical properties (cloudiness and surface state) of an observed area do not change throughout the day. This assumption introduces a major error into the results over areas with a diurnal cloud variance that is stronger than the day-to-day variance due to transient disturbancies. This error is most likely to occur over low latitudes, where only one measurement was obtained per area per day.

The incoming fluxes of solar radiation can also be computed from Equation 5, setting $r = 1$. In integrating the equation, refraction in the atmosphere was taken into account with a simple model derived from Table IX in Reference 39.

*Levine, J. S., "The Planetary Albedo Based on Satellite Measurements Taking into Account the Anisotropic Nature of the Reflected and Backscattered Solar Radiation," Master's Thesis, New York Univ., Graduate School of Arts and Science (private communication).

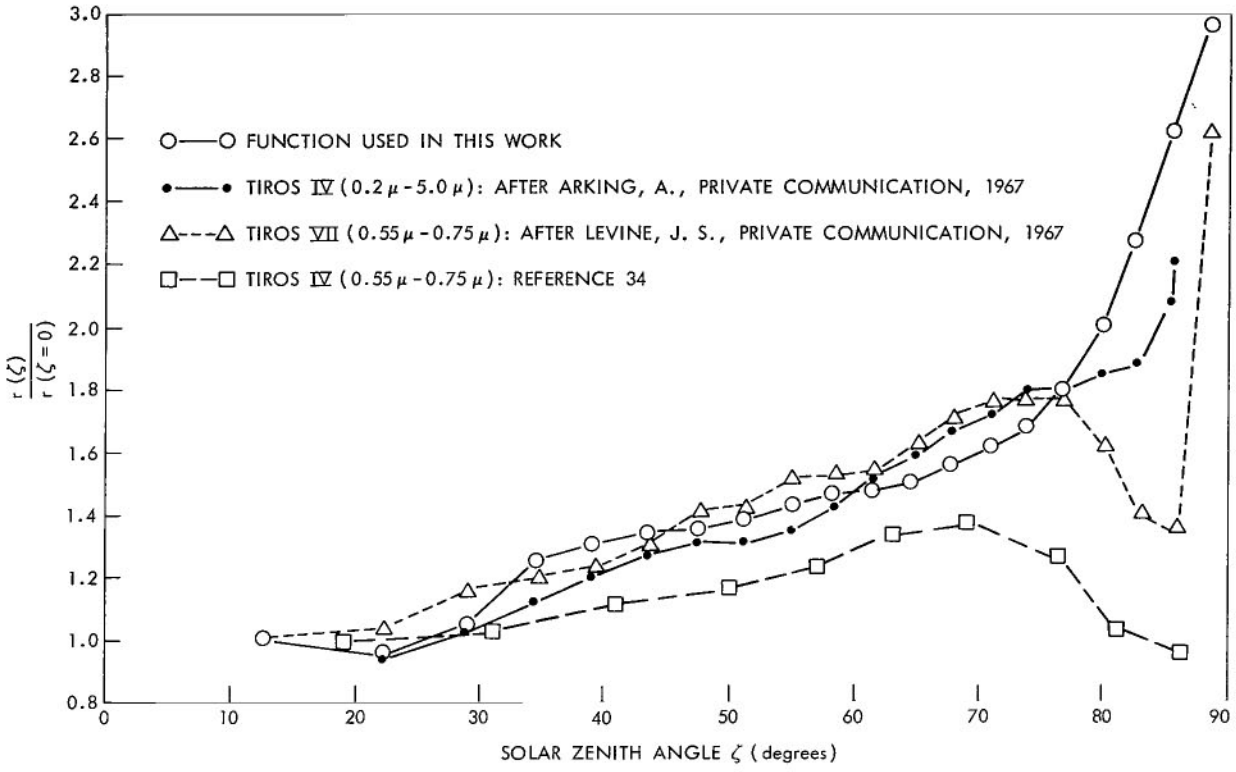

Figure 4—The relative change of the directional reflectance (r) of the earth-atmosphere system with the sun's zenith angle (ζ).

In the earlier investigations of radiation balance by satellites (References 14, 16, 40), the earth-atmosphere system was assumed to be a Lambert reflector. The albedo (References 18, 41) was then obtained by multiplying ρ_f' in Equation 3 by π.

GEOGRAPHIC DISTRIBUTIONS OF RESULTS

Geographic distributions of the outgoing long-wave radiation, albedo, and radiation balance are shown in Mercator projections, 70°N to 60°S, and polar-stereographic projections for both polar regions (Appendix E).

The albedo maps for all five periods show essentially the same patterns. Albedos of more than 55 percent were obtained over the arctic icecap and over snow-covered surfaces, especially in May. From May to July the mean albedo of the polar ice shield diminishes from about 75 to 60 percent, because of the melting of the snow cover and some pack ice. The albedo over the Greenland ice-shield remains nearly constant at 75 to 80 percent. Although over the Arctic a mean cloud coverage of more than 6/10 (see Appendix F) was reported, the pattern of albedo clearly indicates the change of the mean pack-ice boundary with the season, demonstrating the influence of the reflection properties of the earth's surface on the albedo of the earth-atmosphere system above clouds. The pack ice was an average albedo of 50 to 60 percent contributes much to the flux of reflected

solar radiation above clouds. For comparison, the albedo over the open oceans is less than 10 percent. (See Reference 21 for a more comprehensive description of radiation balance and its components.)

Toward the equator the albedo decreases rapidly with decreasing cloudiness, showing minima of less than 20 percent over the subtropical oceans on both sides of the equator. High cloudiness, especially over Central Africa, and the Monsoon over Southeast and South Asia, cause albedos of more than 20—30 percent and 40 percent, respectively. The Sahara and Arabian deserts have albedos upward of more than 30 to 35 percent. South of 30°S, the albedo increases nearly zonally toward 60°S because of the increasing cloud cover and decreasing sun elevation. The sun did not illuminate latitudes poleward of 67—71°S during Nimbus II observations.

The pattern in the maps of the outgoing long-wave radiation is narrowly correlated to the temperature of underlying surfaces (Reference 42). Very low values are obtained, especially over the South Pole (= winter pole), Greenland, and the ice shield over the East Siberian Sea. Elsewhere, at mean and low latitudes, fluxes of less than 0.36 cal cm^{-2} min^{-1} are associated with cloud fields in areas of high cyclonic activity and areas of the intertropical convergence zone (ITC). The ITC is more pronounced in outgoing long-wave radiation than in the albedo, possibly because of the large temperature difference between high tropical cloud surfaces and the adjacent nearly cloud-free and warm subtropical ocean and land surfaces (these are the regions of highest loss of long-wave radiation to space). The temperatures over the Sahara and Arabia increase markedly from May to July.

The maps of the radiation balance or the net radiation flux at the top of the atmosphere clearly show major regions of gain and deficit of radiative energy between 16 May and 28 July 1968. Owing to the sun's declination during this season, the northern hemisphere south of 70°—75°N and the southern tropics absorb more radiation than they re-emit to space. Maxima of energy gain occur over the very low-reflecting northern subtropical oceans. In contrast to these, the large desert areas of North Africa and Arabia (both are highly reflecting and emitting areas) have only a small radiation surplus (in May) or even a small deficit. The latter was predicted already by Budyko (Reference 6) for the annual average.

The Arctic, especially the inner ice-shield over Greenland, reflects and emits more energy to space than it gains by absorption of incoming solar radiation. The radiation balance over central arctic regions reaches positive values only during the first half of July. The southern hemisphere approximately south of 5°—10°S is an area of radiation deficit during this season. Because of the continuous decrease of incoming solar radiation to 70°S (where the influx is almost zero) and decreasing temperatures toward the Antarctic, the maximum deficit occurs in a zonal belt between about 60° and 70°S. Over most land surfaces, especially the southern hemisphere, the radiation deficit is larger and the gain is smaller than over ocean surfaces at the same latitude.

In all maps, the patterns of isolines over the southern hemisphere is almost zonal by latitude, because of the preponderance of ocean. It is very pronounced in the maps of the radiation balance, possibly because the meridional gradient of incoming solar radiation is very strong over the southern

hemisphere during this season. Over the northern hemisphere the wide continental surfaces dissolve the zones in several maxima and minima.

GLOBAL AND HEMISPHERICAL BUDGET

Table 1 summarizes the global and hemispherical averages of all components required in the balance equation; also the average albedos. The global average of the incoming flux of solar radiation S ranges between 0.484 and 0.488 cal cm^{-2} min^{-1}, changing its value according to changes in sun-earth distance. During the entire period the southern hemisphere receives only half as much solar radiation as the northern hemisphere. The global albedo was only 29.1—30.6 percent, which is considerably less than earlier accepted values of 33 percent and more, which were estimated or obtained from calculations with climatological data (References 1, 5, 43—46) and from observations of earth-shine on the moon (References 47, 48). Changes of the planetary value and of the

Table 1

Hemispherical and Global Averages of the Incoming Flux (S) and Reflected (R) Flux of Solar Radiation of the Albedo (R/S), of the Outgoing Long-Wave Radiation (E) and its Equivalent Black-Body Temperature, of the Absorbed Solar Radiation (S-R), and of the Net Radiation Flux (Q).

Period (1966)	Hemisphere(s)	S	R	R/S × 100 (percent)	E		S-R	Q
		cal cm^{-2} min^{-1}			Equivalent Temperature (°K)	cal cm^{-2} min^{-1}		
16-31 May	Northern	0.659	0.216	32.8	255.2	0.345	0.443	+0.098
	Southern	0.316	0.078	24.7	252.7	0.333	0.238	-0.095
	Globe	0.488	0.147	30.1	254.0	0.339	0.341	+0.002
1-15 June	Northern	0.674	0.221	32.8	256.0	0.350	0.453	+0.103
	Southern	0.297	0.076	25.6	253.2	0.334	0.221	-0.113
	Globe	0.486	0.149	30.6	254.8	0.342	0.337	-0.005
16-30 June	Northern	0.676	0.217	32.1	256.5	0.353	0.459	+0.106
	Southern	0.291	0.074	25.4	253.5	0.336	0.217	-0.119
	Globe	0.484	0.146	30.1	255.2	0.345	0.338	-0.007
1-15 July	Northern	0.670	0.210	31.4	257.0	0.356	0.460	+0.104
	Southern	0.298	0.072	24.1	253.5	0.336	0.226	-0.100
	Globe	0.484	0.141	29.1	255.2	0.346	0.343	-0.003
16-28 July	Northern	0.653	0.203	31.1	256.8	0.355	0.451	+0.096
	Southern	0.317	0.084	26.5	253.2	0.334	0.233	-0.101
	Globe	0.485	0.143	29.5	255.2	0.345	0.342	-0.003

hemispheric averages might be caused more by insufficient data coverage over parts of the globe than by albedo changes. The data coverage of the globe throughout all five subperiods was not always complete, as indicated by stippled fracture and dashed isolines in the maps. Thus, all averages in Table 1 might be slightly biased by lack of data in these gaps. The average albedo is rated higher over the northern than over the southern hemisphere, since during this season there were no measurements obtained over the Antarctic. Further, the southern hemisphere is predominantly covered with low-reflecting ocean surfaces.

From values of the outgoing flux, the mean "effective" temperature of the planet earth was found to be between 254 and 255.2°K, which is considerably higher than the 251°K previously accepted assuming radiative equilibrium for the earth-atmosphere system and a 35-percent global albedo. Here, the northern hemisphere is about 3 degrees warmer than the southern. From May to July, the emitted long-wave radiation rises slightly in the northern and decreases slightly in the southern hemisphere.

Figure 5 shows separately the temporal trends of the semihemispherical and global averages of the albedo and of the outgoing long-wave radiation. Over the northern hemisphere the outgoing flux rises slightly while the albedo simultaneously decreases. Both trends are caused by the warming of the northern hemisphere during this season and the melting of parts of the arctic ice cap. There seems to be no similar trend in the opposite direction over the southern hemisphere. The albedo, there, was found to be extremely low (24.1 percent) for the first half of July; but no explanation has been found. The period of available Nimbus II measurements was too short to show definite seasonal trends in these large-scale averages of the albedo and of the outgoing long-wave radiation.

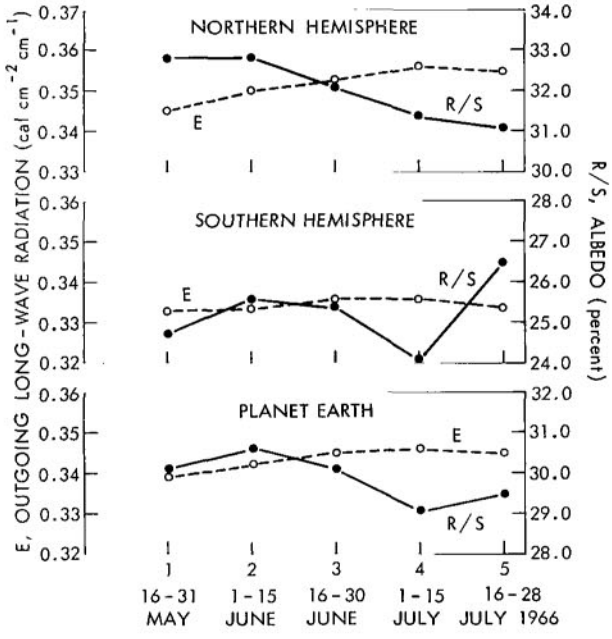

Figure 5—Hemispherical and global averages of the outgoing long-wave radiation, flux (E) and the albedo (R/S).

The last column of Table 1 lists the results on global radiation balance. They indicate for June and July 1966 a minimal radiation deficit of the planet earth, which is less than 2 percent of both components—the absorbed solar radiation and the emitted long-wave radiation. For the second half of May a slight radiation gain was found. Since the value of the solar constant is known at present only within ±2 percent, no final conclusions can be made on the real budget of the earth-atmosphere system during available Nimbus II measurements. However, a similar slight deficit found for this season by Simpson (Reference 3) suggests that the earth may have a slight radiation deficit during this season, possibly due to the larger earth-sun distance. Further measurements

over periods of 1 or 2 years (including simultaneous measurements of the solar constant) will lead to more conclusive results on the earth radiation budget.

The maps in Appendix E also show that the northern hemisphere permanently gains in radiative energy, while the southern hemisphere has a radiation deficit. But the effective emission temperature (T) for both hemispheres at the top of the atmosphere indicate that one or the other is not heating or cooling definitely (Table 1). Thus, atmospheric circulation as well as energy transport by ocean currents accounts for the energy transport from regions of radiation surplus to those of deficit. This, possibly, should also act southward through the equator, although it does not appear pronounced in mean streamline patterns for this season (Reference 49).

Spatial and temporal changes of the radiation budget over different latitudinal zones are better shown in the zonal averages plotted in Figure 6: incoming solar radiation, albedo, outgoing long-wave radiation, and radiation balance. The incoming flux of solar radiation changes considerably north of 40°N and over the southern hemisphere. These changes are explained by changes of the sun's declination which is greatest at the summer solstice.

The zonal averages for the outgoing long-wave radiation show the trend expected over both hemispheres. From May to July the northern hemisphere becomes slightly warmer north of 30°N,

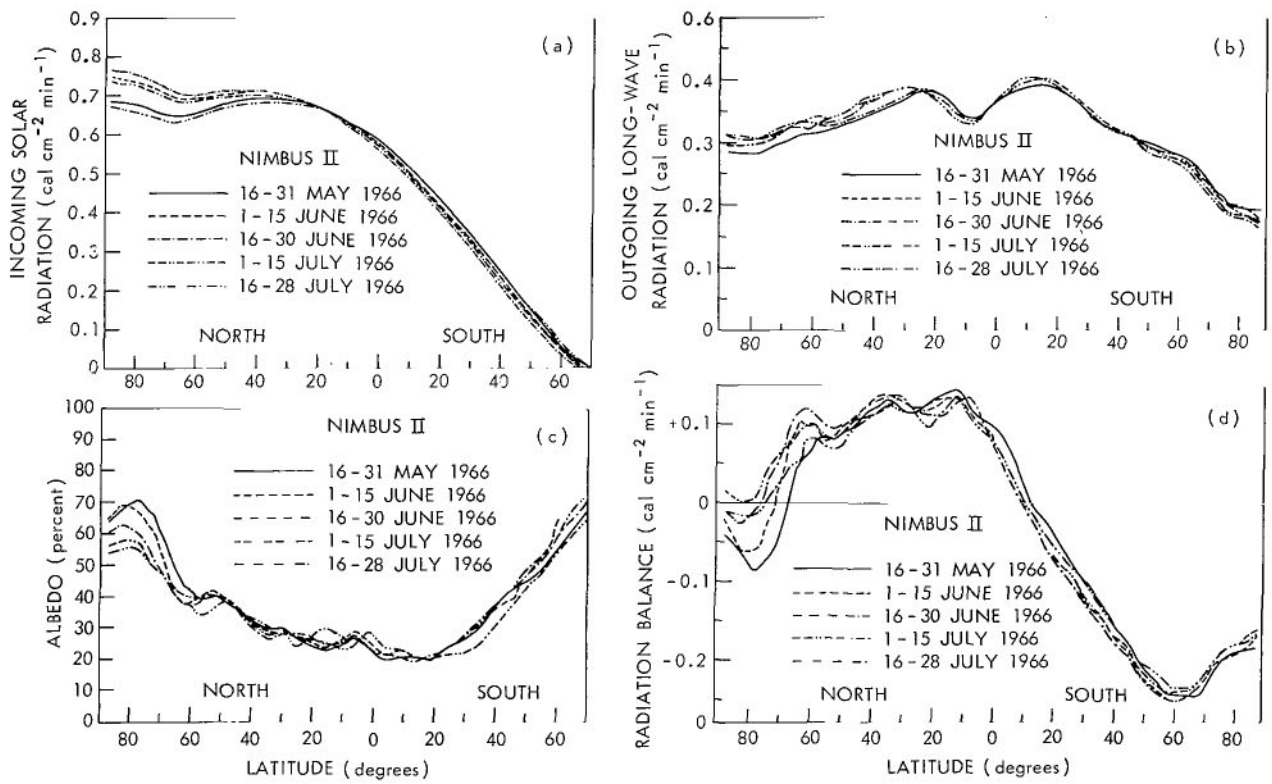

Figure 6—Zonal averages of (a) the incoming solar radiation, (b) the outgoing long-wave radiation, (c) the albedo, and (d) the radiation balance; at the top of the atmosphere.

but slightly colder south of 30°N because of northward shift of subtropical anticyclones and of the ITC (and all cloud fields associated with it). The thermal gradient from the equator to the North Pole decreases slightly, which may result in a slight decrease of the circulation (Figure 27 of Reference 8). The opposite behavior is observed over the southern hemisphere, where warming in the southern tropics (caused by the northward shift of the ITC) and cooling in the Antarctic cause the thermal gradient (and possibly the circulation) to increase slightly. Toward the end of July, radiative cooling at the outer belt of the Antarctic cannot be compensated for completely by advection.

The slight heating over the northern hemisphere is accompanied by a decrease of the albedo north of 60°N, which is due to melting of the snow cover over the arctic pack-ice, and of parts of itself. The radiation balance, however, was found positive over the arctic only during the first half of July. But the deficit is small enough, for parts of the energy transported to the arctic by advection and ocean currents to be available to melt parts of the ice and increase the mean temperature there.

From 50°N to 20°S the albedo shows no definite temporal changes associated with the northward movement of the ITC. Remarkably lower albedos occur during the first half of July over the southern hemisphere; a fact not yet explained. The radiation balance of the earth-atmosphere system south of the equator to 50°S changes its value almost entirely because of solar-influx changes. The maximum deficit of more than 0.24 cal cm^{-2} min^{-1} is observed at the summer solstice at 60°S and decreases there rapidly toward the end of July because of decreasing temperature and increasing insolation. A more detailed description of the results obtained over both polar caps is given elsewhere (Reference 21).

For Nimbus II, even the semimonthly averages might not very well represent the mean radiation balance of the earth-atmosphere system over areas with pronounced diurnal cycles of cloudiness and temperature and small transient disturbances; such was the character of the orbit. These areas are located mainly in tropical and subtropical regions.

COMPARISON OF THE RESULTS WITH DIRECT MEASUREMENTS

A comparison of our averaged results with direct (and ideally simultaneous) measurements should clearly reveal errors inherent in our methods. Because of a satellite's height such measurements should be made from high-flying airplanes or from balloons over areas whose radiation fields are nearly homogeneous in time and in space.

Such areas occur over those regions of the earth where synoptic disturbances (e.g. changes in cloud cover and cloud height) cause—in shorter time intervals—only small variations in both fields, in the outgoing long-wave radiation and in reflected solar radiation (or albedo). They have been found by computations of standard deviations of the albedo and of the outgoing long-wave radiation of all single daily averages within a grid field. Figure 7 shows results for the albedo during June, 1966. The standard deviation was less than 5 percent of the average value for both quantities, the albedo and the outgoing radiation flux (not shown here) over the Arctic (especially Greenland) and

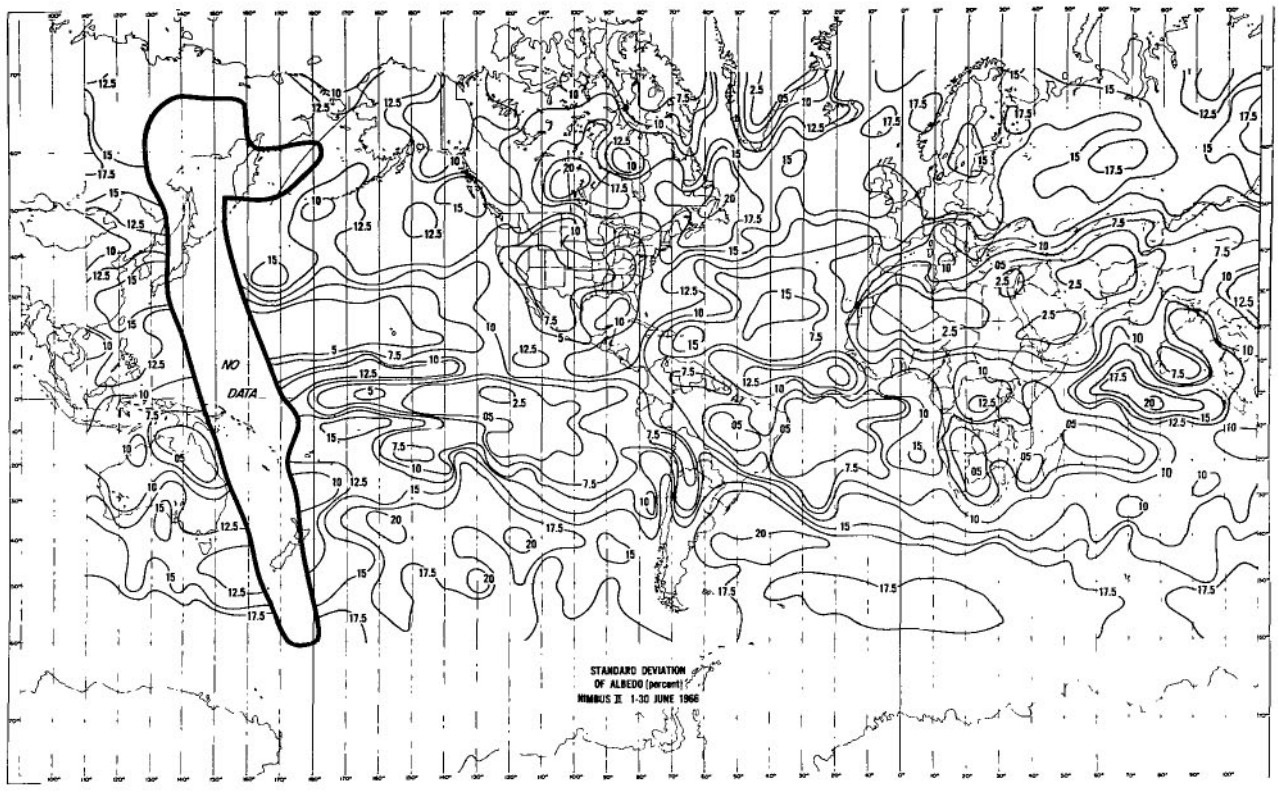

Figure 7—Standard deviation of the albedo in June 1966.

over the Sahara, indicating the predominant influence of surface conditions on the outgoing radiation in these areas. Standard deviation of the albedo over the subtropical oceans is less than 5 percent; but actually this is large, considering that the total mean albedo there is 15 percent or less. Over land areas at the same latitude the standard deviation is small and the mean albedo is much higher. Also, the standard deviation of the outgoing long-wave radiation is very low over the Antarctic.

In-situ measurements of outgoing long-wave radiation were recently discussed by Kuhn*, who conducted radiometer-sonde measurements over six antarctic stations during the same period (16 May—28 July 1966). His results agreed with our results within ±2 percent. It is now highly desirable to make a similar comparison over much warmer areas, such as the Sahara or Australian deserts.

No simultaneous measurements of the outgoing shortwave radiation were available for comparisons with the albedo values obtained from the Nimbus II measurements. But only a few authors reported on results which they obtained on the directional reflectance of surfaces during the same season although in different years. Kasten (Reference 50) obtained over Greenland values of around 72 percent under clear skies in June; this compares quite well with our albedos between 70 and 80 percent which are affected by the atmosphere. The cloud cover over Greenland was about 4/10 to 6/10 during June (see Figures F2 and F3). Diamond and Gerdel (Reference 51) reported similar values; they obtained 77 percent in the forenoon and 87 percent in the afternoon under a

*Kuhn, P. H., "Nimbus II and Balloon Radiation Analyses," to be published in *J. Atm. Sci.*, private communication, 1967.

clear sky. Hubley (Reference 52) obtained over the Lamon Creek Glacier in Alaska a pronounced variation of the directional reflectance with local time. His values range between 80 and 65 percent at forenoon and 65 to 85 percent in the afternoon. Predoehl and Spano (Reference 53) and Spano (Reference 54) reported on airplane measurements over the Antarctic ice cap. These measurements, though conducted during a different season, show by contrast the extent of our results over the Arctic regions. Over the old winter ice they found values between 65 and 74 percent; new ice had considerably less directional reflectance. These values seem to confirm the high albedos of 70 to 80 percent, which were obtained from the Nimbus II measurements over Greenland by the computational methods discussed above. The straight assumption of a Lambert-surface led to considerably smaller values between 55 and 60 percent (Reference 41).

Roach (Reference 55) obtained over the Sahara between El-Adem and Karthoum directional reflectances of about 32 percent. Our values over this region range between 30 and 40 percent and may be affected largely by the cloudiness. This rough comparison shows that our computational results obtained from Nimbus II radiance measurements agree quite well with other measurements. Definite conclusions on the radiation balance of the planet earth, and for specific areas, require a more reliable confirmation.

COMPARISON WITH OTHER RADIATION BALANCE STUDIES

From climatological data Baur and Philipps (Reference 4) and London (Reference 1) obtained results for the same season (summer) for the northern hemisphere only. Gabites (Reference 10) computed monthly averages of the radiation balance and its components only south of 40°S, using observations of the International Geophysical Year 1957—1958. Only Simpson (Reference 3) and Vinnikov (Reference 7) obtained results on a global scale. Houghton (Reference 5) and Budyko (Reference 6) reported only on annual averages.

Measurements of previous TIROS satellites were evaluated by several authors: Rasool and Prabhakara (Reference 16), Winston (Reference 17), Bandeen, et al. (Reference 14). The outgoing flux of long-wave radiation was computed from measurements of infrared radiation between 8 and 12 microns, since measurements in a wide spectral range were unavailable (on TIROS IV) or very inaccurate (on TIROS VII). These measurements and those of the outgoing solar radiation were highly affected by instrumental degradation. The results, then, may still contain some errors, although careful correction methods were applied (Reference 14). The albedo of the earth-atmosphere system was computed in these earlier studies assuming complete isotropy of the reflection properties of the earth-atmosphere system. Although the original measurements were corrected for degradation, the albedos were still too low. Arking and Levine (Reference 56) applied an angular correction on TIROS VII measurements. But they had to use a factor of 1.56 to obtain a 32-percent global albedo; this albedo value was necessary to balance in the annual average the incoming solar radiation with the outgoing radiation fluxes (Reference 14), From Explorer VII data, House (Reference 15) obtained averages for December 1959 through May 1960 only. Thus, our results cannot be compared with those from earlier satellite measurements.

Figure 8 summarizes zonal averages of earlier investigations and compares them with those obtained from Nimbus II measurements throughout July. The estimates of the albedo and outgoing

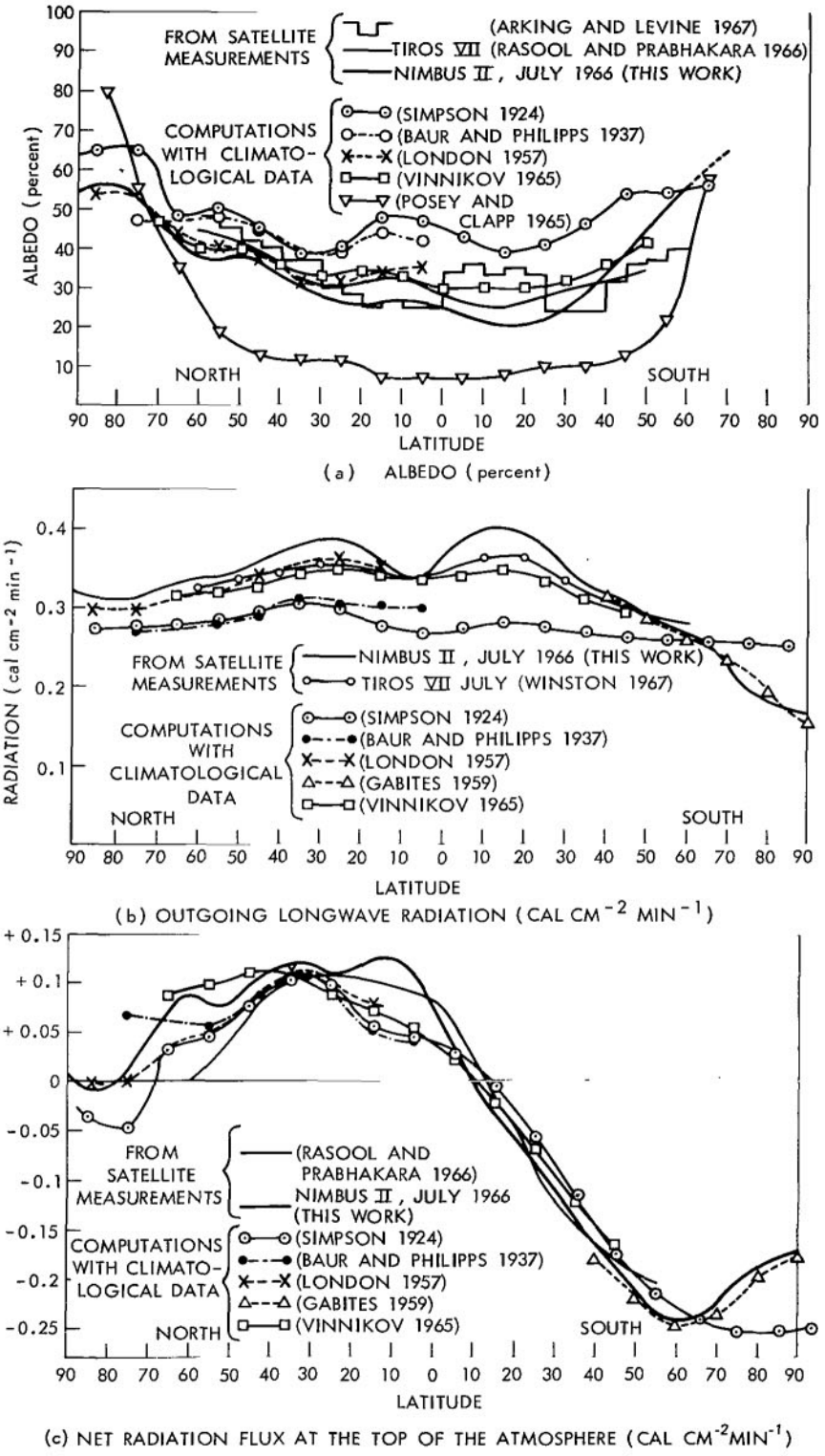

Figure 8—Comparison of zonal averages of (a) the albedo, (b) the outgoing long-wave radiation, and (c) the radiation balance, obtained from Nimbus II measurements during the period 1—28 July 1966, with results of other authors.

long-wave radiation from climatological data resulted in higher albedo values and lower outgoing radiation values between 50°N and 40°S than were obtained from Nimbus II data. This may be due to overestimating the cloud cover, the cloud height, and the reflection properties of clouds. A comparison of the albedos with the surface albedo, as shown in part (a) of the figure, may give some idea of the contribution of clouds to the albedo. (Between 70°N and 90°N Posey and Clapp (Reference 57) may have considerably overestimated the albedo of the polar ice cap and surrounding areas, not taking into account the open sea, which has considerably less albedo.)*

All authors found the radiation gain and deficit lower between 50°N and 50°S—see Figure 8(c). At higher northern latitudes only London's (Reference 1) results show a good agreement. Over the central Arctic (where Nimbus II measurements led to a slight radiation gain of 0.001 cal cm^{-2} min^{-1} for the monthly average), Vowinckel and Orvig (Reference 9) found a much higher surplus of +0.05 cal cm^{-2} min^{-1}, while Fletcher (Reference 8) obtained a deficit of -0.02 cal cm^{-2} min^{-1}. Gabites' results (Reference 10) over high southern latitudes show the closest agreement with our results. Simpson (Reference 3) had estimated too high surface temperatures over the Antarctic continent.

CONCLUSIONS

The main object of these investigations has been to calculate—from Nimbus II measurements of the radiance of outgoing long-wave and short-wave radiation—the outgoing flux of long-wave radiation and the albedo of the earth-atmosphere system. Both of these quantities and the incoming flux of solar radiation (obtained on the basis of the solar constant S_0 = 2.0 cal cm^{-2} min^{-1}) were used to compute the radiation balance, which is essentially the net radiation flux at the top of the atmosphere. Results are presented in geographic maps for the entire globe for five semimonthly periods covering the entire period of available Nimbus II measurements (16 May to 28 July, 1966). The spatial resolution was chosen to be between 500 km × 500 km (at the equator) and about 280 km × 280 km (poleward of latitude 60°). These maps show for the first time *global* distributions of the albedo, the outgoing long-wave radiation and the radiation balance as obtained from satellite measurements.

Other main results are:

1. Consideration of the anisotropic reflection characteristics of the earth-atmosphere system, in simple models, in albedo computations led to results that reasonably agree with measurements by other authors. But only a few comparisons were possible.
2. Outgoing long-wave radiation-flux measurements over the Antarctic agreed within 2 percent with simultaneous radiometersonde measurements. Similar comparisons over warmer areas are desired.

*But also the orbital characteristics of Nimbus II have caused errors over areas where the diurnal cycle of cloudiness and cloud height (and thus of the outgoing long-wave radiation and the albedo) is very pronounced as compared with day-to-day changes due to transient disturbances. Merritt, et al. (Reference 58), for instance, obtained a semi-diurnal cycle of cloudiness over Indonesia and Malaysia, with maxima in the early morning and late afternoon, while at local noon the cloudiness was somewhat less. Nimbus II daylight measurements are obtained over these areas around local noon; thus, the albedo may have been somewhat lower than if measured throughout the whole day. But the differences between the older studies and our investigations are too pronounced to be due only to these diurnal effects.

3. Global averages of the radiation balance of the earth-atmosphere system range, for all five subperiods, within 0.002 cal cm^{-2} min^{-1} gain and 0.007 cal cm^{-2} min^{-1} deficit (which is less than 2 percent of both components, the absorbed solar radiation remaining at the planet earth, and the emitted long-wave radiation being lost to space). These results indicate that the earth-atmosphere system is—even in smaller time periods—close to radiative equilibrium. (But, the results might be biased also by a systematic error in the solar constant.)
4. Zonal and global averages of the albedo and outgoing long-wave radiation are lower and higher, respectively, than those obtained from climatological data. This disagreement occurs mainly at low latitudes. This suggests that ground-based observations considerably overestimate the cloud cover.

For future efforts (recommended in research programs, such as the "Global Atmospheric Research Program," Reference 62, and the "World Weather Watch," Reference 63) the directions are very clear:

1. The solar constant must be measured simultaneously with other measurements of radiation emerging from the earth.
2. Higher spatial and temporal resolutions of the results require more sophisticated computational efforts, which permit the study of climatological peculiarities over different areas.
3. Simultaneous but independent measurements of the outgoing long-wave radiation flux and reflected solar radiation must be conducted over selected areas, to check the quality of the results obtained from satellite measurements of the radiance.

The results obtained so far from Nimbus II measurements on the radiation balance of the earth-atmosphere system clearly demonstrated the validity of satellite measurements. Results over several years (as well as studies of their relation to the general circulation pattern) have a fundamental bearing on the energy exchange of the planet earth. Once approved, similar methods could be applied for other planets.

ACKNOWLEDGMENT

The author is indebted to Dr. W. Nordberg and Mr. W. R. Bandeen of the Laboratory of Atmospheric and Biological Sciences for their helpful discussions and suggestions while this research was done. He also should like to express his appreciation to Mr. Robert Hite and Mr. Hugh Powell for their extensive efforts in the computer processing of the vast amount of satellite radiation measurements utilized in this study.

Goddard Space Flight Center
National Aeronautics and Space Administration
Greenbelt, Maryland, January 8, 1968
160-44-05-02-51

REFERENCES

1. London, J., "A Study of the Atmospheric Heat Balance," Final Report, Contr. AF 19(122)-165, Research Division, Col. of Engineering, New York U., N. Y., 1957.

2. Dines, W. H., "The Heat Balance of the Atmosphere," *Quart. J. Roy. Met. Soc.* 43:151-158, 1917.

3. Simpson, G. C., "The Distribution of Terrestrial Radiation," *Memoirs of the Royal Meteor. Soc.* 3(23), 1924.

4. Baur, F., and Philipps, H., "Der Wärmehaushalt der Lufthülle der Nordhalbkugel in Januar und Juli und zur Zeit der Äguinoktien und Solstitien," *Gerl. Beitr. Geophys.* 42:160-207, 1934; 45:82-132, 1937.

5. Houghton, H. G., "On the Annual Heat Balance of the Northern Hemisphere," *J. Meteor.*, 11: 3-9, 1954.

6. Budyko, M. I., ed., "Atlas of the Heat Balance of the Earth (Atlas Teplovogo Bolansa Zemnogo Shara)," Moscow, 1963.

7. Vinnikov, K. Ya, "A New Calculation of the Heat Balance of the System Earth-Atmosphere" (in Russian), *Meteorologija i Gidrologija* 8:32-37, 1965. "Outgoing Radiation of the System Earth-Atmosphere" (in Russian), *Glavnaja Geofisicheskaja Observatoria* 168, 1965. "The Albedo of the System Earth-Atmosphere and the Field of Outgoing Shortwave Radiation," (in Russian), *Glavnaja Geofisicheskaja Observatoria* 170, 1965.

8. Fletcher, J. O., "The Heat Budget of the Arctic Basin and its Relation to Climate," The RAND Corporation, R-444-PR, 1965.

9. Vowinkel, E., and Orvig, S., "Radiation Balance of the Troposphere and of the Earth-Atmosphere System in the Arctic," *Sci. Rep.* Contr. AF 19(604)-7415, Dept. of Meteor., Montreal, Can., No. 9, January 1964.

10. Gabites, J. F., "The Heat Balance of the Antarctic Through the Year," in: *Antarctic Meteorology,* Proceedings of Melbourne Symposium, February 1959, New York: Pergamon Press, pp. 370-377.

11. Weinstein M., and Suomi, V., "Analysis of Satellite Infrared Radiation Measurements on a Synoptic Scale," *Monthly Weather Rev.* 89:419-428, 1961.

12. Malkevich, M. S., Pokras, V. M., and Yurkova, L. I., "Measurements of Radiation Balance from the Satellite Explorer VII," *Planet. Space Sci.* 11:839-865, 1962.

13. Bignell, K. J., "Heat-Balance Measurements from an Earth-Satellite—an Analysis of Some Possibilities," *Quart. J. Roy. Met. Soc.* 87:231-244, 1961.

14. Bandeen, W. R., Halev, M., and Strange, I., "A Radiation Climatology in the Visible and Infrared from the TIROS Meteorological Satellites," NASA Technical Note D-2534, 1965.

15. House, F. B., "The Radiation Balance of the Earth, from a Satellite," Ph. D. Thesis, Dept. of Meteor., U. of Wisconsin, 1965.

16. Rasool, S. I., and Prabhakara, C., "Heat Budget of the Southern Hemisphere: Problems in Atmospheric Circulation," ed. by Garcia and Malone, Washington, D. C.: Spartan Books, 1966, pp. 76-92.

17. Winston, J. S., "Planetary Scale Characteristics of Monthly Mean Long-Wave Radiation and Albedo and Some Year-to-Year Variations," *Monthly Weather Rev.* 95:235-256, 1967.

18. Winston, J. S., and Taylor, V. R., "Atlas of World Maps of Long-Wave Radiation and Albedo," ESSA Technical Report NESC-43, Washington, D. C., 1967.

19. Nordberg, W., McCulloch, A. W., Foshee, L. L., and Bandeen, W. R., "Preliminary Results from Nimbus II," *Bull. Am. Meteor. Soc.* 47:857-872, 1966.

20. Raschke, E., and Pasternak, M., "The Global Radiation Balance of the Earth-Atmosphere System Obtained from Radiation Data of the Meteorological Satellite Nimbus II," NASA Goddard Space Flight Center Document X-622-67-383; to be published in Space Research VIII, Proceedings of the COSPAR Meeting, London, July 1967.

21. Raschke, E., Möller, F., and Bandeen, W. R., "The Radiation Balance of the Earth-Atmosphere System over both Polar Regions Obtained from Radiation Measurements of the Nimbus II Meteorological Satellite," NASA Goddard Space Flight Center Document X-622-67-460 (Paper presented at 6th International Polar Meeting, Stuttgart, Germany), 1967.

22. "Nimbus II User's Guide," NASA Goddard Space Flight Center, Greenbelt, Maryland.

23. Wark, D. Q., Yamamoto, G., and Lienesch, J. H., "Methods of Estimating Infrared Flux and Surface Temperature from Meteorological Satellites," *J. Atm. Sci.* 19:369-384, 1962.

24. Lienesch, J. H., and Wark, D. Q., "Infrared Limb Darkening of the Earth from Statistical Analyses of TIROS Data," *J. Appl. Meteor.* 6:674-682, 1967.

25. Korb, G., Michalowski, J., and Möller, F., "Die Absorption der Sonnenstrahlung in der Wolken freien und bewölkten Atmosphäre," *Beitr. Phys. Atm.* 30:63-77, 1957.

26. Coulson, K. L., "Characteristics of the Radiation Emerging from the Top of a Rayleigh Atmosphere," *Planet. Space Sci.* 1:265-284, 1959.

27. Sekera, Z., and Viezee, W., "Distribution of the Intensity and Polarization of the Diffusely Reflected Light Over a Planetary Disk." The RAND Corporation, R-389-PR, 1961.

28. Heger, K., "Die von der Atmosphäre nach aussen gestreute Strahlung. II. Ergebnisse numerischer Auswertung," *Beitr. Phys. Atm.* 39:12-36, 1966.

29. Plass, G. N., and Kattawar, G. W., "Monte Carlo Calculations of Light Scattering from Clouds" (Paper presented at the Meeting of the American Geophysical Union), Washington, D. C., 1967.

30. Bartman, F. L., "The Reflectance and Scattering of Solar Radiation by the Earth," Technical Report, 1967.

31. Cherrix, T., and Sparkman, B., "A Preliminary Report on Bidirectional Reflectances of Stratocumulus Clouds Measured with Airborne Medium Resolution Radiometer," NASA Goddard Space Flight Center Document X-622-67-48, 1967.

32. Salomonson, V. V., "Anisotropy of Reflected Solar Radiation from Various Surfaces as Measured with an Aircraft-Mounted Radiometer," Research Report, Contr. NASr-147, Colorado State U., 1967.

33. Arking, A., "The Angular Distribution of Scattered Solar Radiation and the Earth Albedo as Observed from TIROS," Institute for Space Studies, Research Reports, July 1, 1964—June 30, 1965, New York, 1965, pp. 47-67.

34. Ruff, I., Koffler, R., Fritz, S., Winston, J. S., and Rao, P. K., "Angular Distribution of Solar Radiation Reflected from Clouds as Determined from TIROS IV Radiometer Measurements," ESSA Technical Report NESC-38, Washington, D. C., 1967.

35. Raschke, E., and Bandeen, W. R., "Studies of Reflection Characteristics of the Planet Earth from a Synchronous Satellite—Preliminary Results," NASA Goddard Space Flight Center Document X-622-67-572, 1967.

36. Viezee, W., Mancuso, R. L., and Davis, P. A., "Variations of Daytime Radiation Data with Viewing Geometry," Contr. AF 19(628)-2777, SRI Project 4448, Stanford Research Institute, Menlo Park, Calif., 1964.

37. Råbbe, A., "Angular Dependence of Albedo from Stratiform Clouds as Measured by TIROS IV Scanning Radiometers," SMRP Research Paper, No. 58, Dept. of Geoph. Sciences, U. of Chicago, 1966.

38. Johnson, F. S., "The Solar Constant," *J. Meteor.* 11:431-439, 1954.

39. Baur, F., ed., Linke's "Taschenbuch der Meteorologie. 2. Ausgabe, Vol. III," Leipzig, 1953.

40. Möller, F., "Eine Karte der Strahlungsbilanz des Systems Erde—Atmosphäre für einen 14-tägigen Zeitraum," *Meteor. Rundschau* 20:97-98, 1967.

41. Pasternak, M., "An Atlas of Total Outgoing Long-Wave Radiation and of Short-Wave Reflectances from Nimbus II Observations," NASA Goddard Space Flight Center Document X-622-67-500, 1967.

42. Möller, F., and Raschke, E., "Evaluation of TIROS III Radiation Data," NASA Contractor Report-112 (Grant NSG-305 with the U. of Munich, Germany), 1964.

43. Wegner, A., "Thermodynamik der Atmosphäre," Leipzig: J. A. Barth, 1911, pp. 3-5.

44. Aldrich, L. B., "The Reflecting Power of Clouds," *Smith. Miscell. Collections* 69:(10), 1919,

45. Fritz, S., "The Albedo of the Planet Earth and of Clouds," *J. Meteor.* 6:277-282, 1949.

46. Ångstrom, A., "Atmospheric Turbidity, Global Illumination and Planetary Albedo of the Earth," *Tellus* 14:435-450, 1962.

47. Danjon, A., "Nouvelles Recherches sur la Photométrie de la Lumière Cendrée et l'Albedo de la Terre," *Ann. Obs. Strasbourg* 3:(3), 1936.

48. Penndorf, R., "Die Albedo der Erde Meteor. Zeitscyrift," 54:348-349, 1937.

49. Riehl, H., "Tropical Meteorology," New York: McGraw-Hill Book Company, 1954, pp. 1-17.

50. Kasten, F., "Meteorologisch—Optische Untersuchungen auf dem Gränländischen Inlandeis," *Polarforsch.* 5:202-207, 1963.

51. Diamond, M., and Gerdel, R. W., "Radiation Measurements on the Greenland Ice Cap," *Comptes Rendus et Rapports—Assemblee Generale de Toronto,* 4:403-426, 1958.

52. Hubley, R. C., "Measurements of Diurnal Variations in Snow Albedo on Lemon Creek Glacier, Alaska," *J. Glaciol.* 2:560-563, 1955.

53. Predoehl, M. C., and Spano, A. F., "Airborne Albedo Measurements over the Ross Sea, October-November 1962," *Monthly Weather Rev.* 93:687-696, 1965.

54. Spano, A. F., "Results of an Airborne Program in Antarctica, 1963," *Monthly Weather Rev.* 93:697-703, 1965.

55. Roach, W. T., "Some Aircraft Observations of Fluxes of Solar Radiation in the Atmosphere," *Quart. J. Roy. Met. Soc.* 87:346-363, 1961.

56. Arking, A., and Levine, J. S., "Earth Albedo Measurements: July 1963 to June 1964," *J. Atm. Sci.* 24:721-724, 1967.

57. Posey, J. W., and Clapp, P. F., "Global Distribution of Normal Surface Albedo," *Geofísica Internacional* 1:33-48, 1965.

58. Merritt, E. S., Sherr, P. E., Widger, F., and Bowley, C. J., "Studies of TIROS and Nimbus Radiometric Observations," Final Report, Contr. NAS 5-10151, Allied Research Assoc. Inc., Concord, Mass., 1967.

59. List, R. J., ed., "Smithsonian Meteorological Tables, 6," Revised Edition, Smithsonian Institution, 1963.

60. Boileau, A. R., and Gordon, J. I., "Atmospheric Properties and Reflectances of Ocean Water and Other Surfaces for a Low Sun," *Appl. Optics* 5:803-813, 1966.

61. Deirmendjian, D., "Scattering and Polarization Properties of Water Clouds and Fluxes in the Visible and Infrared," *Appl. Optics* 3:187-196, 1964.

62. "Global Atmospheric Research Programme (GARP)," Report of a Study Conference, Stockholm, June 28—July 11, 1967. ICSU/IUGG, Committee on Atmos. Sci., COSPAR, World Meteorological Organization, 1967.

63. "The Role of Meteorological Satellites in the World Weather Watch," Planning Report No. 18, World Meteorological Organization, 1967.

Appendix A

Computation of Angles θ, ψ, ζ

Solar Zenith Angle:

$$\zeta = \cos^{-1}\left[\cos\phi\cos\delta\cos\left(\lambda_G - \lambda\right) + \sin\phi\sin\delta\right] , \tag{A1}$$

where λ, ϕ are the geographic longitude and latitude, respectively, of an observed surface element (λ is counted westward; ϕ is positive north and negative south of the equator), λ_G is the Greenwich hour angle, and δ is the declination of the sun.

Zenith Angle of Measurement θ:

$$\begin{aligned} \theta &= \sin^{-1}\left(\frac{R+H}{R}\sin\alpha\right) \\ &= \sin^{-1}\left(K\cdot\sin\alpha\right) , \end{aligned} \tag{A2}$$

where α is the nadir angle of measurement, which can be obtained from the data tape (Reference 22). The earth's mean radius R is assumed to be 6371 km and the satellite height H to be constant: H = 1140 km.

Then $K = (R+h)/R = 1.17893$.

Azimuth Angle of Measurement ψ:

The azimuth angle ψ is determined with respect to the ray of incident solar radiation (Figure 1), by

$$\psi = \cos^{-1}\left(\frac{\cos\Gamma - \cos\zeta\cos\theta}{\sin\zeta\sin\theta}\right) , \tag{A3}$$

where

$$\cos\Gamma = \frac{\left[K\cdot\cos\phi_s\cos\left(\lambda_s-\lambda_G\right)\cos\phi_s\cos\left(\lambda-\lambda_G\right)\right]\cos\delta + \left[K\sin\phi_s - \sin\phi\right]\sin\delta}{\sqrt{K^2+1-2K\left(\cos\phi_s\cos\phi\cos\left(\lambda-\lambda_s\right)+\sin\phi_s\sin\phi\right)}} , \tag{A4}$$

where λ_s and ϕ_s are the geographic longitude and latitude, respectively, of the subsatellite point.

The Length of a Day $\Delta\lambda$:

Sunrise and sunset are defined as the instants when the upper edge of the disk of the sun is on the horizon at normal refraction (Table IX in Reference 39). Assuming that a semidiameter of the sun subtends a 16-minute angle, with a constant 34-minute refraction (Reference 59), then the length of a day $\Delta\lambda^*$ (in degrees of arc on the celestial sphere) is

$$\Delta\lambda^* = 2 \cdot \Delta\lambda = 2 \cdot \cos^{-1} \frac{-0.0143 - \sin\phi \sin\delta}{\cos\phi \cos\theta} = 2\cos^{-1}(\text{arg}) , \qquad \text{(A5)}$$

where $\Delta\lambda$ is 180° (= 12 hours), if (arg) $\leq$ - 1.

Appendix B

Computation of Outgoing Long-Wave Radiation Flux E

If $N_f(\theta)$ is the measured filtered radiance in the spectral range from 5.0 to 30.0 microns, then the unfiltered radiance N (Figure 2) is:*

$$N(\theta) = \frac{1}{\pi}\left[0.0439 + 5.4318 \times 10^{-3} \cdot N_f(\theta) + 1.0245 \times 10^{-5} \cdot N_f(\theta)^2 + \theta^3 \cdot \left(1.36 \times 10^{-8} - 7.9262 \times 10^{-10} \cdot N_f(\theta) + 1.1488 \times 10^{-11} \cdot N_f(\theta)^2\right)\right], \quad \text{(B1)}$$

where $N(\theta)$ and $N_f(\theta)$ are in cal cm^{-2} min^{-1} sr^{-1}.

The outgoing flux E, then, is determined by

$$E = 2.901 \cdot N(\theta) \Big/ \left[1 + 1.933 \times 10^{-4} \cdot \theta - 4.247 \times 10^{-5} \cdot \theta^2 + 6.149 \times 10^{-7} \cdot \theta^3 - 7.807 \times 10^{-9} \cdot \theta^4\right] \text{ cal } cm^{-2} \, min^{-1}. \quad \text{(B2)}$$

The denominator in Equation B2 was found statistically by Lienesch* from measurements of TIROS satellites. It describes the zenith-angle dependence of outgoing long-wave radiation.

*Lienesch, J. H., private communication, 1966.

Appendix C

Relations to Determine Directional Reflectance r from Bidirectional Reflectance ρ'

General Equation for $r(\zeta)$:

To integrate Equation 5 we need to know how the directional reflectance of an observed surface element varies with the solar zenith angle. Since only one or two satellite measurements were possible over the same area throughout the day, an empirical model was set up, to determine $r(\zeta)$ from the bidirectional reflectance $\rho'(\theta, \psi, \zeta')$, as obtained from a measured radiance (Equation 3):

$$r(\zeta) = \frac{r(\zeta)}{r(\zeta = 0)} \cdot \frac{r(\zeta = 0)}{r(\zeta')} \cdot \frac{r(\zeta')}{\rho(\theta, \psi, \zeta')} \cdot \pi\rho'(\theta, \psi, \zeta') , \qquad \text{(C1)}$$

(See Figures 3 and 4)

where ζ' and ζ are the solar zenith angle at the moment of measurement and at any arbitrary time, respectively, throughout the day.

Derivation of the Relation $r(\zeta)/r(\zeta = 0)$:

The general relation for the change of the directional reflectance with the sun's zenith angle was derived from several measurements. A main condition for the selection of measured reflectances was: that these measurements should be made in a wide spectral interval comparable with that of the Nimbus II MRIR (0.2—4.0 microns). Further, these measurements should have been obtained at a certain distance above reflecting surfaces (ground or clouds), so that they should also contain the effect of the atmosphere above those surfaces.

Up to that time (when these calculations were made), only a few measurements were available; these were obtained from airplanes (References 31, 32) and from balloons (Reference 30). The underlying surfaces were clear ocean, clouds, and snow. These measurements were obtained only in three narrow ranges of the solar zenith angle: $10° \leq \zeta \leq 20°$; $50° \leq \zeta \leq 60°$; $65° \leq \zeta \leq 75°$. Arking (Reference 33) obtained results on the angular behavior of the reflectance from a statistical analysis of TIROS IV measurements.

The heterogeneity of these available data required the assumption of a multiplicative law, to give an equation for the mean dependence of r on ζ:

$$\frac{r(\zeta)}{r(\zeta = 0)} = \frac{\rho(0, 0, \zeta)}{\rho(0, 0, 0)} \cdot \frac{r(\zeta)}{\rho(0, 0, \zeta)} \cdot \frac{\rho(0, 0, 0)}{r(\zeta = 0)} , \qquad \text{(C2)}$$

where $\rho(0, 0, \zeta) = \pi \cdot \rho'(0, 0, \zeta)$ at the subobserver point on the earth's surface.

Figure C1 shows the dependence of the product of the last two factors in Equation C2 on ζ, which describes the change of the ratio between the directional reflectance and the bidirectional reflectance at the subobserver point with the sun's zenith angle. A smooth curve drawn through the various kinds of data point was adopted in these computations. For comparison, the results of Arking* and Levine† are drawn in Figure C1.

The factor $\rho(0, 0, \zeta)/\rho(0, 0, 0)$, which describes the dependence of the bidirectional reflectance of the subobserver point on the solar zenith angle, was obtained from Arking's and Levine's statistical analysis of TIROS IV measurements. Figure C2(a) shows those authors' results. The relation of $\rho(0, 0, \zeta)/\rho(0, 0, 0)$ to ζ adopted for this work was obtained by curve-smoothing and is shown in Figure C2(b). This curve has some similarity with scattering functions obtained theoretically for water droplets (see for instance, Reference 61); this may be incidental and be due to data sampling.

The final relation of $r(\zeta)/r(\zeta = 0)$ to ζ was obtained through Equation C2 and is shown in Figure 4 in the main body of this report.

Diagrams $X = r/\rho$:

According to the third factor in Equation C1, we need relations to convert the bidirectional reflectance ρ' obtained from Equation 3 to the directional reflectance r. These relations, assumed to represent the mean behavior of the earth-atmosphere system, replace the measurements which, in fact, are required under all angles θ, ψ, ζ over one area. Bartman (Reference 30) and Salomonson (Reference 32) obtained measurements over different surfaces for many values of θ and ψ. Cherrix and Sparkman (Reference 31 at the time had results for azimuthal angles ψ of 0°, 180°, 45°, 135°, 90° only; thus, in order to provide models at least

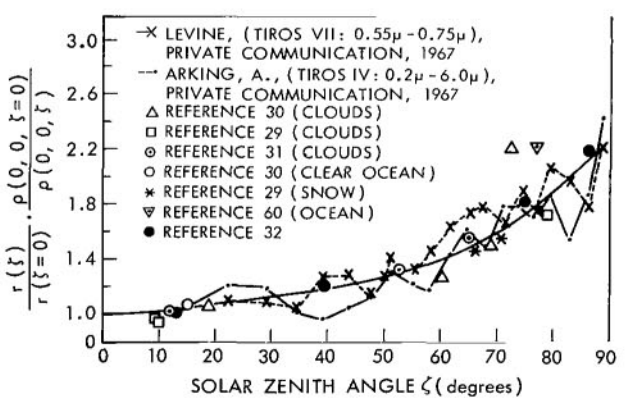

Figure C1—The relative change of the ratio between the directional reflectance (r) and the bidirectional reflectance ($\rho = \rho/\pi$) at the subobserver point ($\theta = 0°, \psi = 0°$) with the solar zenith angle (ζ).

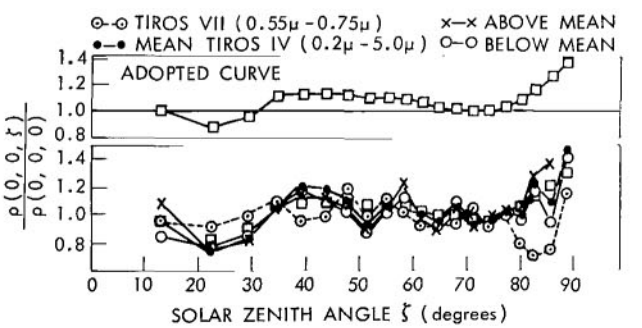

Figure C2—The relative change of the bidirectional reflectance ($\rho' = \rho/\pi$) at the subobserver point ($\theta = 0°$, $\psi = 0°$) with the solar zenith angle (ζ); experimental and smoothed curves.

*Arking, A., private communication, 1967.

†Levine, J. S., "The Planetary Albedo Based on Satellite Measurements Taking into Account the Anisotropic Nature of the Reflected and Backscattered Solar Radiation," Master's Thesis, New York Univ., Graduate School of Arts and Science (private communication).

on the average behavior, all available data have been summarized only for these azimuthal angles. Symmetry was assumed with respect to the principle plane (ψ: 0°—180°).

Figures C3 through C5 show the mean curves r/ρ, which were also obtained by smoothing. The single measurements, average for $\Delta\theta$ = 10 degrees, are indicated by several signatures according to the data source. All values r/ρ are normalized with respect to the relation shown in Figure C1. To draw the mean curves in Figures C3 through C5, most weight was given to measurements which were obtained in all five planes (ψ = 0°, 180°, 45°, 135°, 90°) over cloud surfaces.

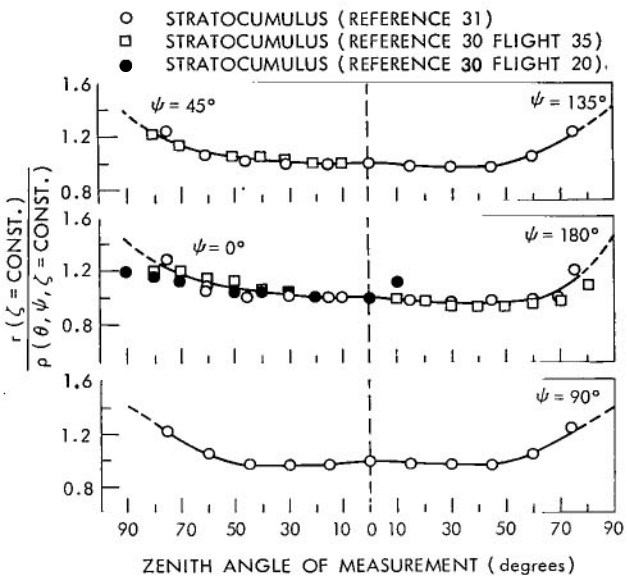

Figure C3—The ratio between the directional reflectance (r) and the bidirectional reflectance ($\rho' = \rho/\pi$) at values of azimuthal angle (ψ: 0°, 180°, 45°, 135°, 90°) as obtained from measurements at solar zenith angles ($10° \leq \zeta \leq 20°$).

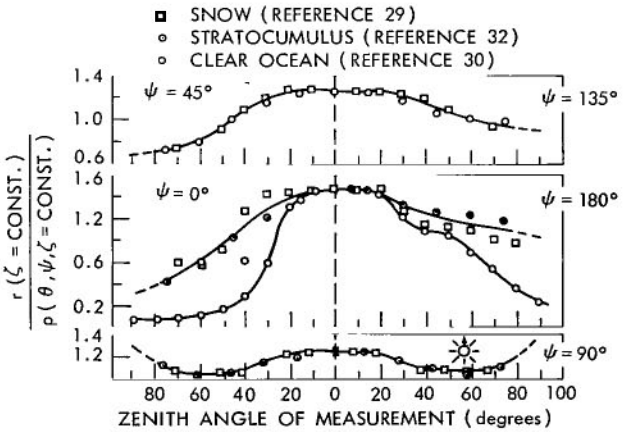

Figure C4—The ratio between the directional reflectance (r) and the bidirectional reflectance ($\rho' = \rho/\pi$) at values of azimuthal angle (ψ: 0°, 180°, 45°, 135°, 90°) as obtained from measurements at solar zenith angles ($50° \leq \zeta \leq 60°$).

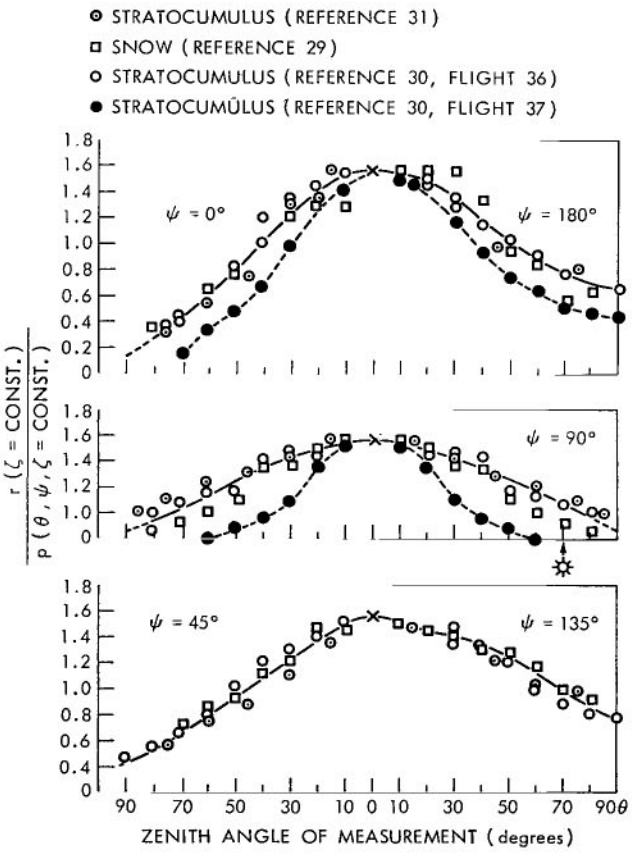

Figure C5—The ratio between the directional reflectance (r) and the bidirectional reflectance ($\rho' = \rho/\pi$) at values of azimuthal angle (ψ: 0°, 180°, 45°, 135°, 90°) as obtained from measurements at solar zenith angles ($65° \leq \zeta \leq 75°$).

The deviations of all single values from the mean smoothed curves in Figures C3—C5 is rather large, showing that the reflection properties of single cloud decks and snow covers deviate from each other. But the smooth curves indicate, at least, a general trend, which is used here to account for the angular dependence of Nimbus II measurements of reflected solar radiation.

The diagrams shown in Figures 3, C6, and C7 were obtained from the mean curves in Figures C3 through C5 by graphical interpolation. The angular dependence of the reflectance observed for $10° \leq \zeta \leq 20°$ was adopted for all Nimbus II measurements for $0° \leq \zeta \leq 35°$; that observed for $50° \leq \zeta \leq 60°$, for $35° < \zeta \leq 60°$; and that observed at $65° \leq \zeta \leq 75°$, for $60° < \zeta \leq 80°$. The sparsity of observations then available made it impossible to determine more detailed models.

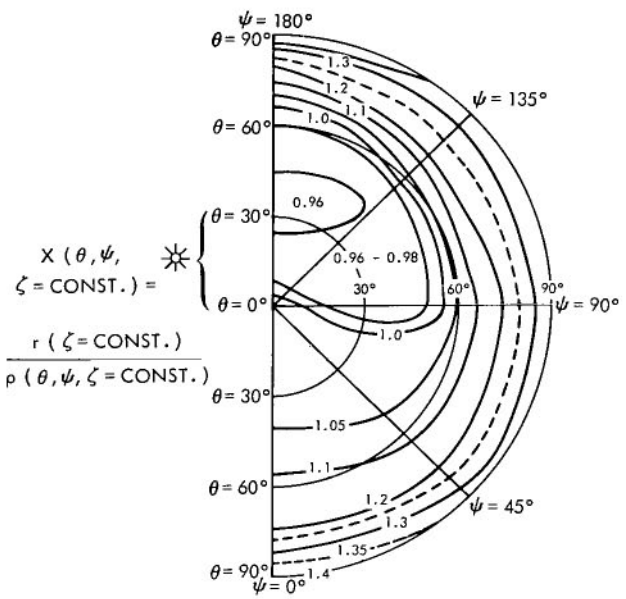

Figure C6—Dependence of the ratio $X = r/\rho$ on the angles θ and ψ of the measurement at very high sun ($0° \leq \zeta \leq 35°$).

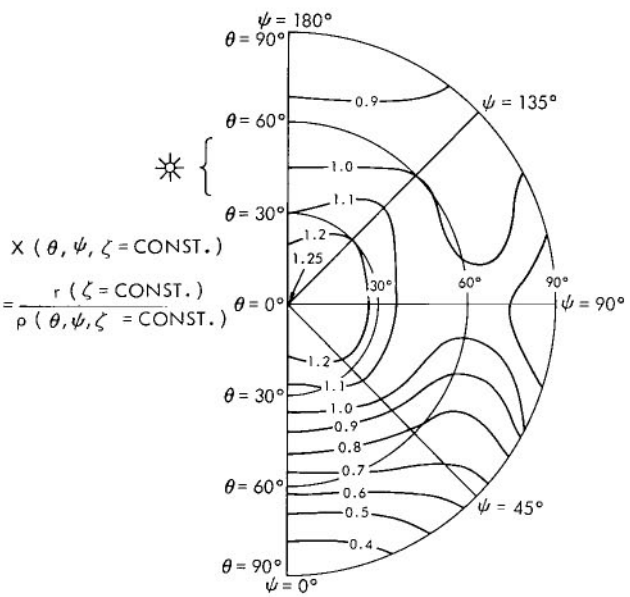

Figure C7—Dependence of the ratio $X = r/\rho$ on the angles θ and ψ of the measurement at solar zenith angles ($35° < \zeta \leq 60°$).

Appendix D

Summary of Computer Program

Figure D1 is a system flow chart that summarizes all phases in the computational procedure.

Phase 1 computes all required radiation fluxes for all orbits of one day or parts of a day. The NMRT—MRIR tape (see Reference 23) contains the measurements. Control parameters are required to read the tapes as well as those parameters required in several equations. The results of each orbit for one day or parts of a day will be stored in matrices (which correspond to standardized matrices) for geographic mapping of the satellite data.

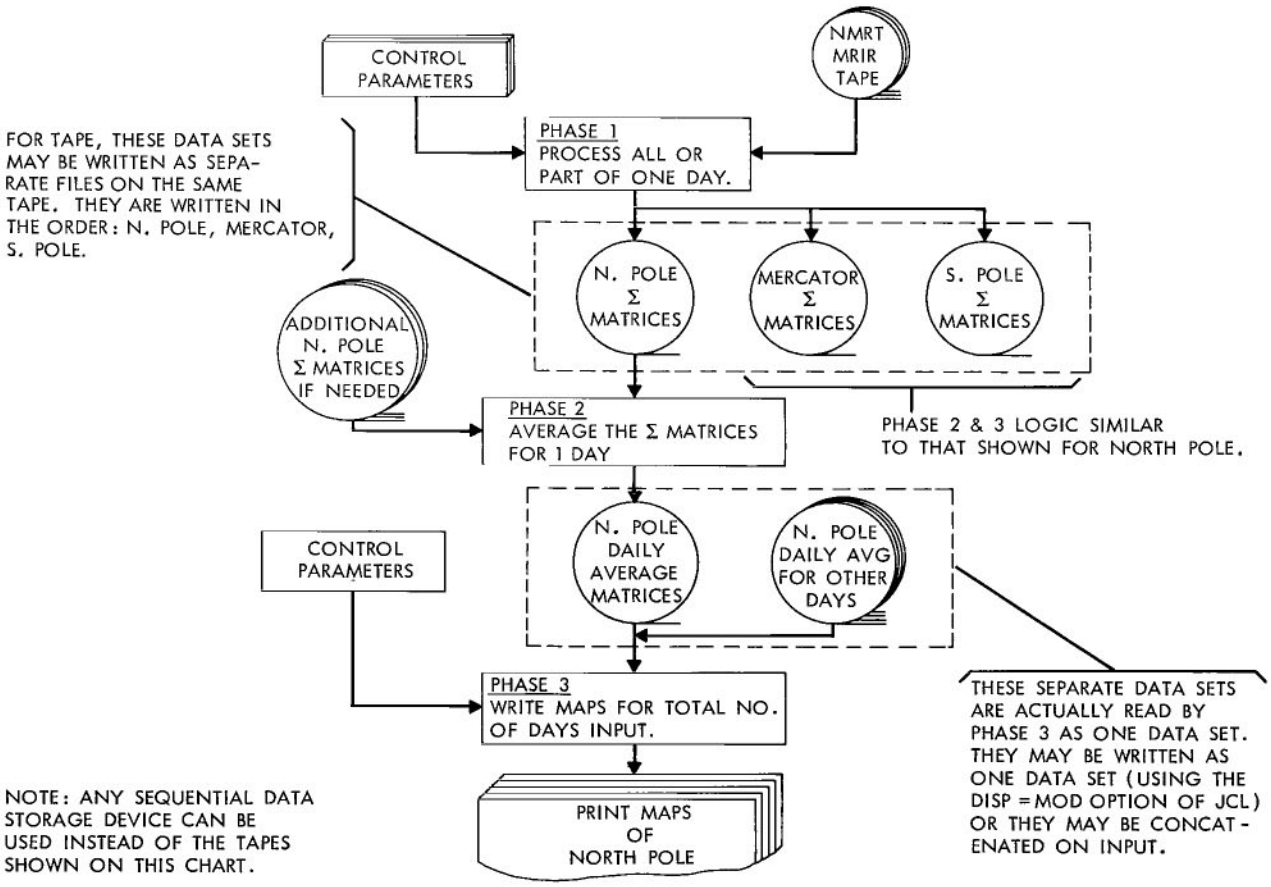

Figure D1—System flow chart of the computer program.

Phase 2 summarizes all matrices and gives averages within each gridfield for each day (24-hour interval, counted from 00.00 to 24.00 GMT) separately.

Phase 3 computes averages for a number of days, as given by the control parameters. Zonal averages will be determined only for the Mercator matrices between 75°N and 75°S. Separate programs were set up to compute standard deviations, relative dispersions, and differences between day and night values of the outgoing long-wave radiation for each gridfield. Furthermore, zonal averages can be determined for several zones on the globe. Maximum and minimum values of the albedo and the outgoing long-wave radiation (day and night separately) are determined for several climatological studies.

Appendix E

Maps of Results

The geographic distributions of the albedo of the outgoing long-wave radiation and of the radiation balance or net radiation flux are shown here, separately, in maps for all five semimonthly periods. (See Figures E1 through E40.)

In the polar sterographic projections, the spatial resolution for each gridfield ranges from about 280 km × 280 km at the pole to about 260 km × 280 km at 60° latitude. In the Mercator projections, a gridfield at the equator covers an area of 5° × 5° of longitude and latitude (500 km × 500 km) and at 60° latitude an area of 5° × 2.5° of longitude and latitude (280 km × 280 km). Isolines were drawn by hand almost everywhere at equidistant intervals. Intermediate isolines were added over special areas (e.g., Sahara, subtropical oceans, and both polar caps) to demonstrate a specific pattern. Dashed isolines were obtained by interpolation and extrapolation over areas where measurements were made on only one or two days (or not at all) during a semimonthly period. Larger gaps in the data coverage are marked with stippled fracture. Such gaps were found for daytime measurements between about 110°E and 170°E of longitude and for night measurements between about 30°W and 10°E. An orientation error was found in the Mercator projections after the maps were drawn; all data were misplaced by 2.5 degrees of longitude eastward.

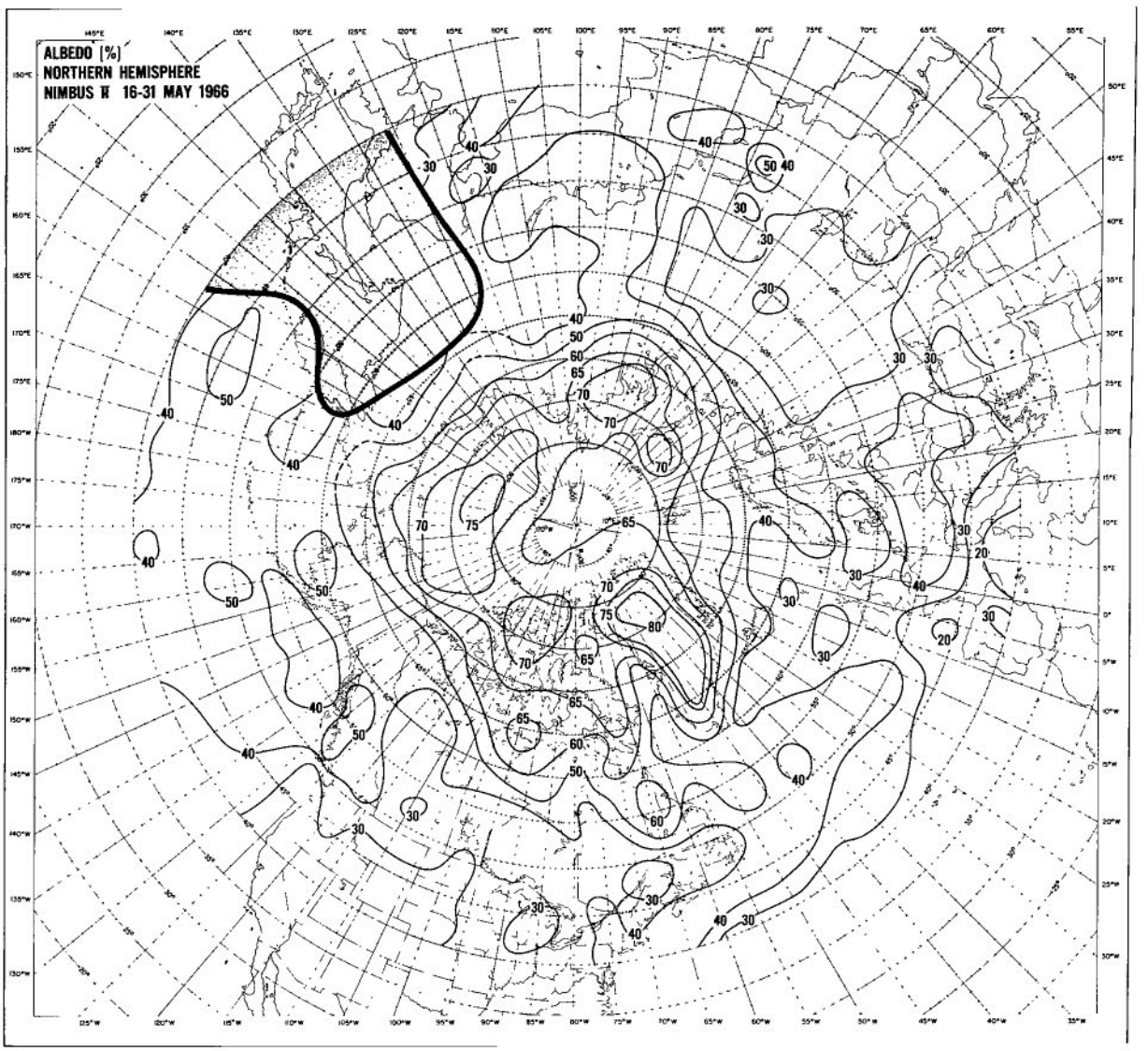

Figure E1—Albedo of the earth-atmosphere system over the northern hemisphere during the period 16—31 May 1966.

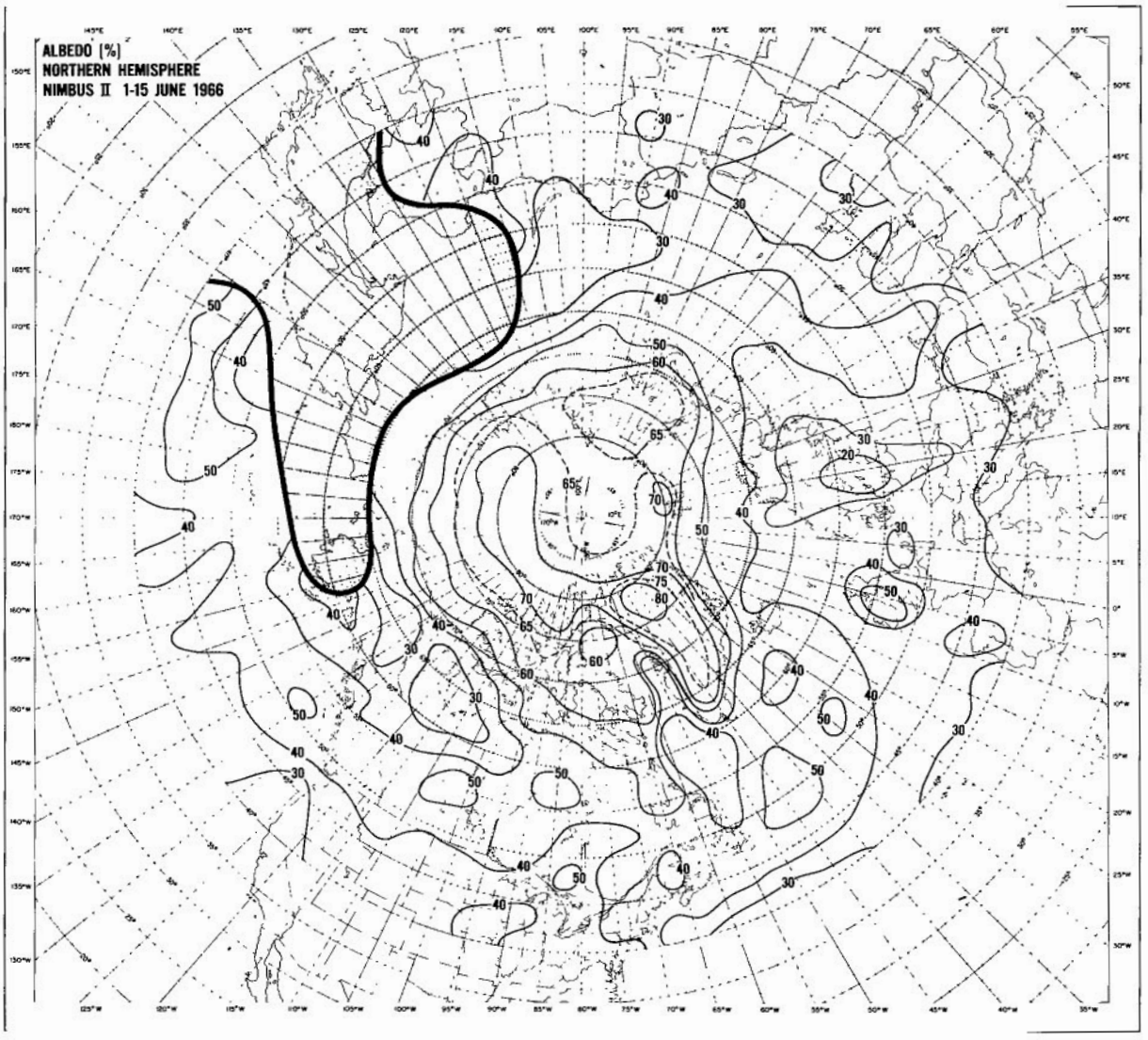

Figure E2—Albedo of the earth-atmosphere system over the northern hemisphere during the period 1—15 June 1966.

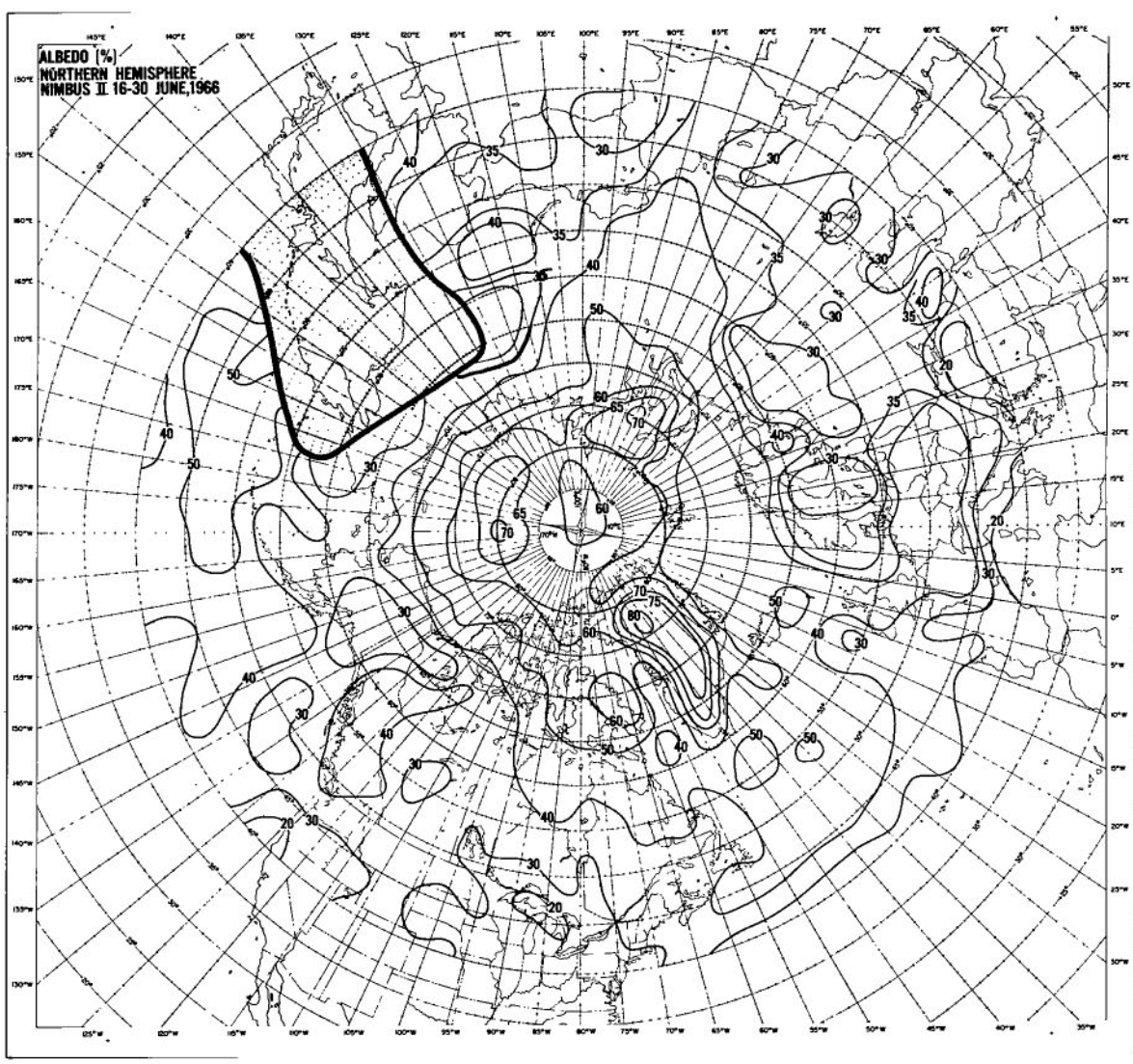

Figure E3—Albedo of the earth-atmosphere system over the northern hemisphere during the period 16—30 June 1966.

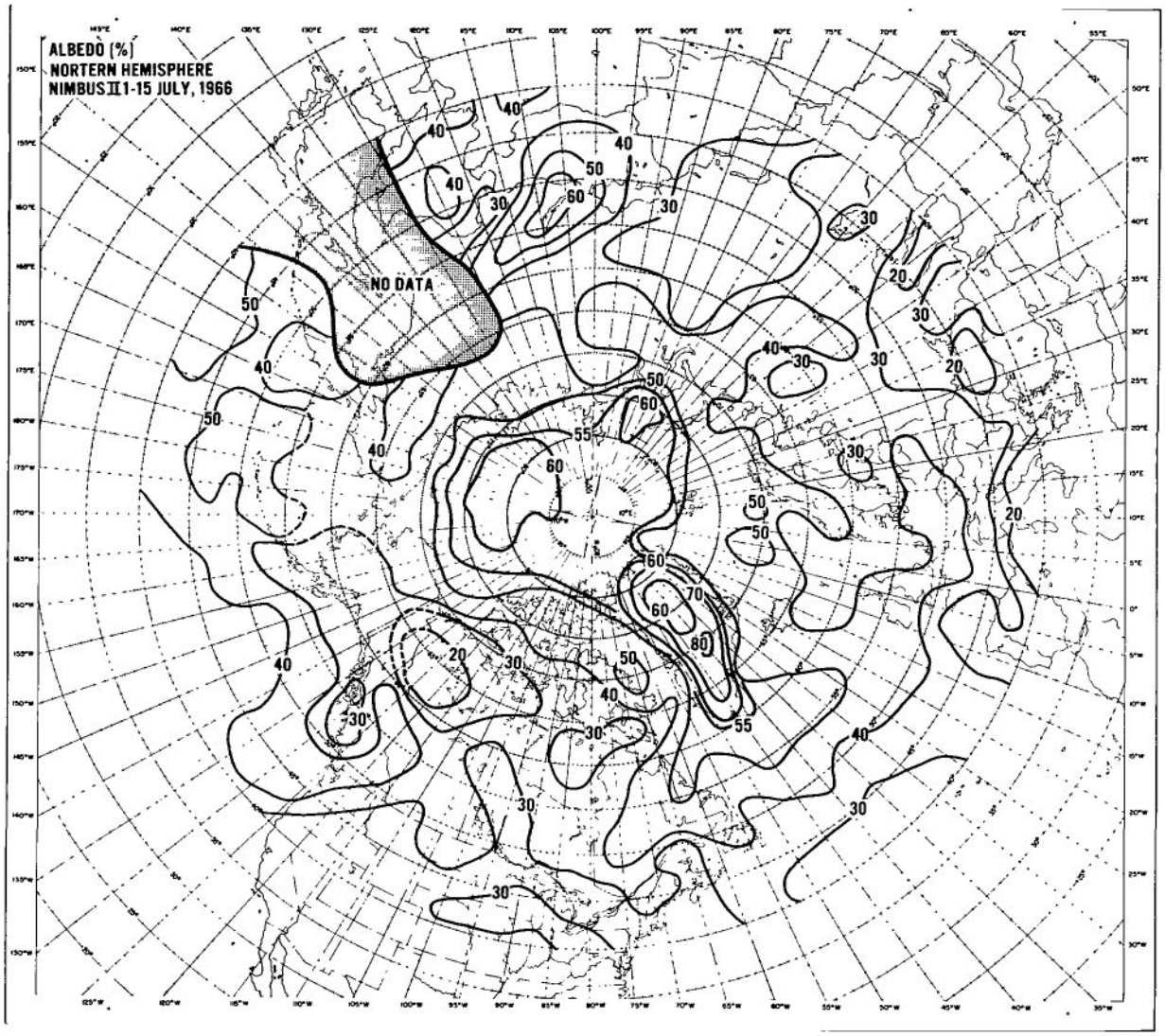

Figure E4—Albedo of the earth-atmosphere system over the northern hemisphere during the period 1–15 July 1966.

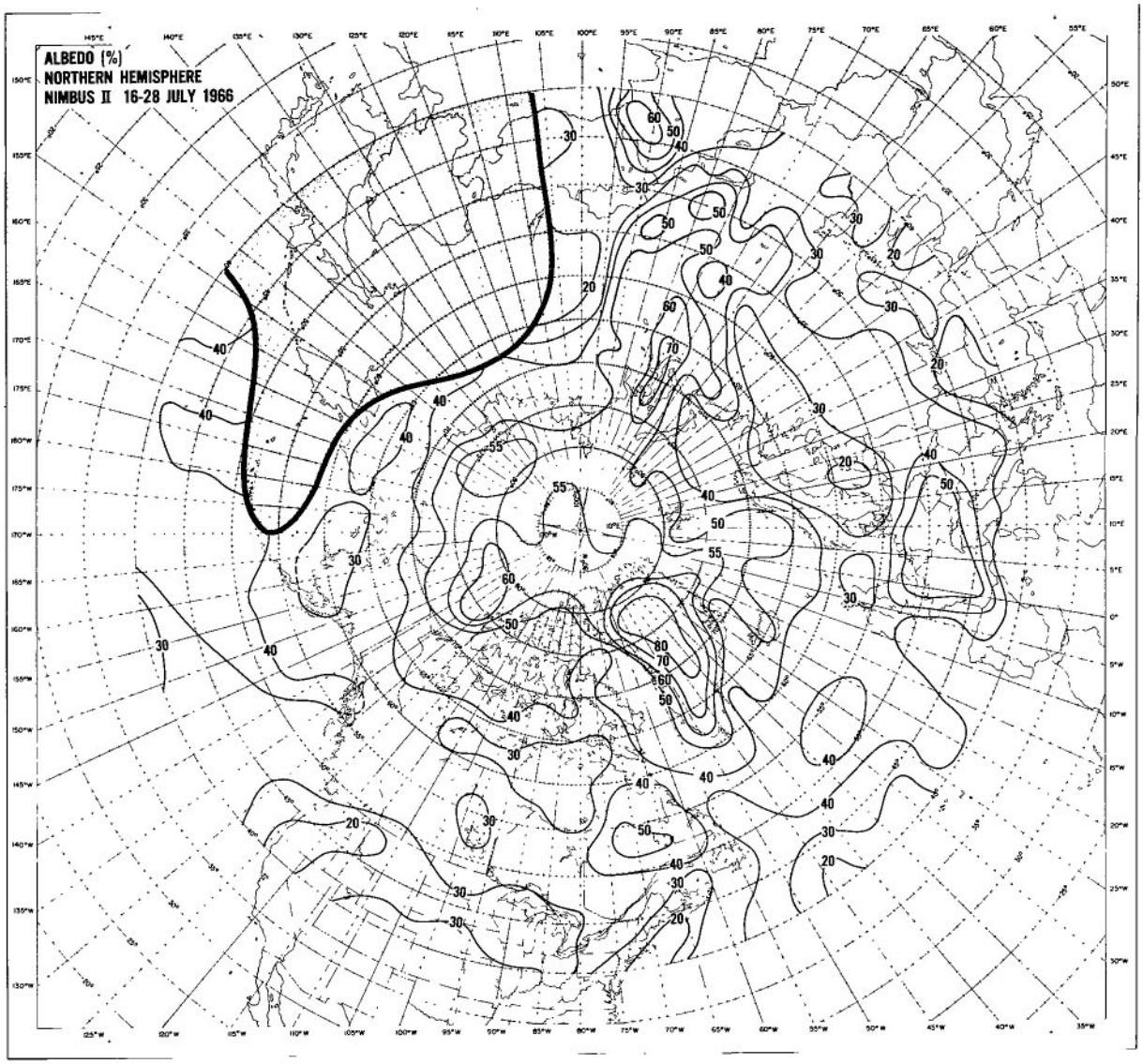

Figure E5—Albedo of the earth-atmosphere system over the northern hemisphere during the period 16—28 July 1966.

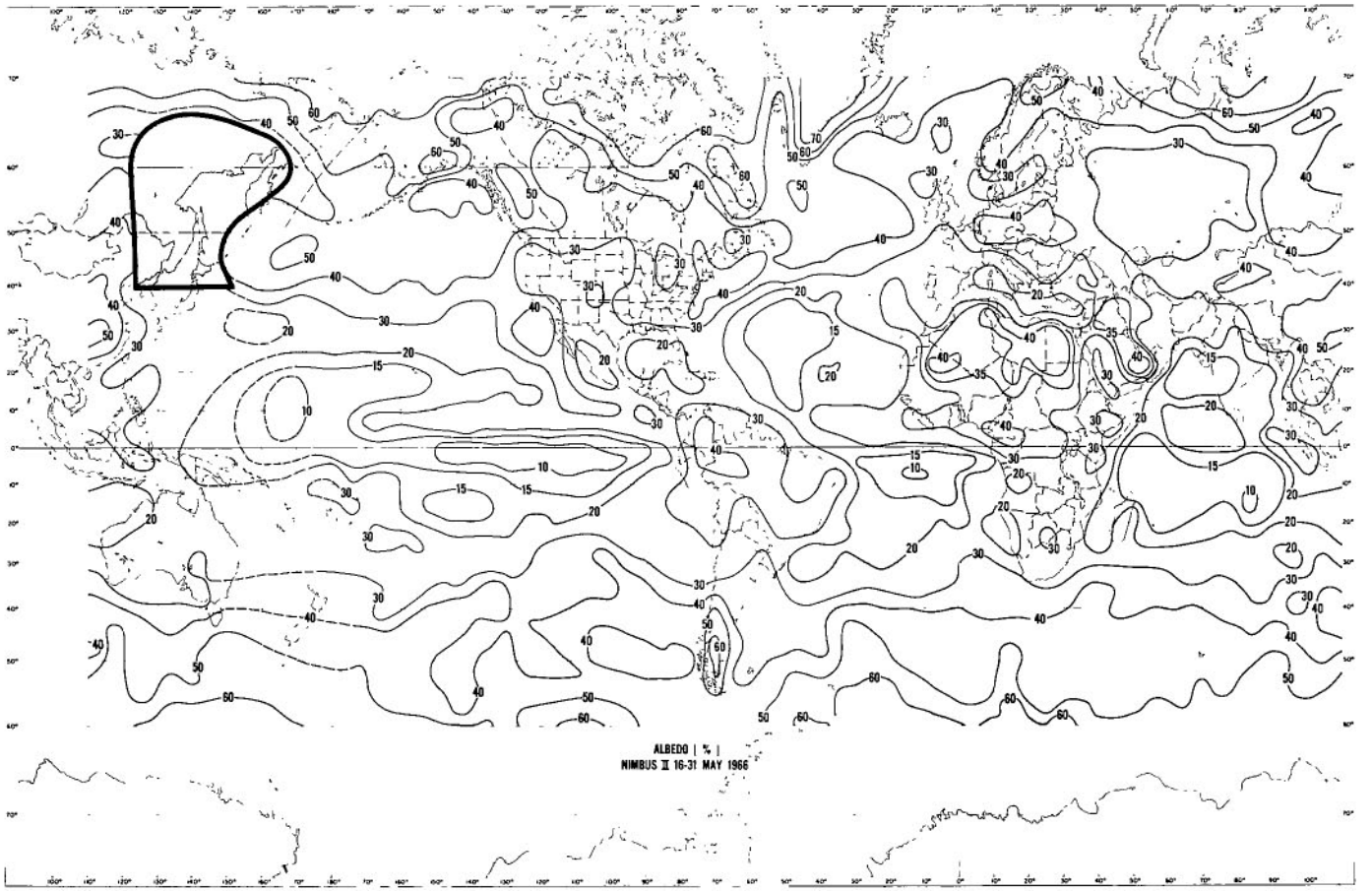

Figure E6—Albedo of the earth-atmosphere system between 70°N and 60°S during the period 16—31 May 1966.

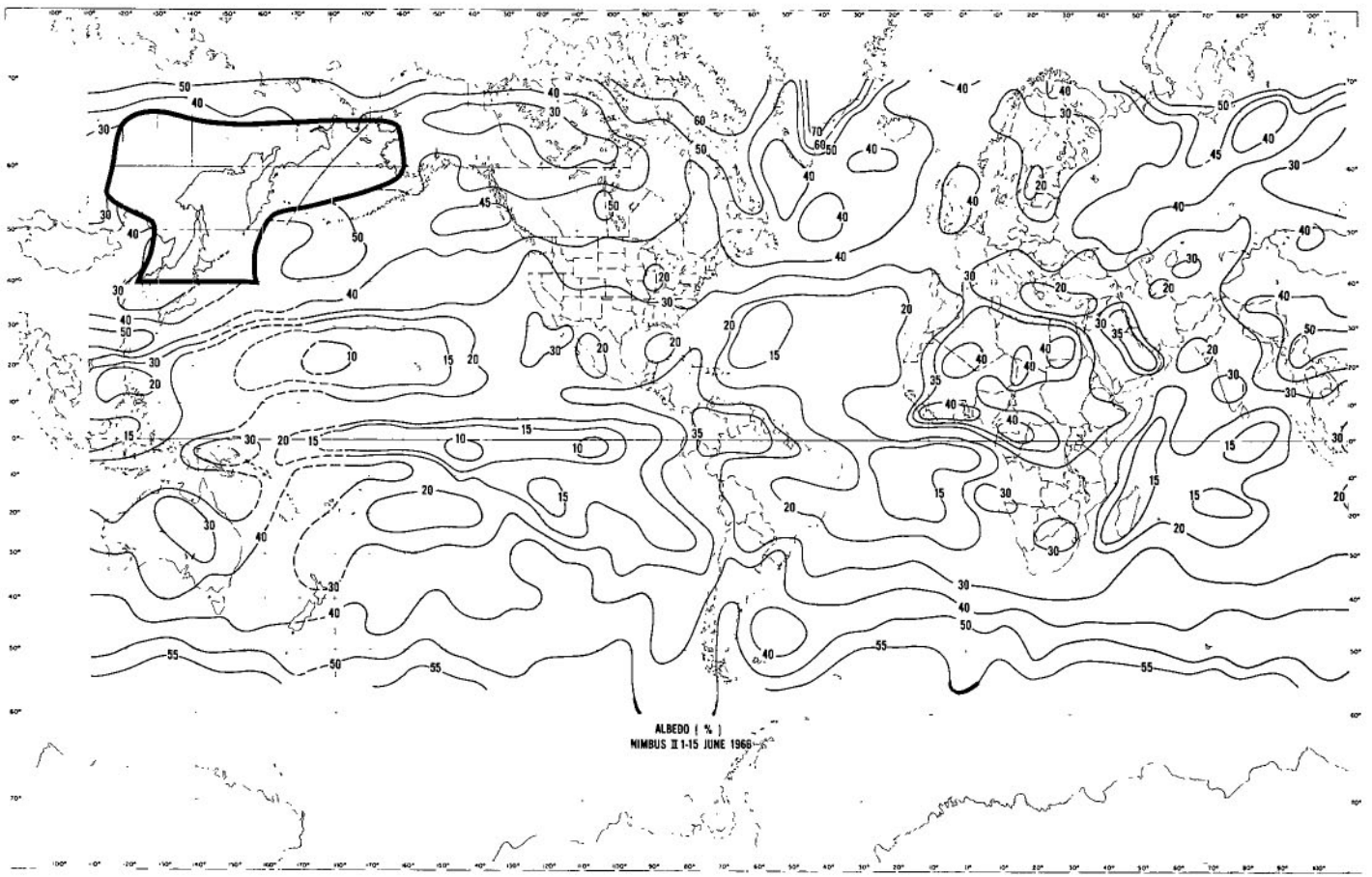

Figure E7—Albedo of the earth-atmosphere system between 70°N and 60°S during the period 1—15 June 1966.

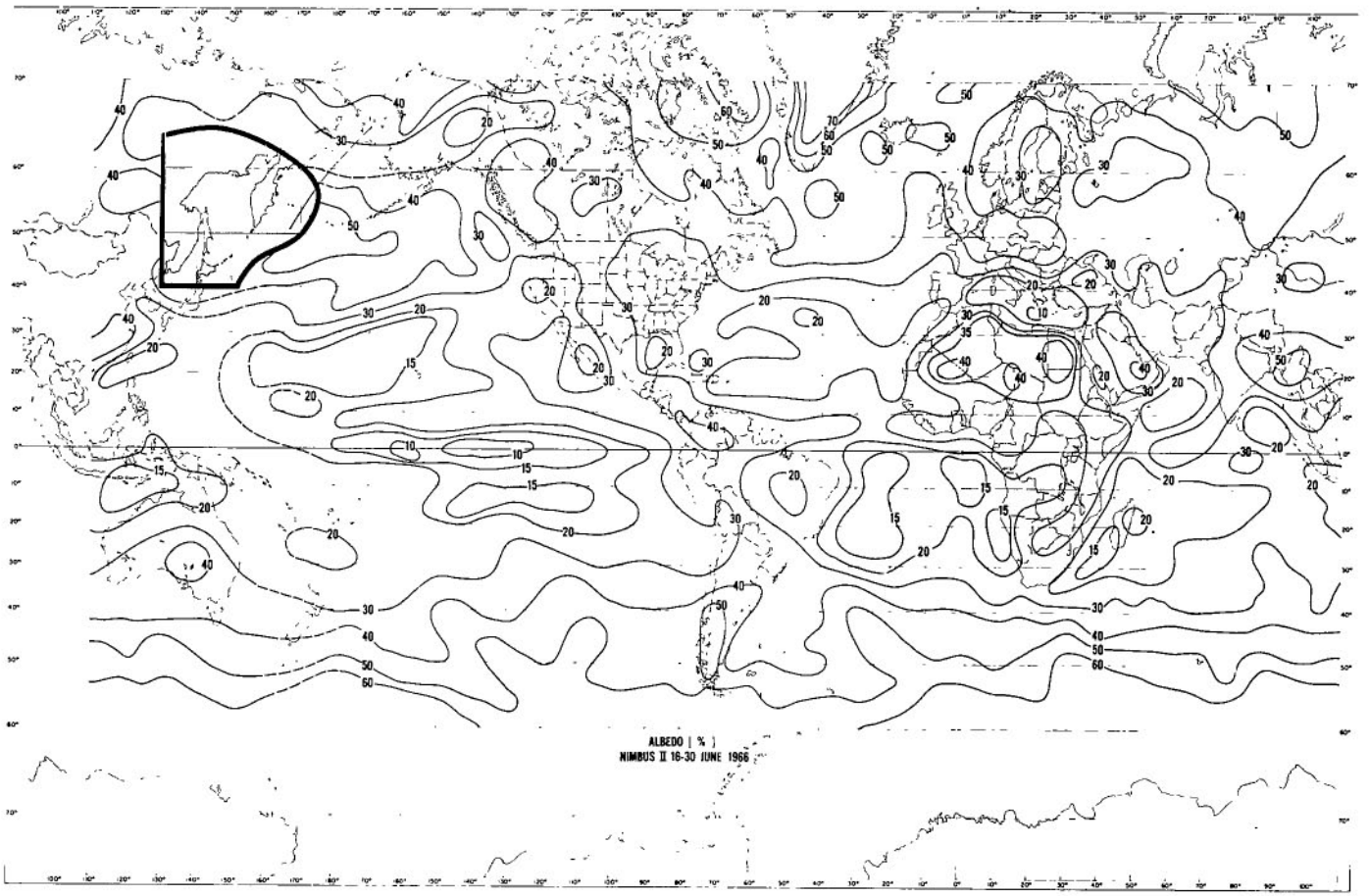

Figure E8—Albedo of the earth-atmosphere system between 70°N and 60°S during the period 16—30 June 1966.

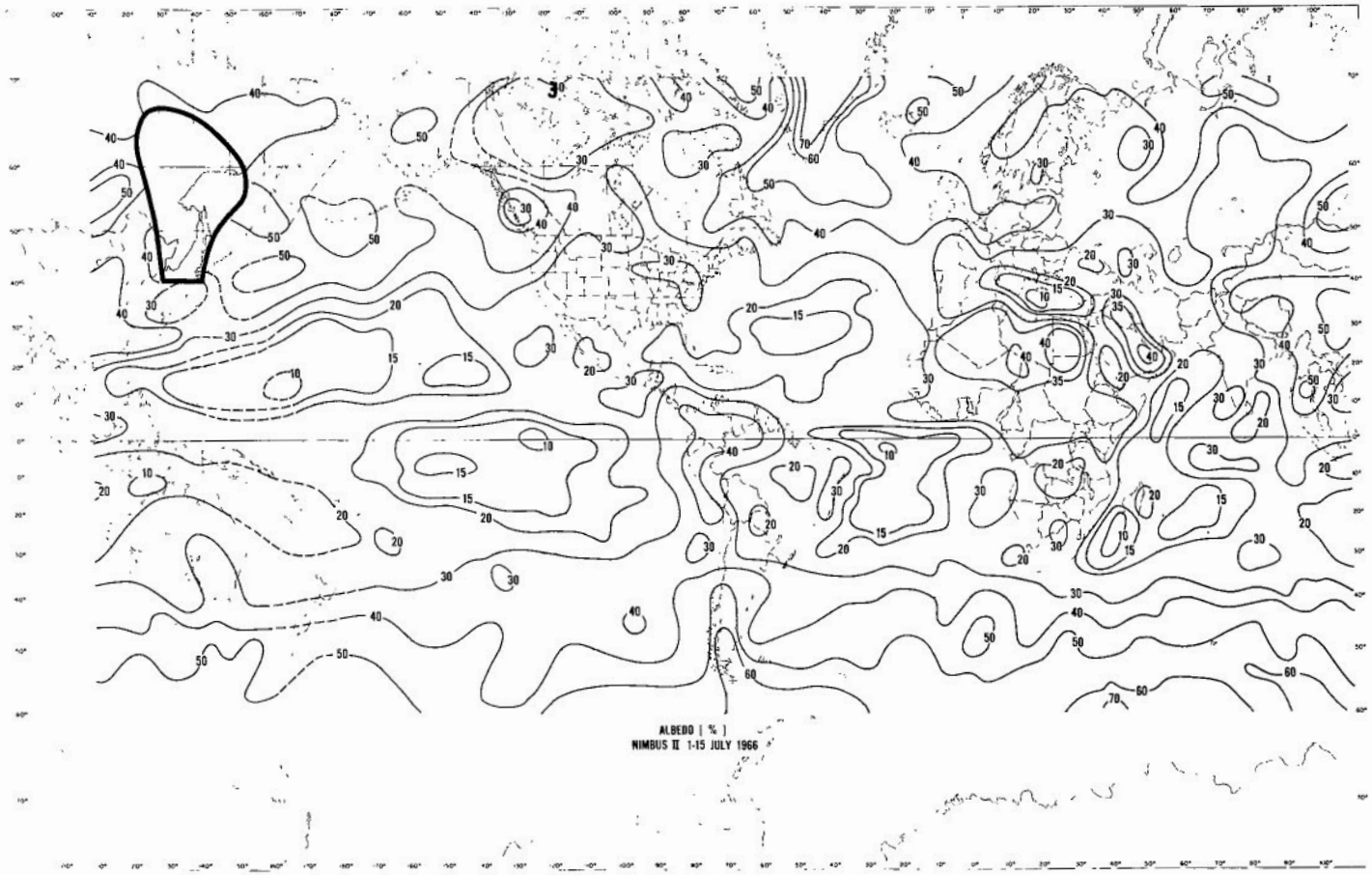

Figure E9—Albedo of the earth-atmosphere system between 70°N and 60°S during the period 1—15 July 1966.

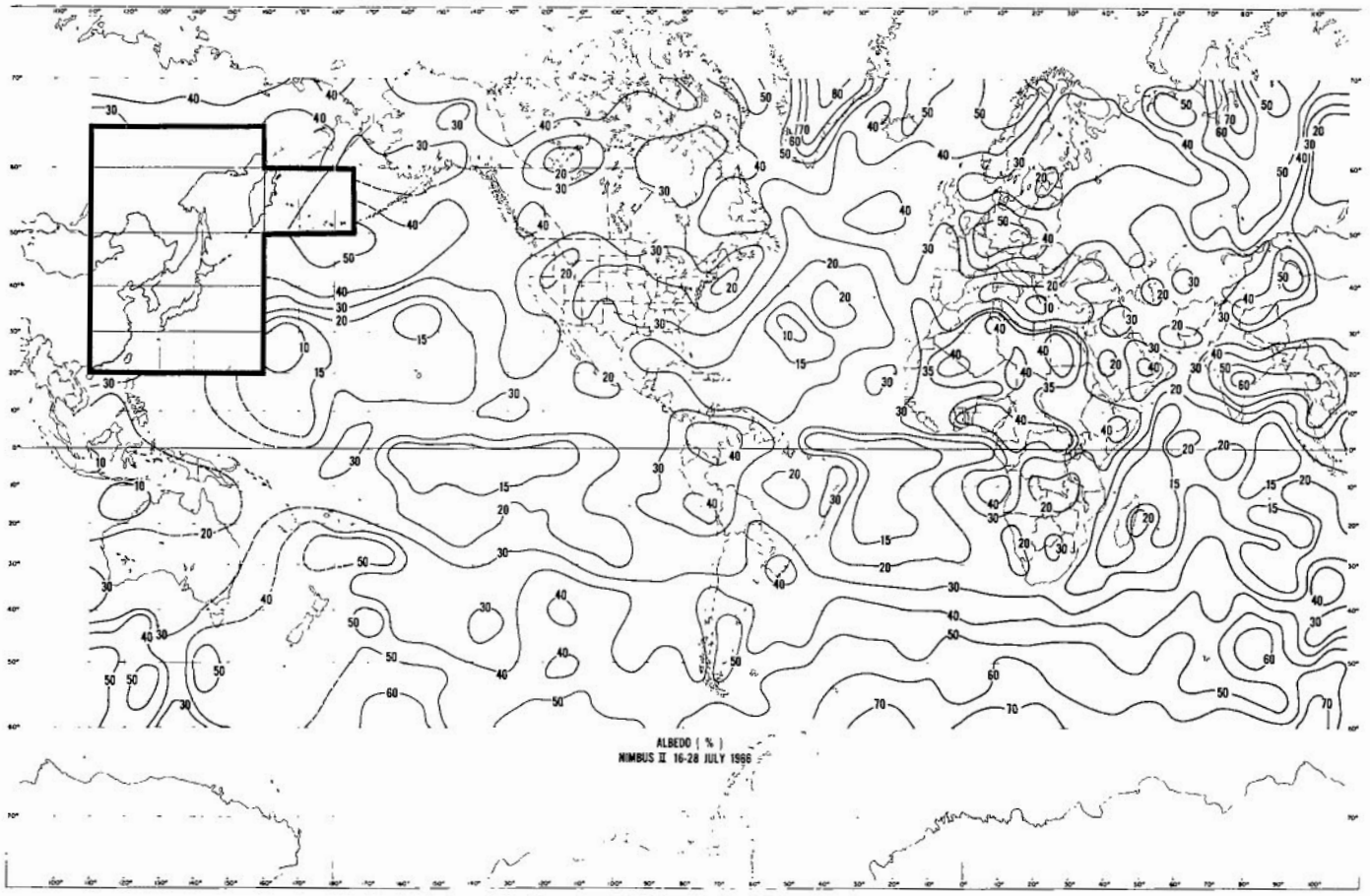

Figure E10—Albedo of the earth-atmosphere system between 70°N and 60°S during the period 16—28 July 1966.

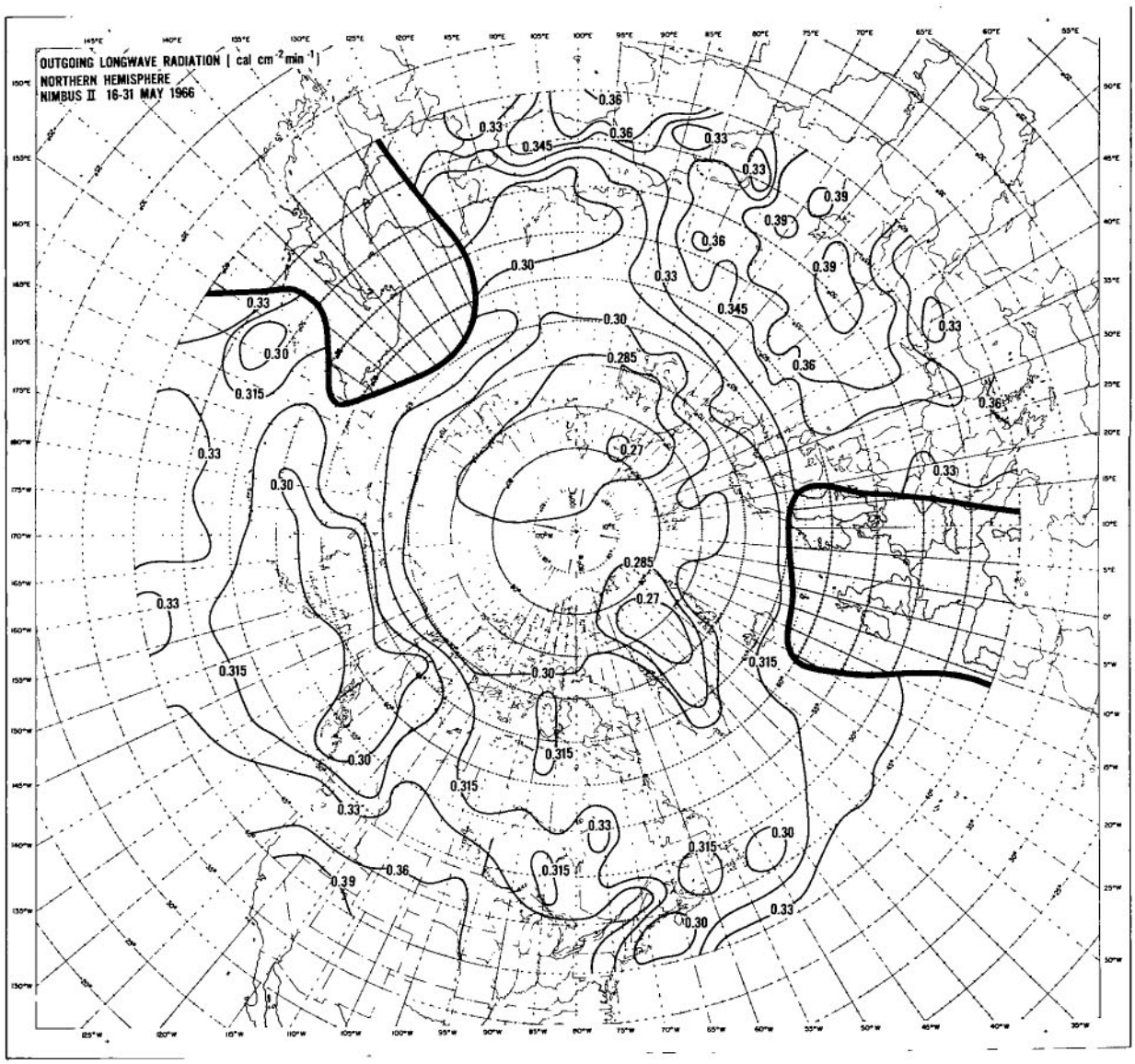

Figure E11—Outgoing long-wave radiation flux at the top of the atmosphere over the northern hemisphere during the period 16—31 May 1966.

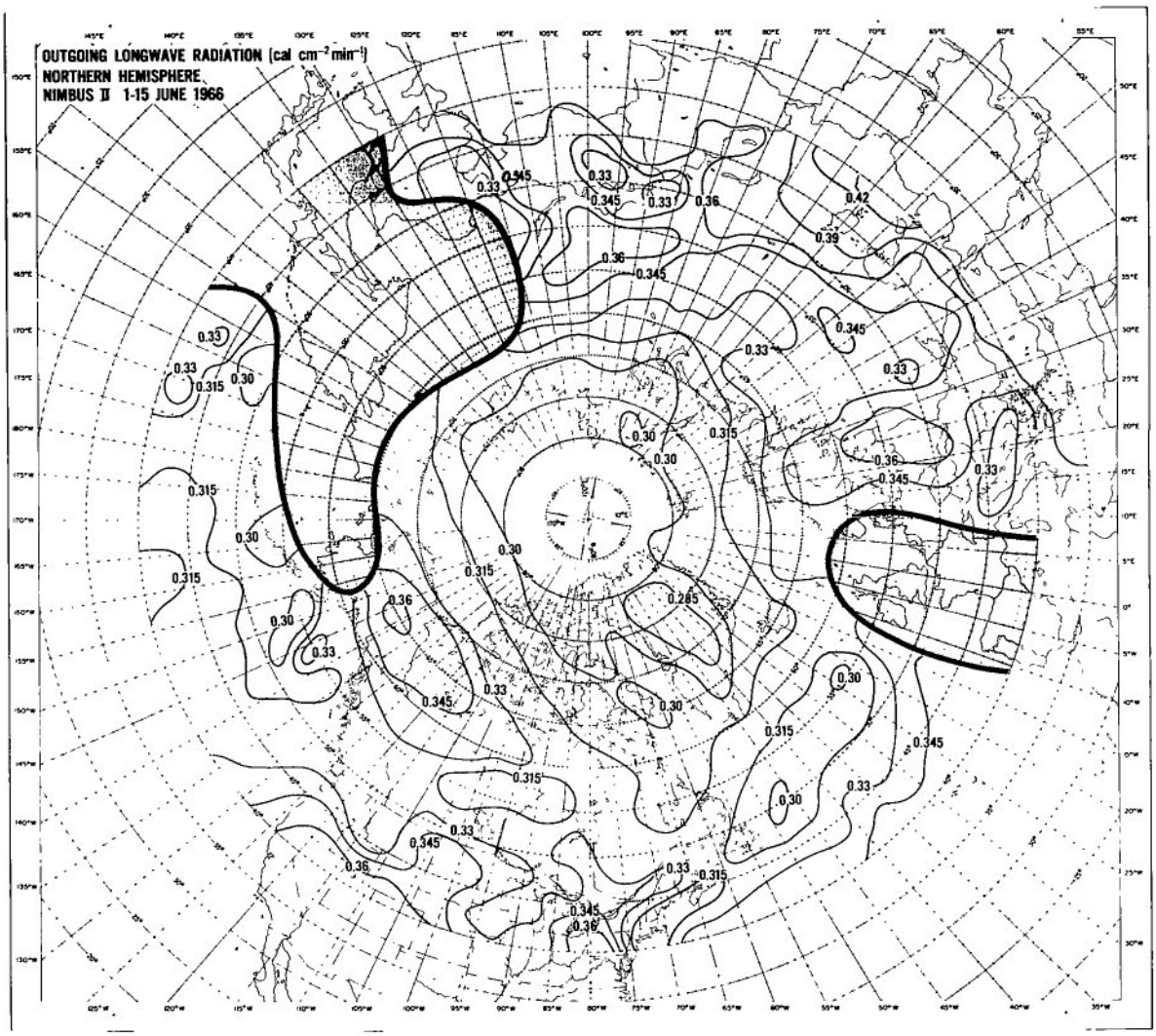

Figure 12—Outgoing long-wave radiation flux at the top of the atmosphere over the northern hemisphere during the period 1—15 June 1966.

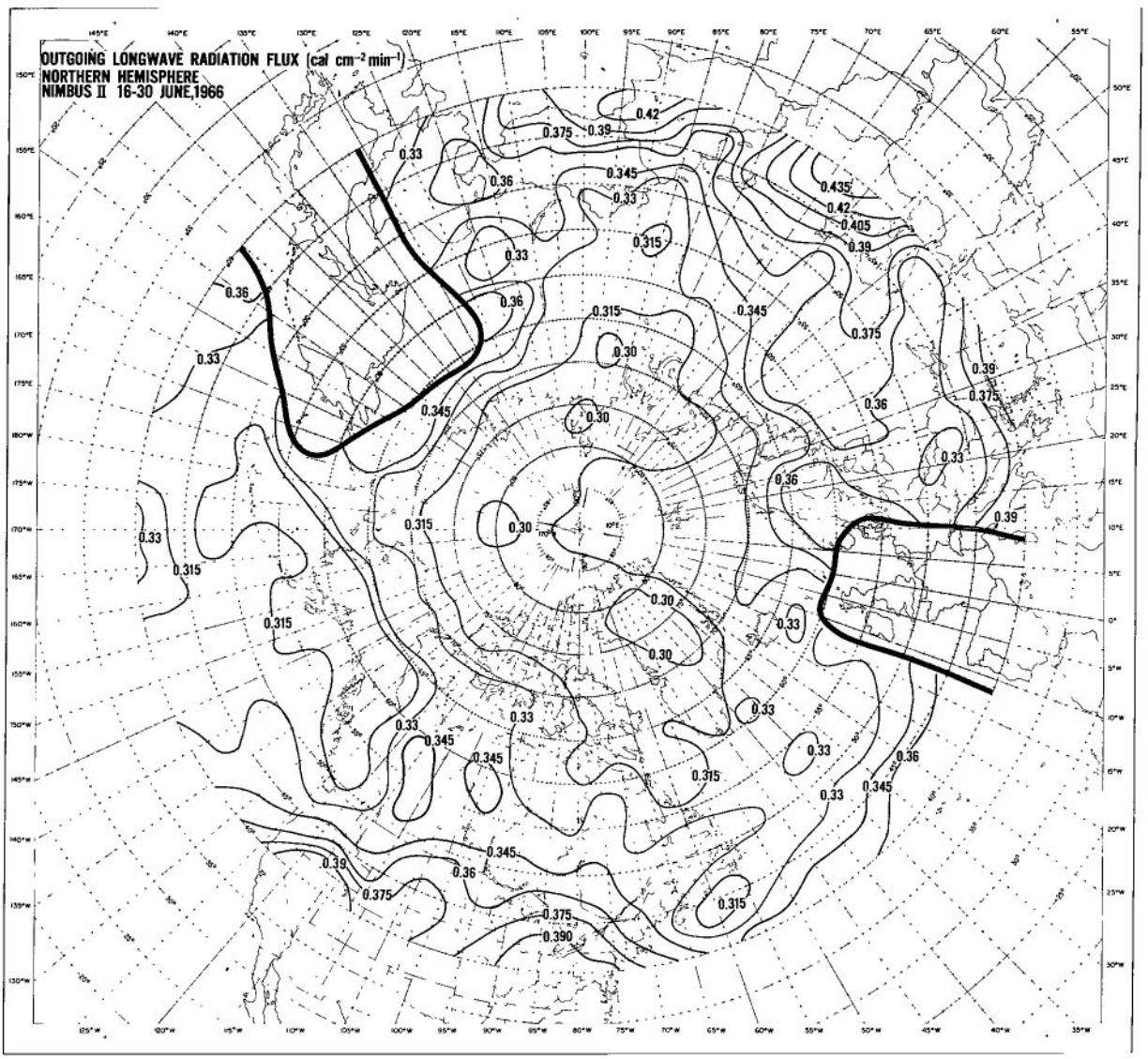

Figure E13—Outgoing long-wave radiation flux at the top of the atmosphere over the northern hemisphere during the period 16—30 June 1966.

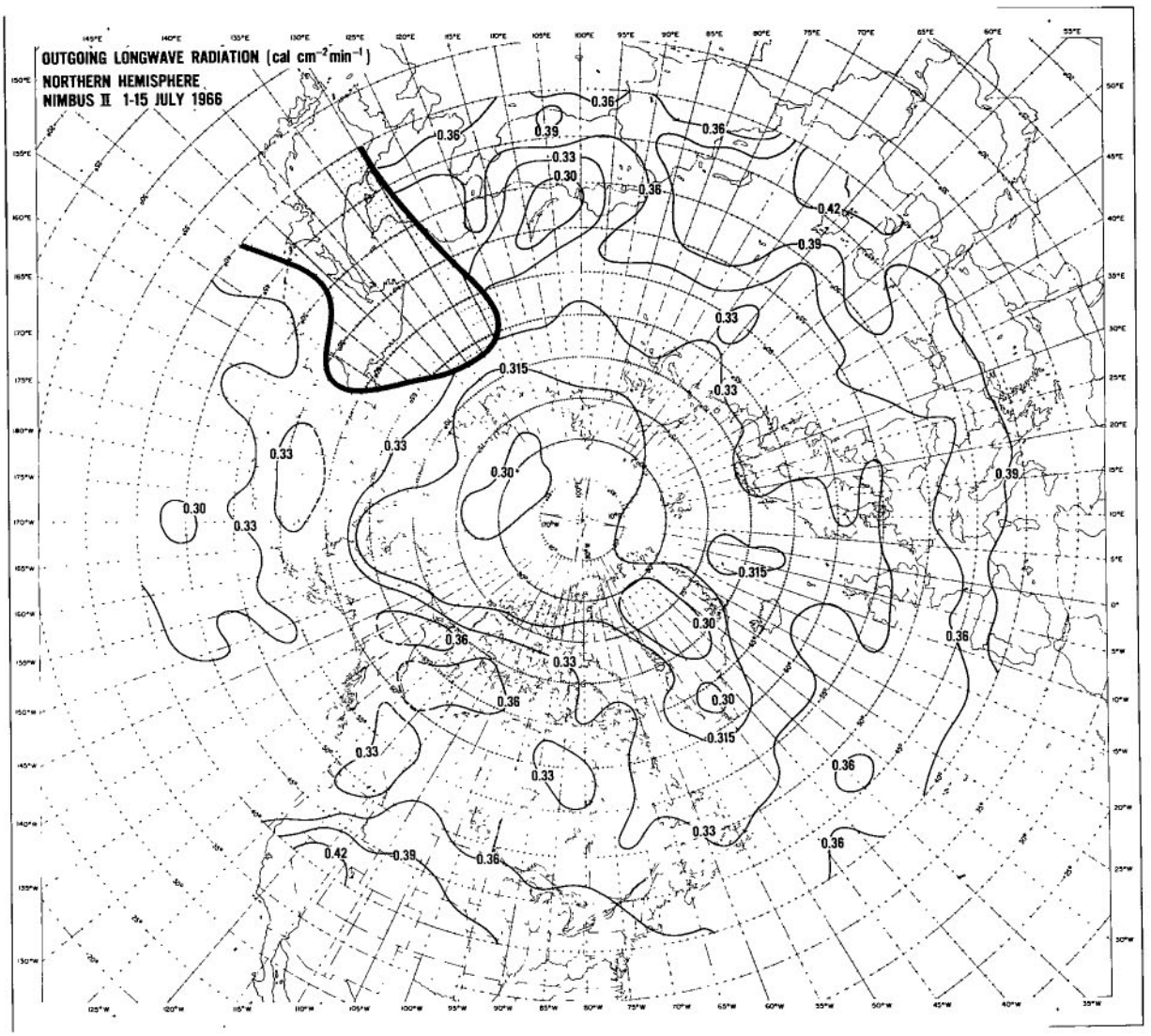

Figure E14—Outgoing long-wave radiation flux at the top of the atmosphere over the northern hemisphere during the period 1—15 July 1966.

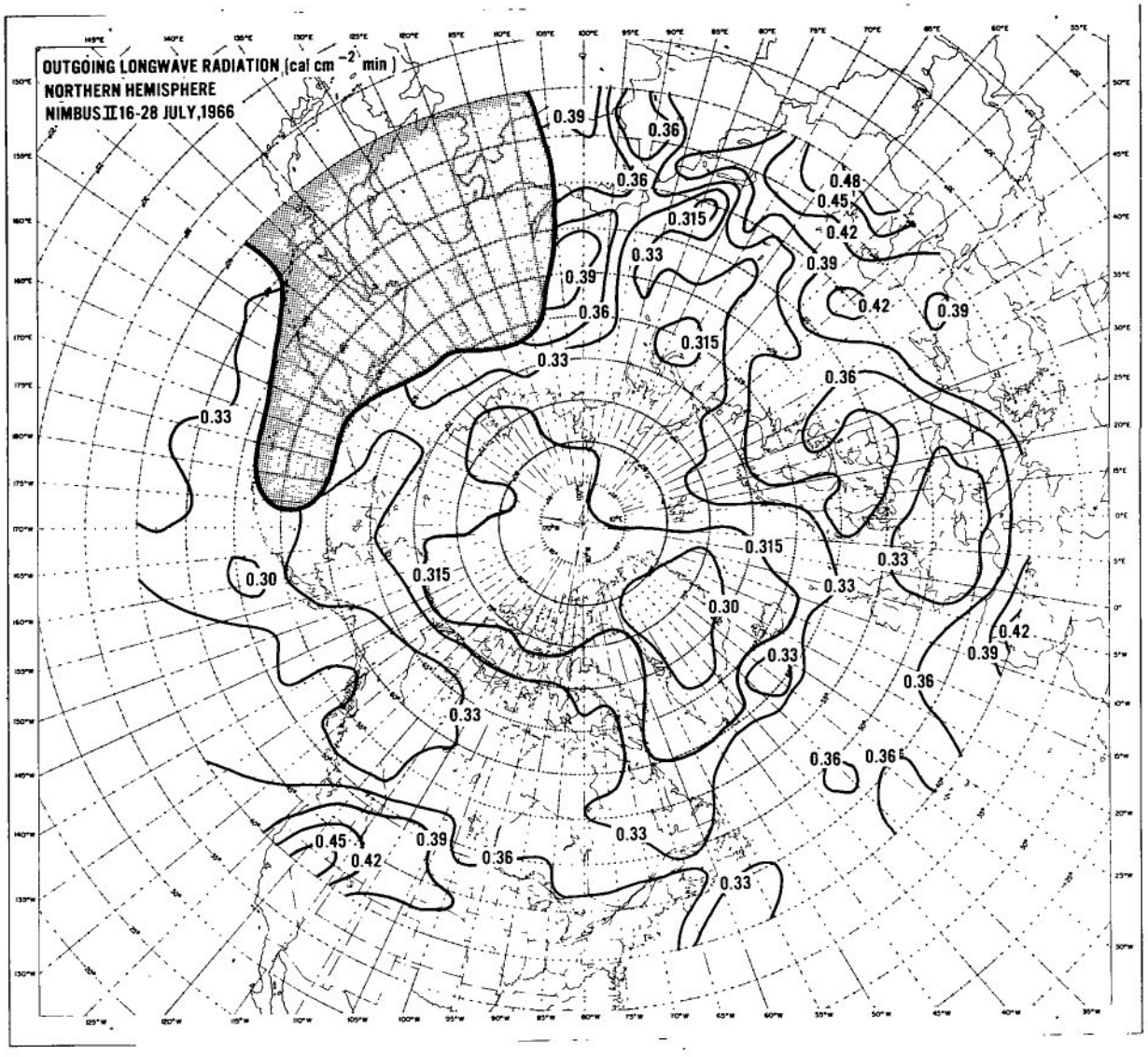

Figure 15—Outgoing long-wave radiation flux at the top of the atmosphere over the northern hemisphere during the period 16–28 July 1966.

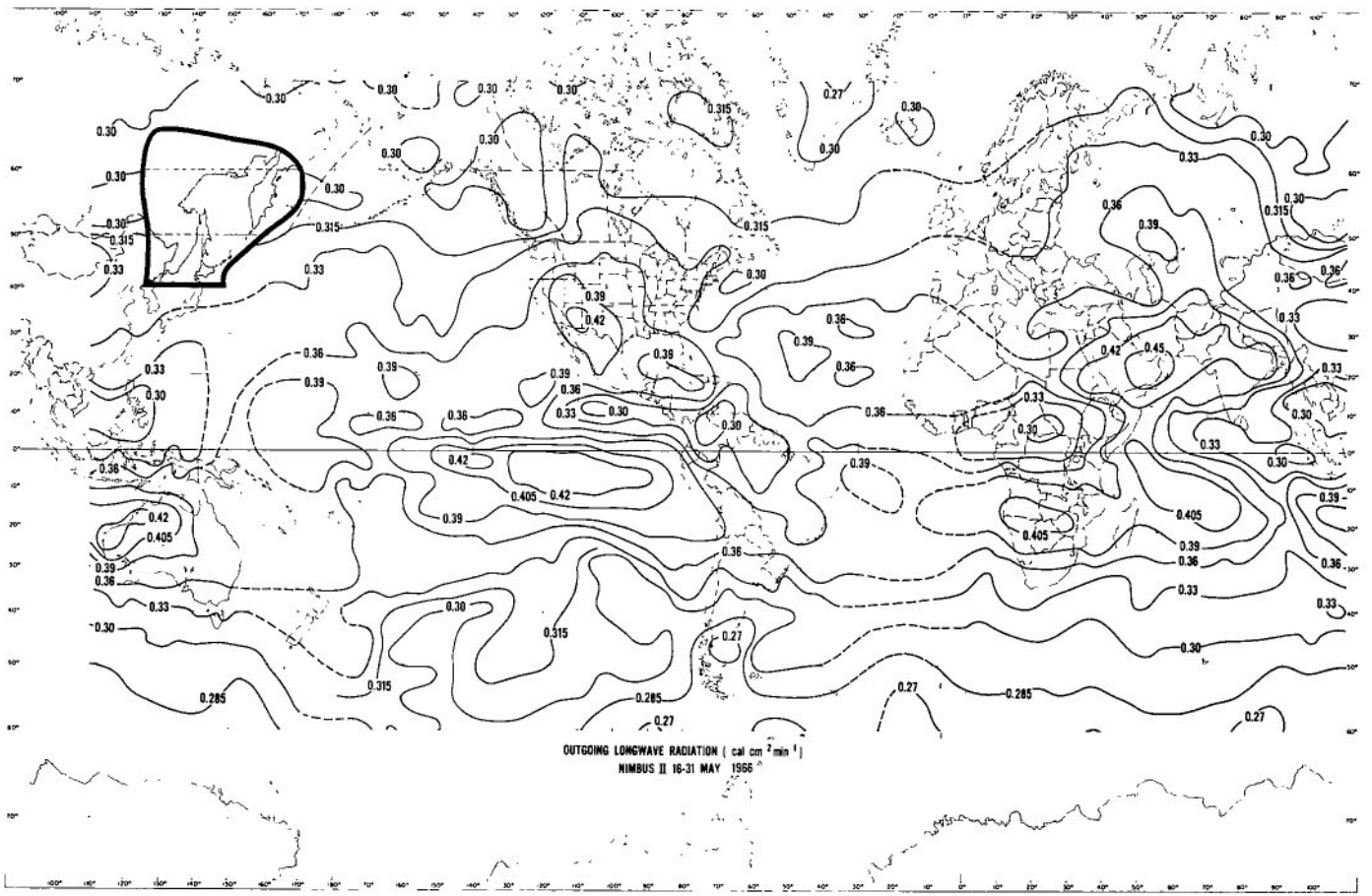

Figure E16—Outgoing long-wave radiation flux at the top of the atmosphere between 70°N and 60°S during the period 16—31 May 1966.

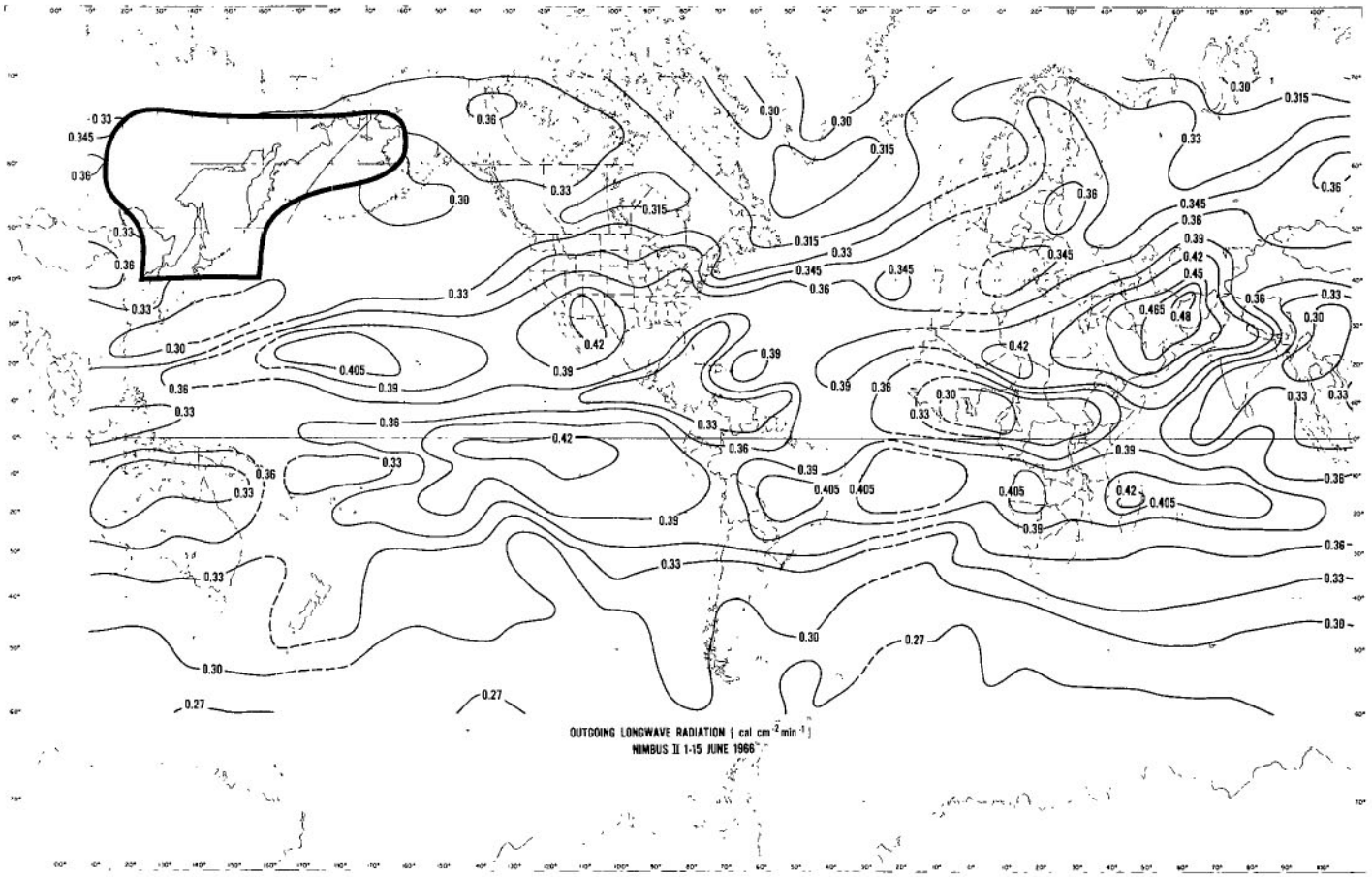

Figure E17—Outgoing long-wave radiation flux at the top of the atmosphere between 70°N and 60°S during the period 1—15 June 1966.

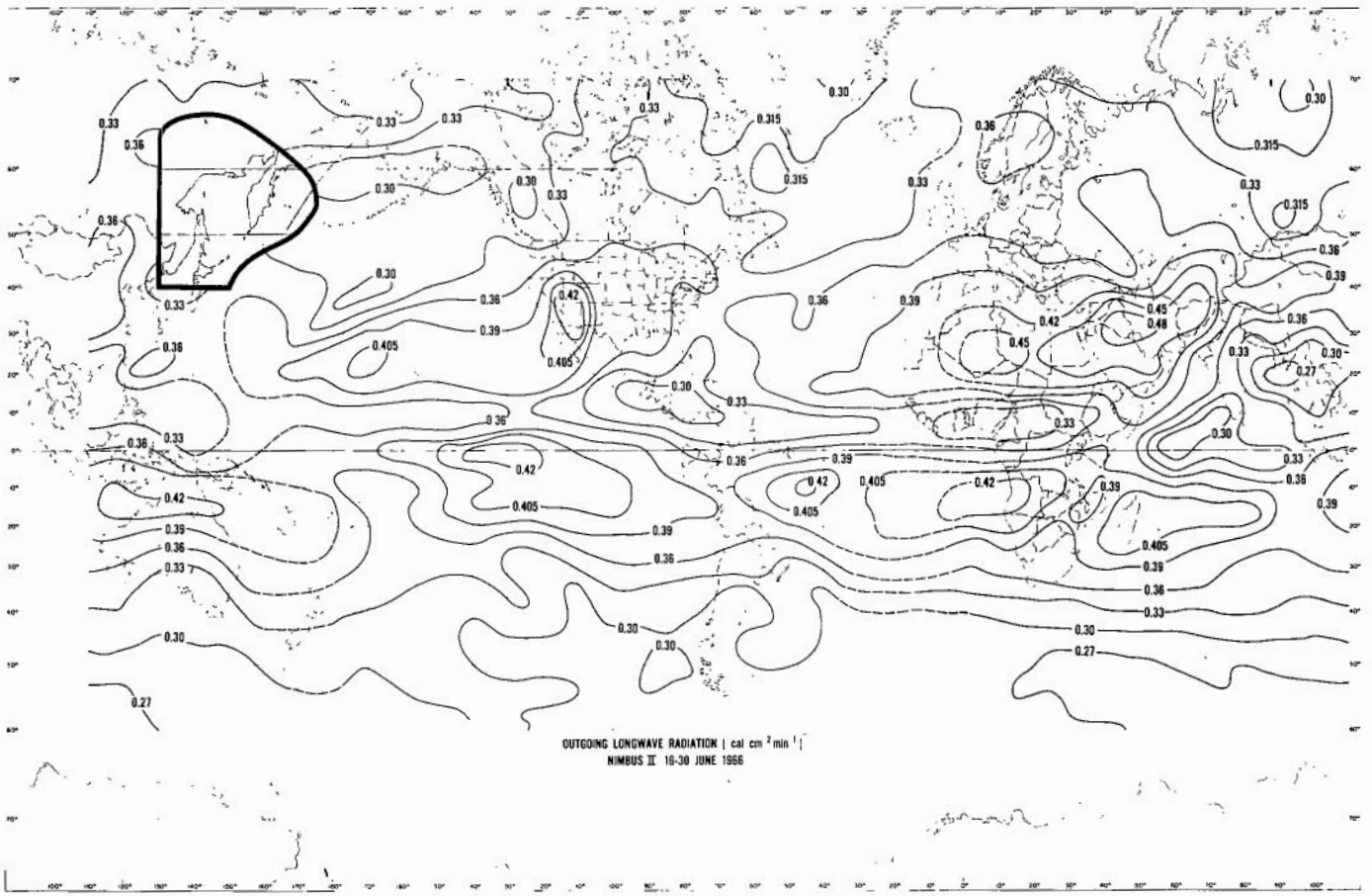

Figure E18—Outgoing long-wave radiation flux at the top of the atmosphere between 70°N and 60°S during the period 16—30 June 1966.

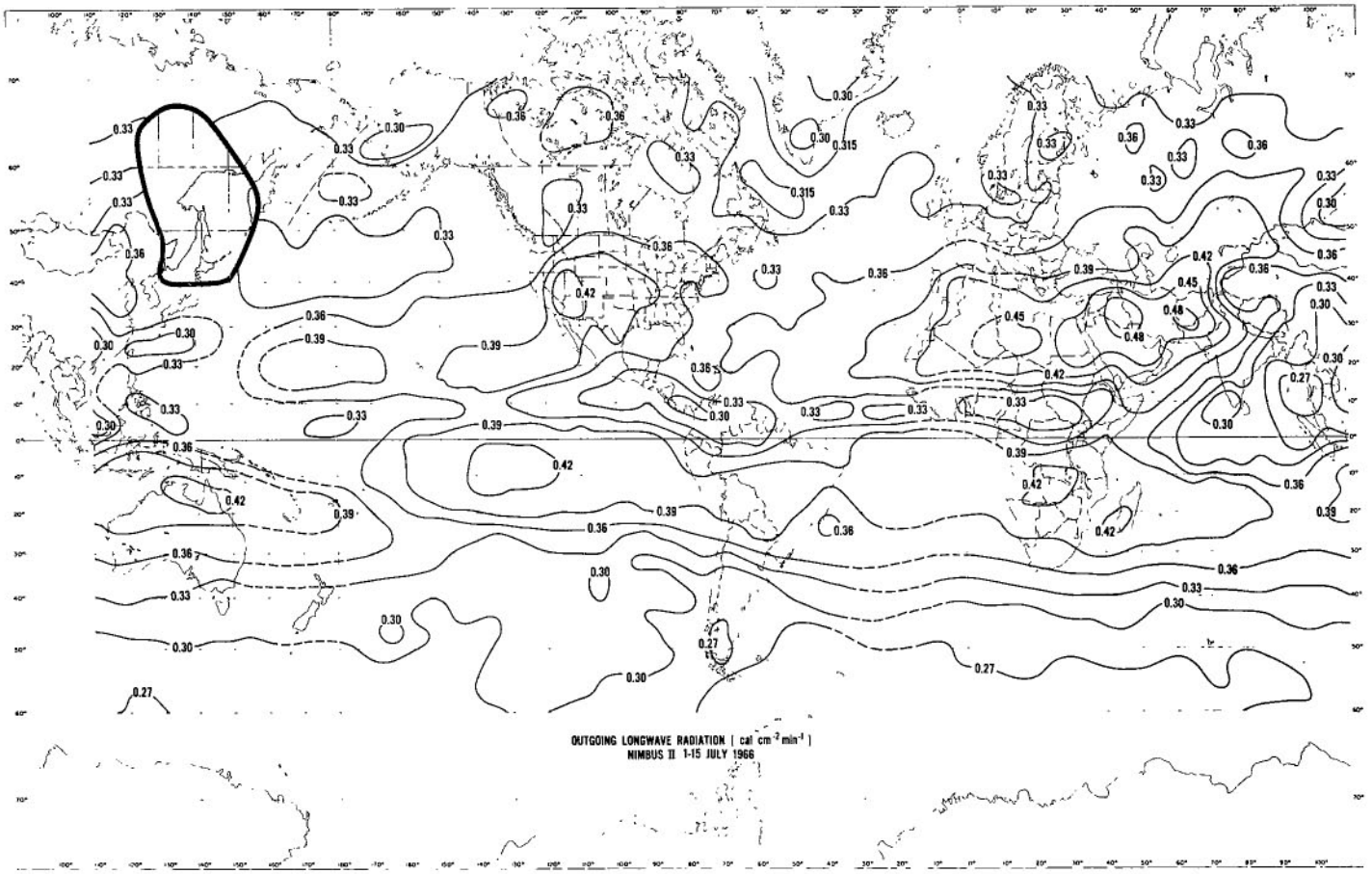

Figure E19—Outgoing long-wave radiation flux at the top of the atmosphere between 70°N and 60°S during the period 1—15 July 1966.

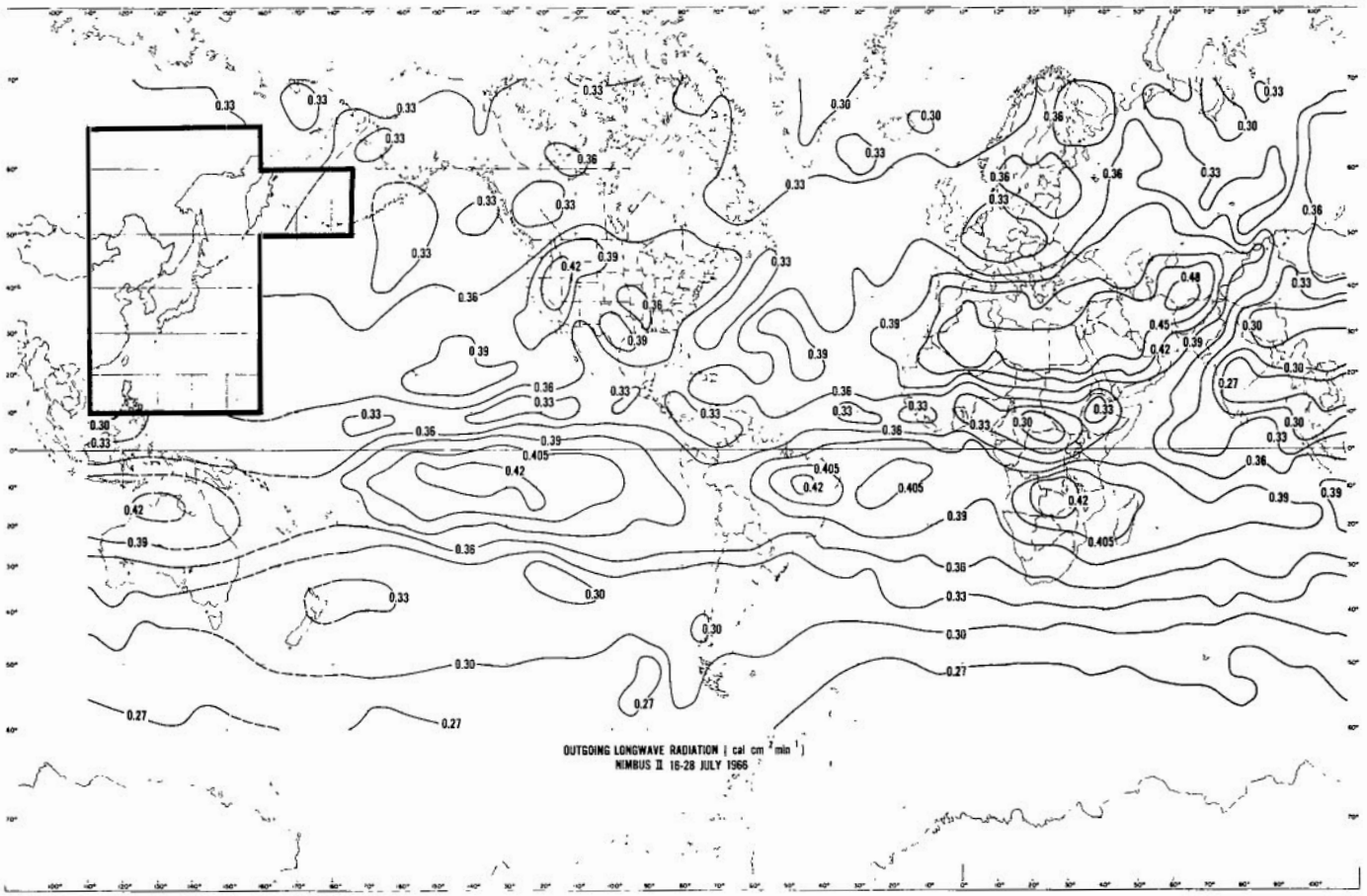

Figure 20—Outgoing long-wave radiation flux at the top of the atmosphere between 70°N and 60°S during the period 16–28 July 1966.

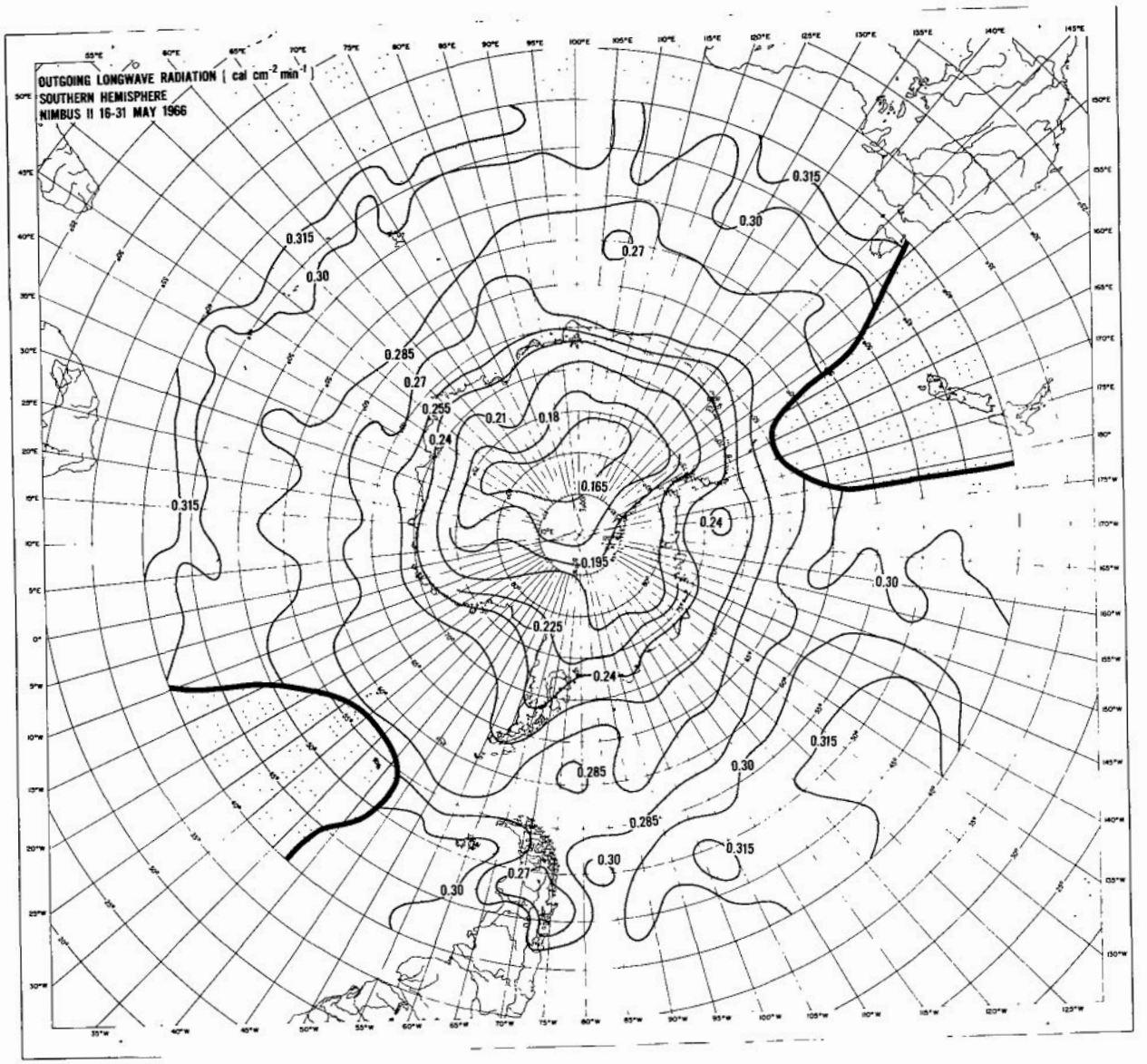

Figure E21—Outgoing long-wave radiation flux at the top of the atmosphere over the southern hemisphere during the period 16—31 May 1966.

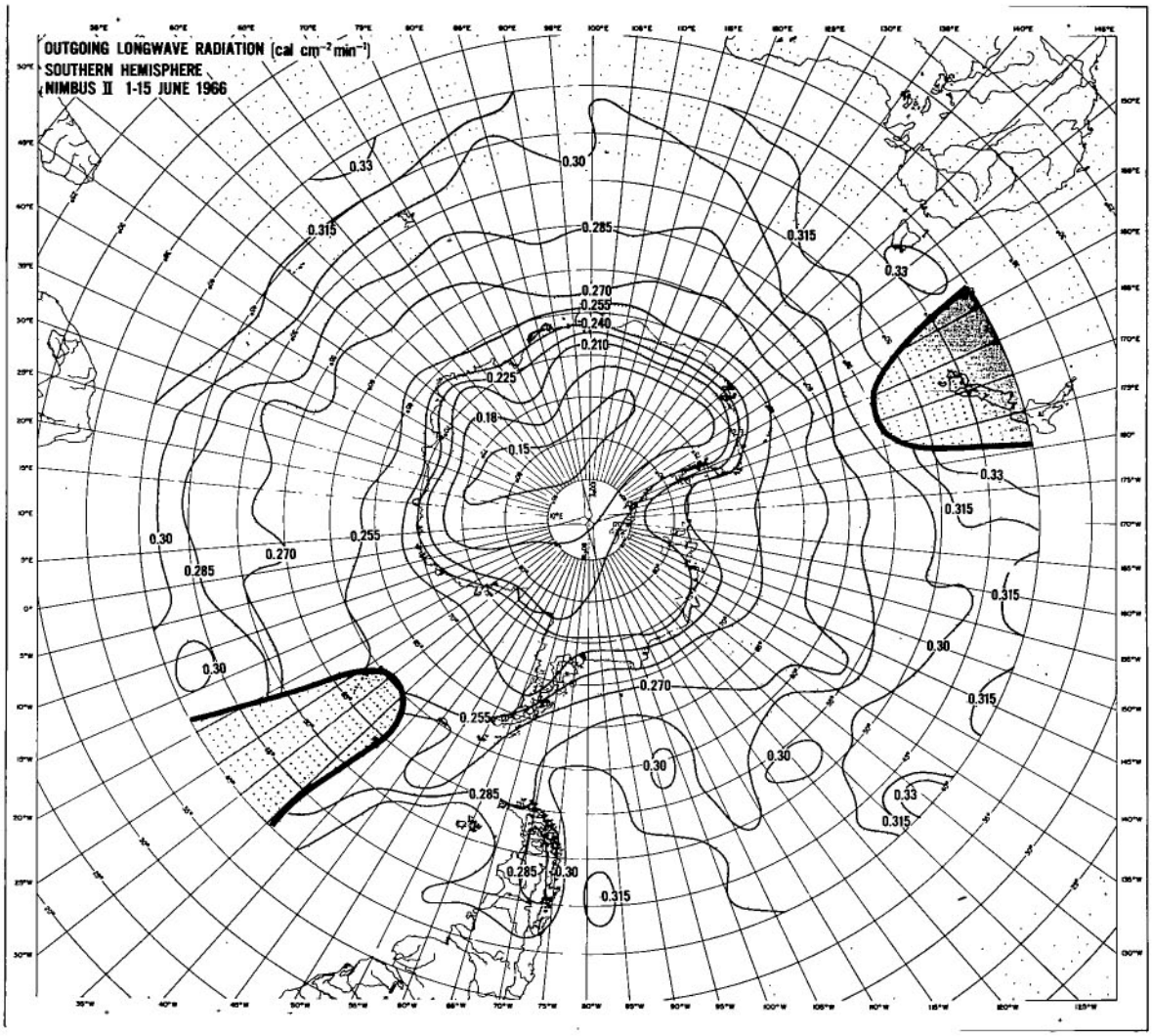

Figure E22—Outgoing long-wave radiation flux at the top of the atmosphere over the southern hemisphere during the period 1—15 June 1966.

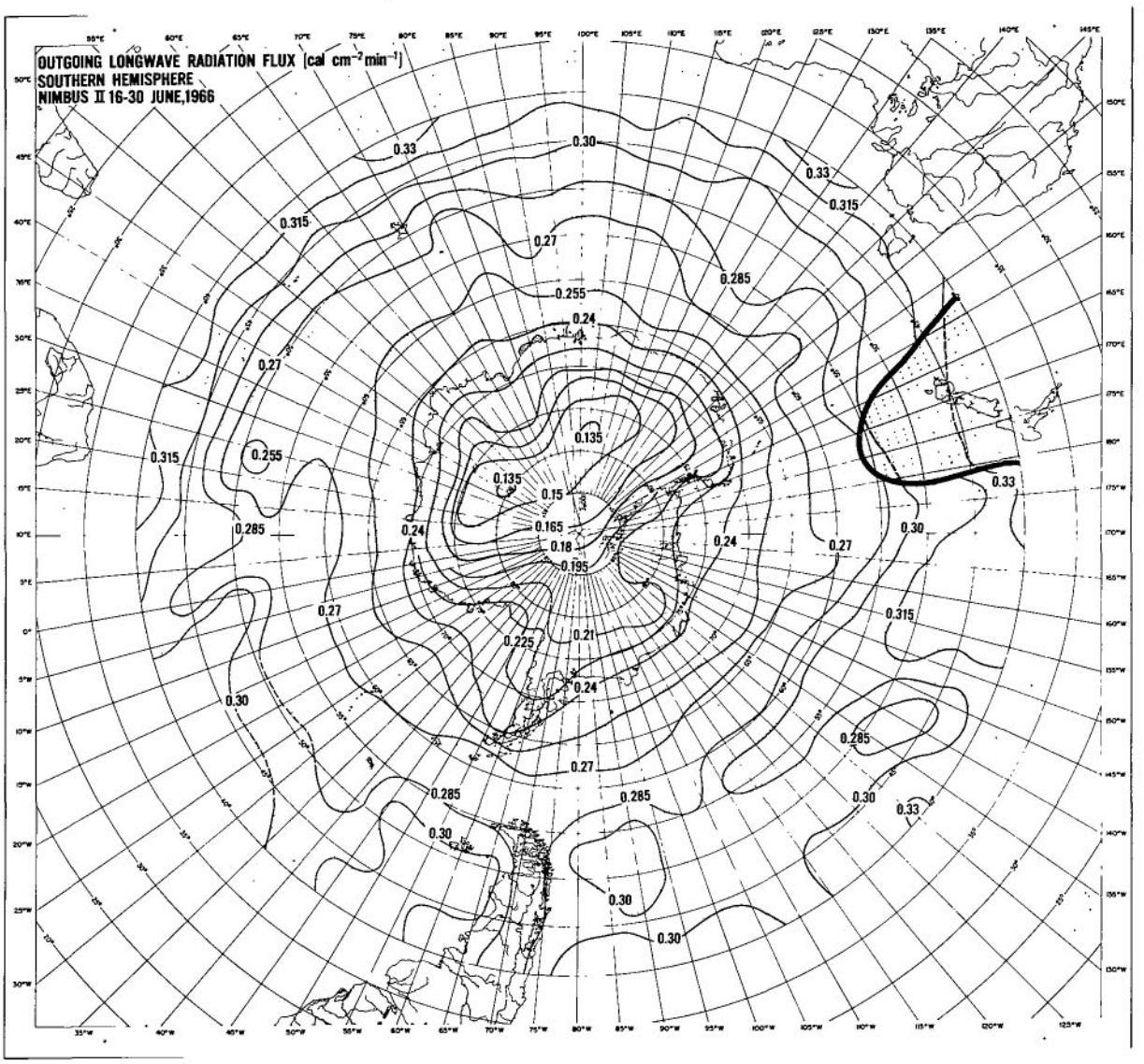

Figure E23—Outgoing long-wave radiation flux at the top of the atmosphere over the southern hemisphere during the period 16—30 June 1966.

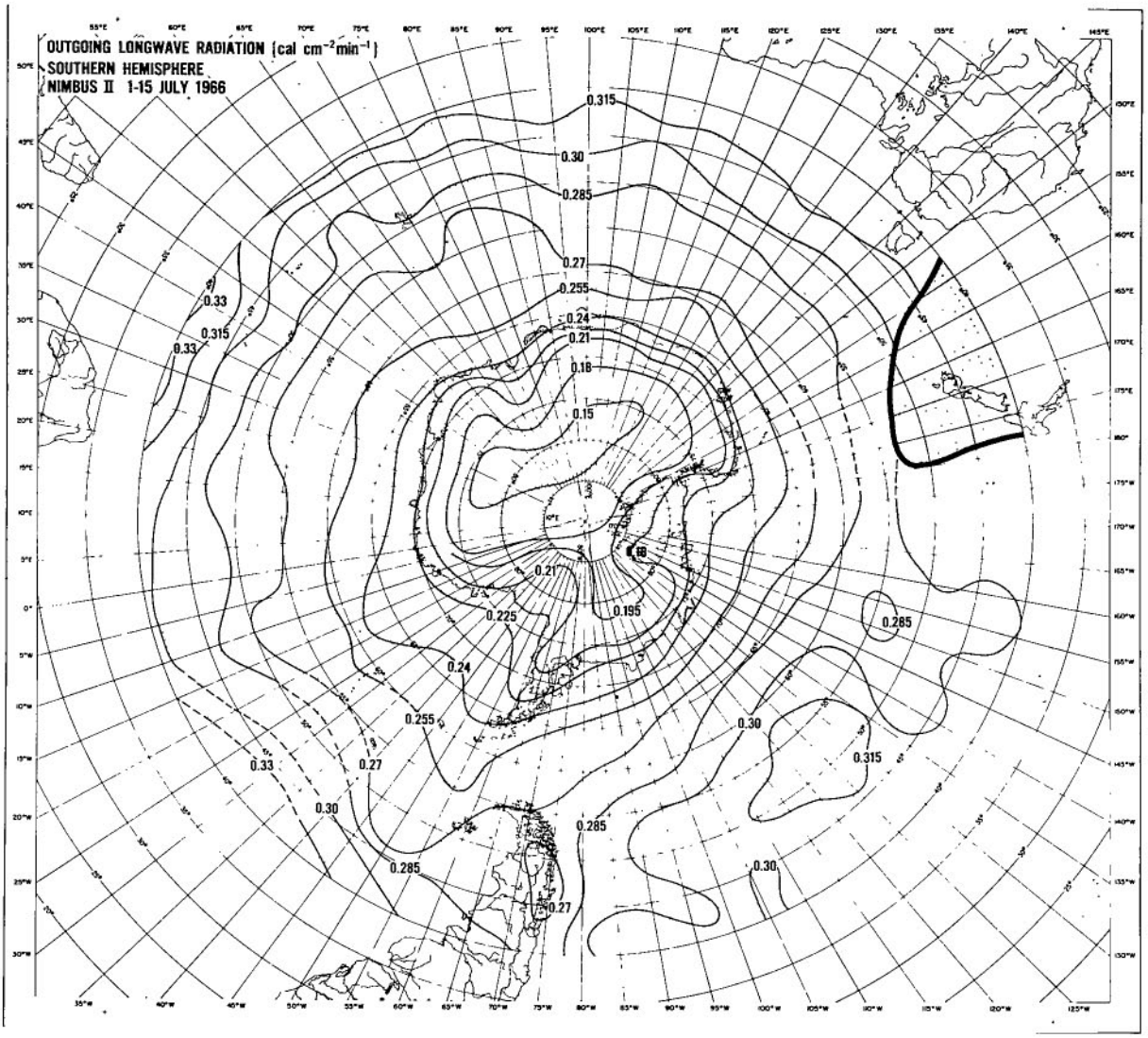

Figure E24—Outgoing long-wave radiation flux at the top of the atmosphere over the southern hemisphere during the period 1—15 July 1966.

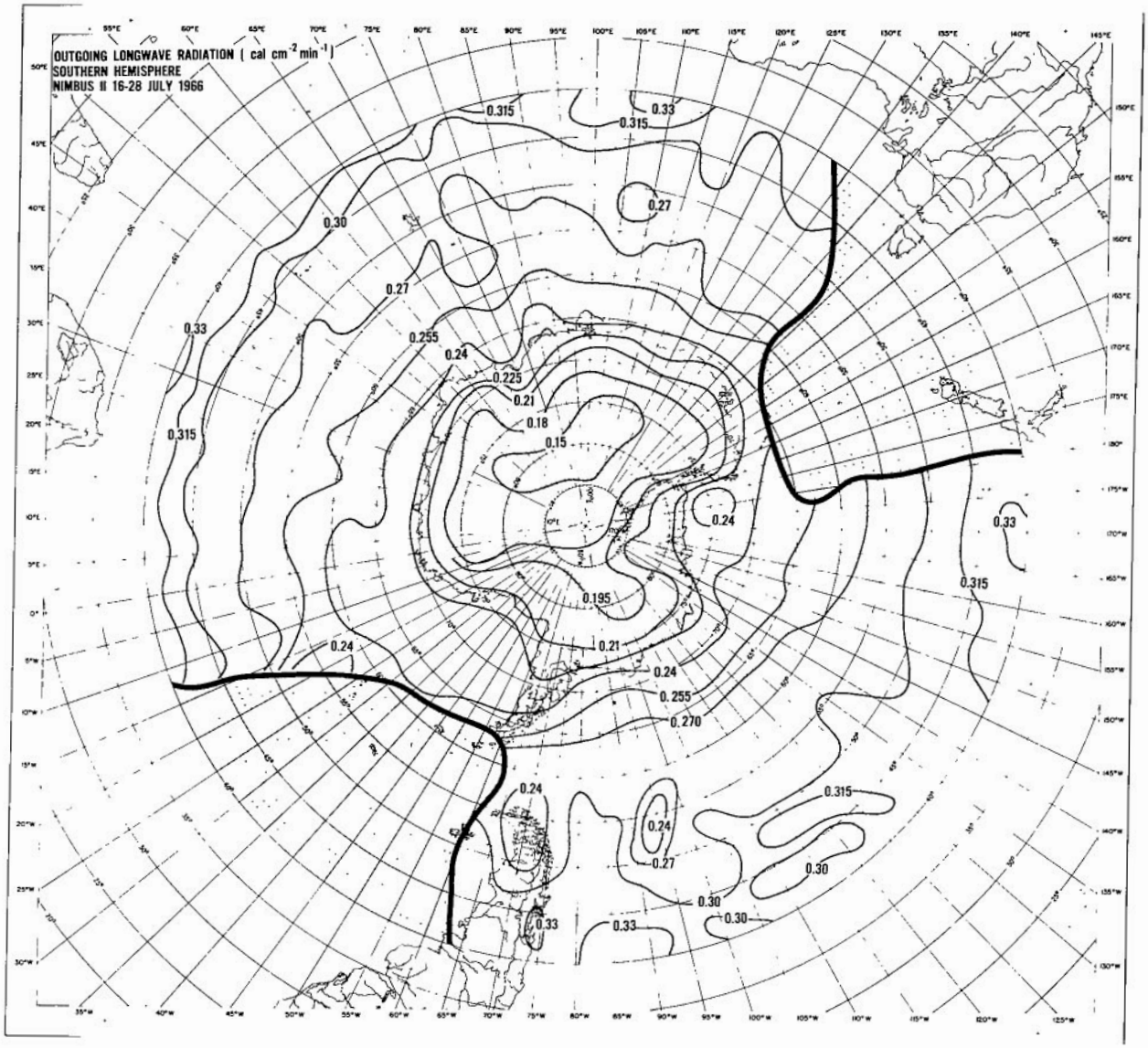

Figure E25—Outgoing long-wave radiation flux at the top of the atmosphere over the southern hemisphere during the period 16—28 July 1966.

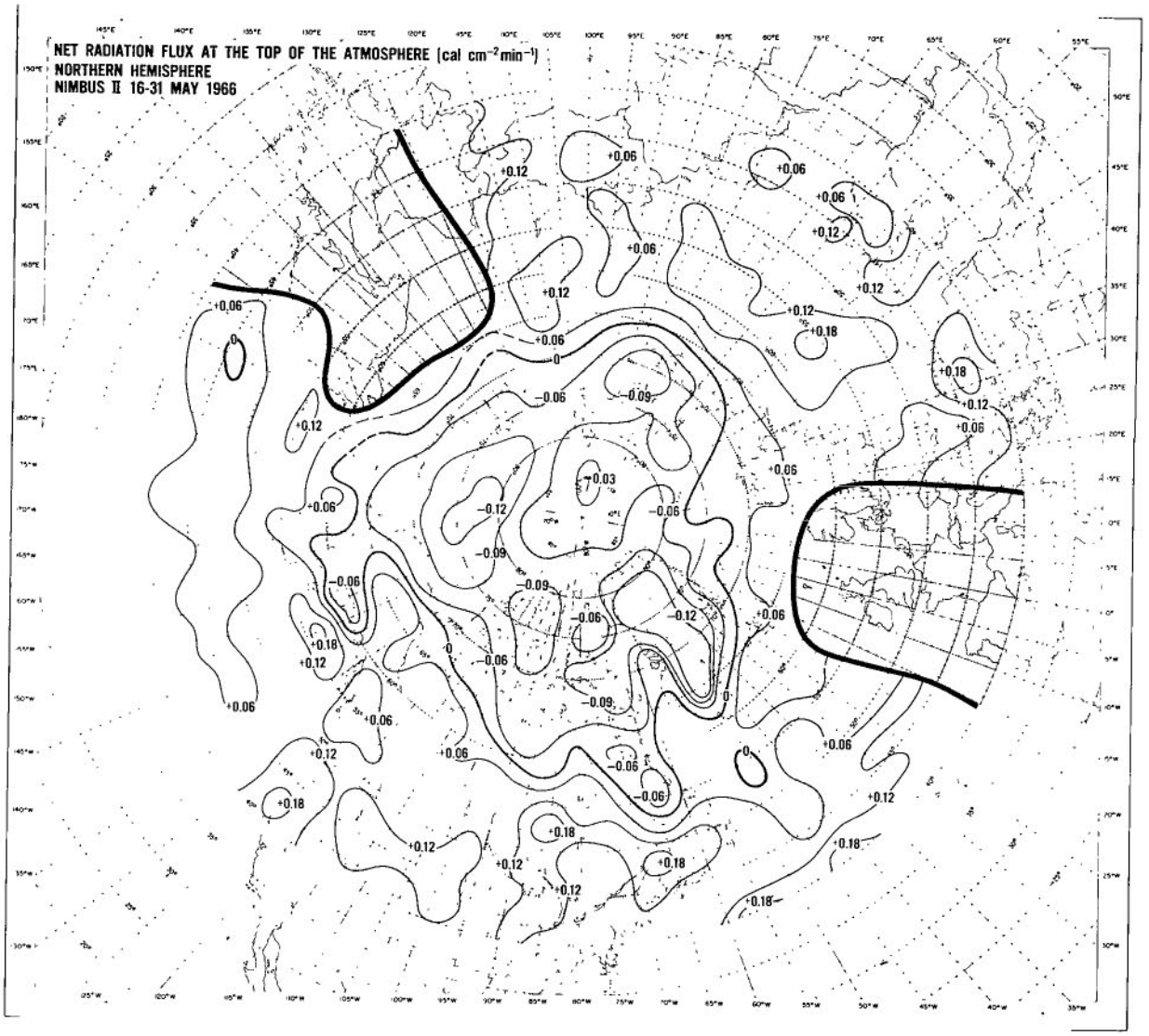

Figure E26—Radiation balance of the earth-atmosphere system over the northern hemisphere during the period 16—31 May 1966.

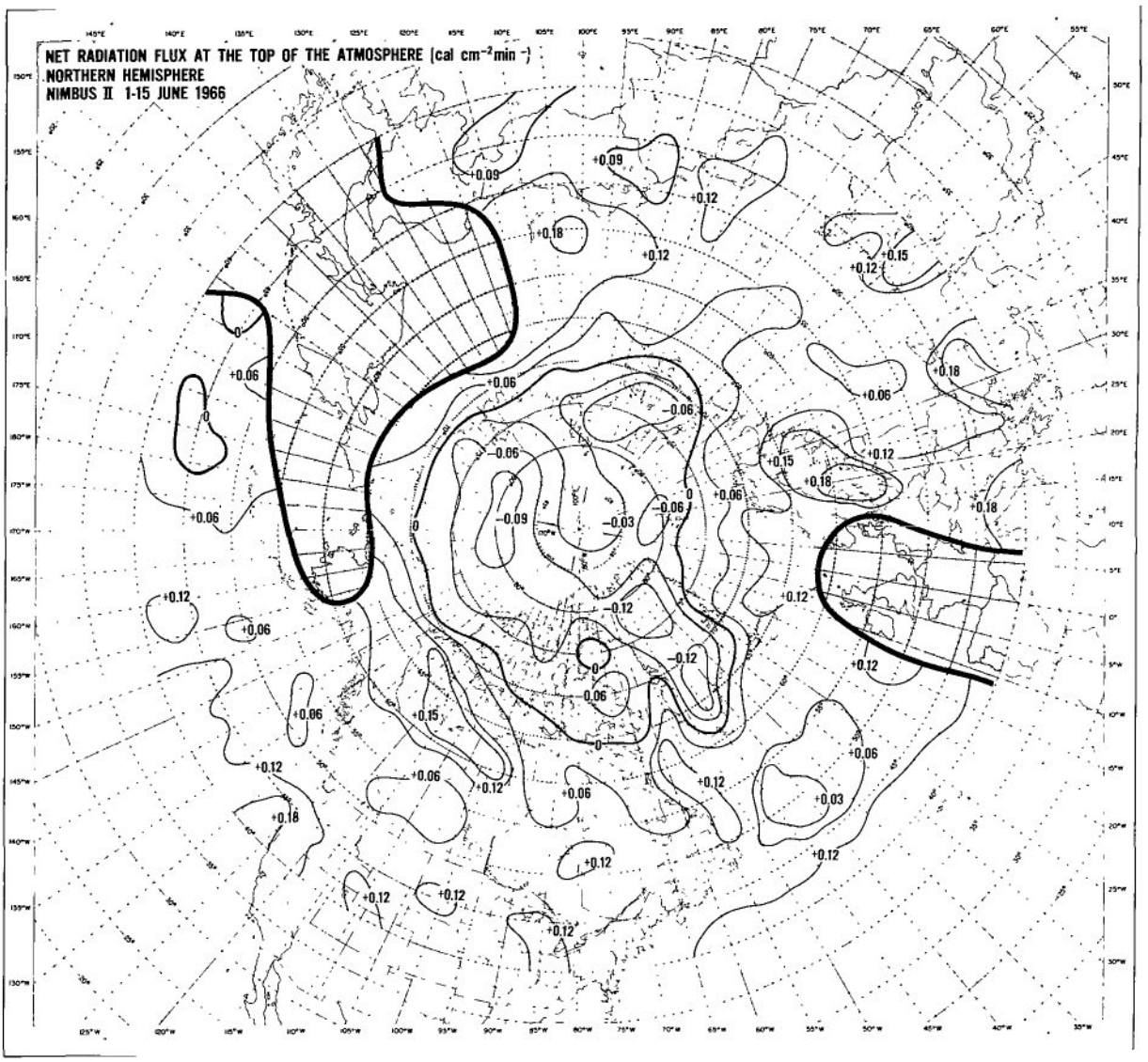

Figure E27—Radiation balance of the earth–atmosphere system over the northern hemisphere during the period 1—15 June 1966.

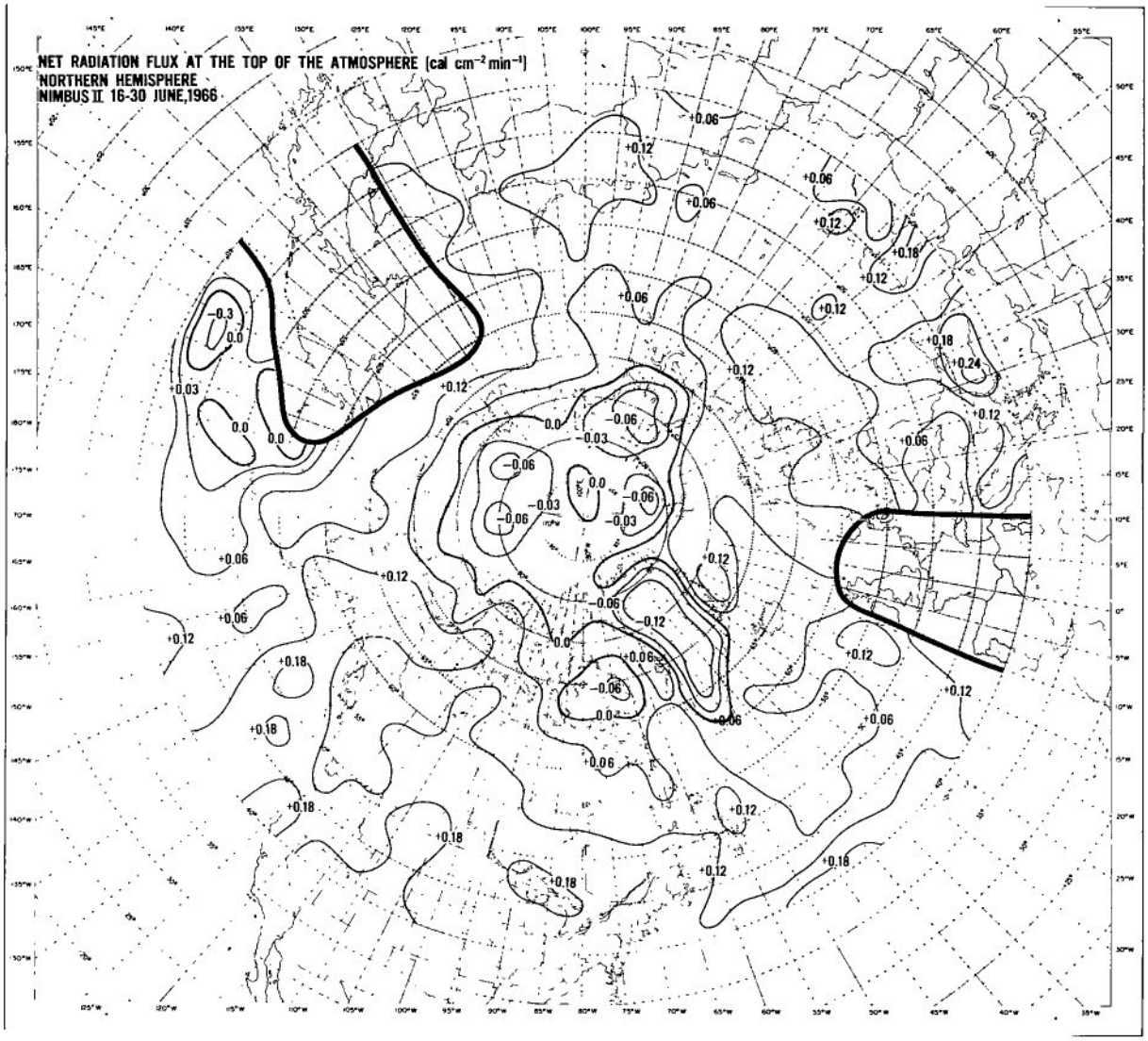

Figure E28—Radiation balance of the earth-atmosphere system over the northern hemisphere during the period 16—30 June 1966.

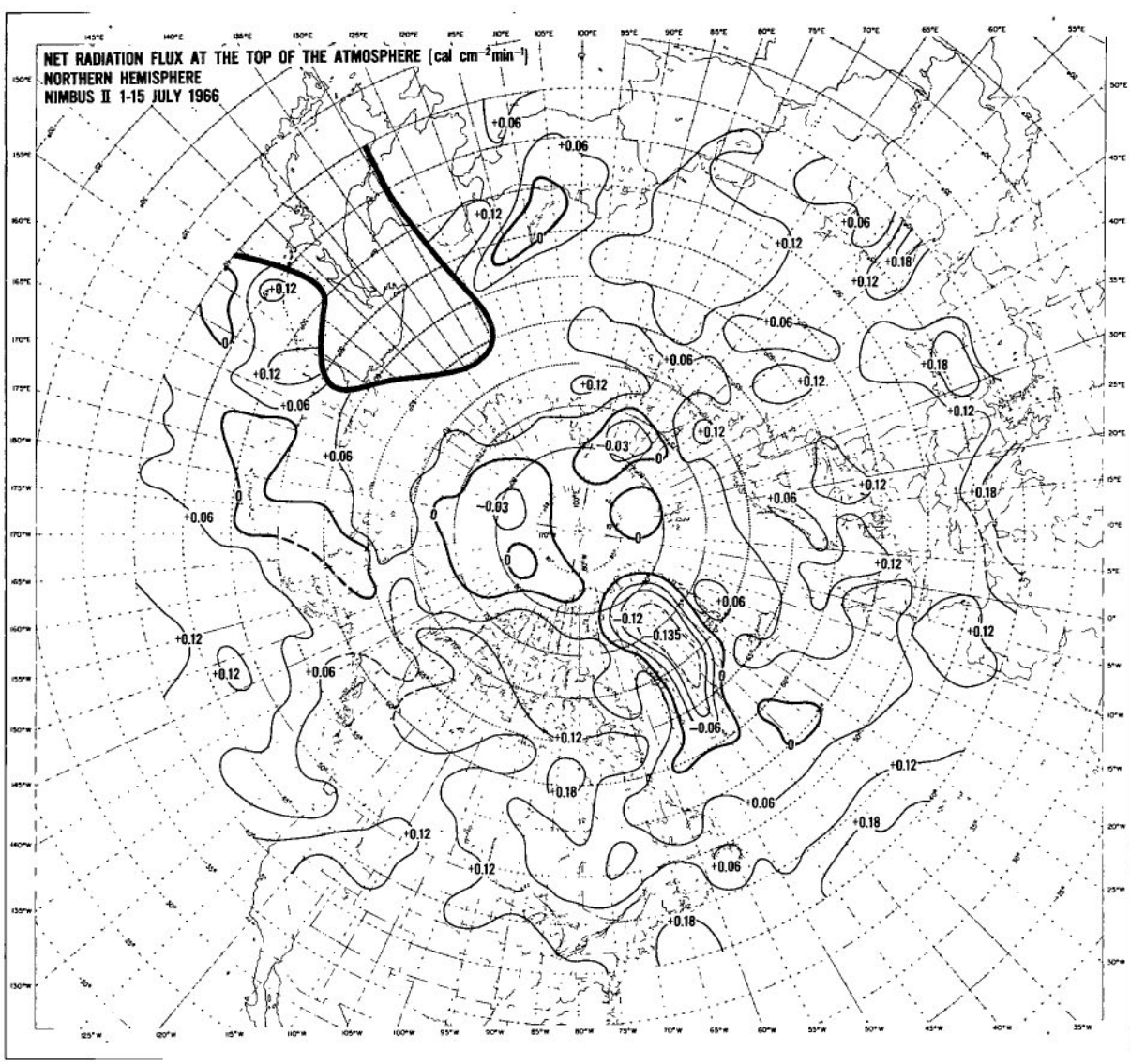

Figure E29—Radiation balance of the earth-atmosphere system over the northern hemisphere during the period 1—15 July 1966.

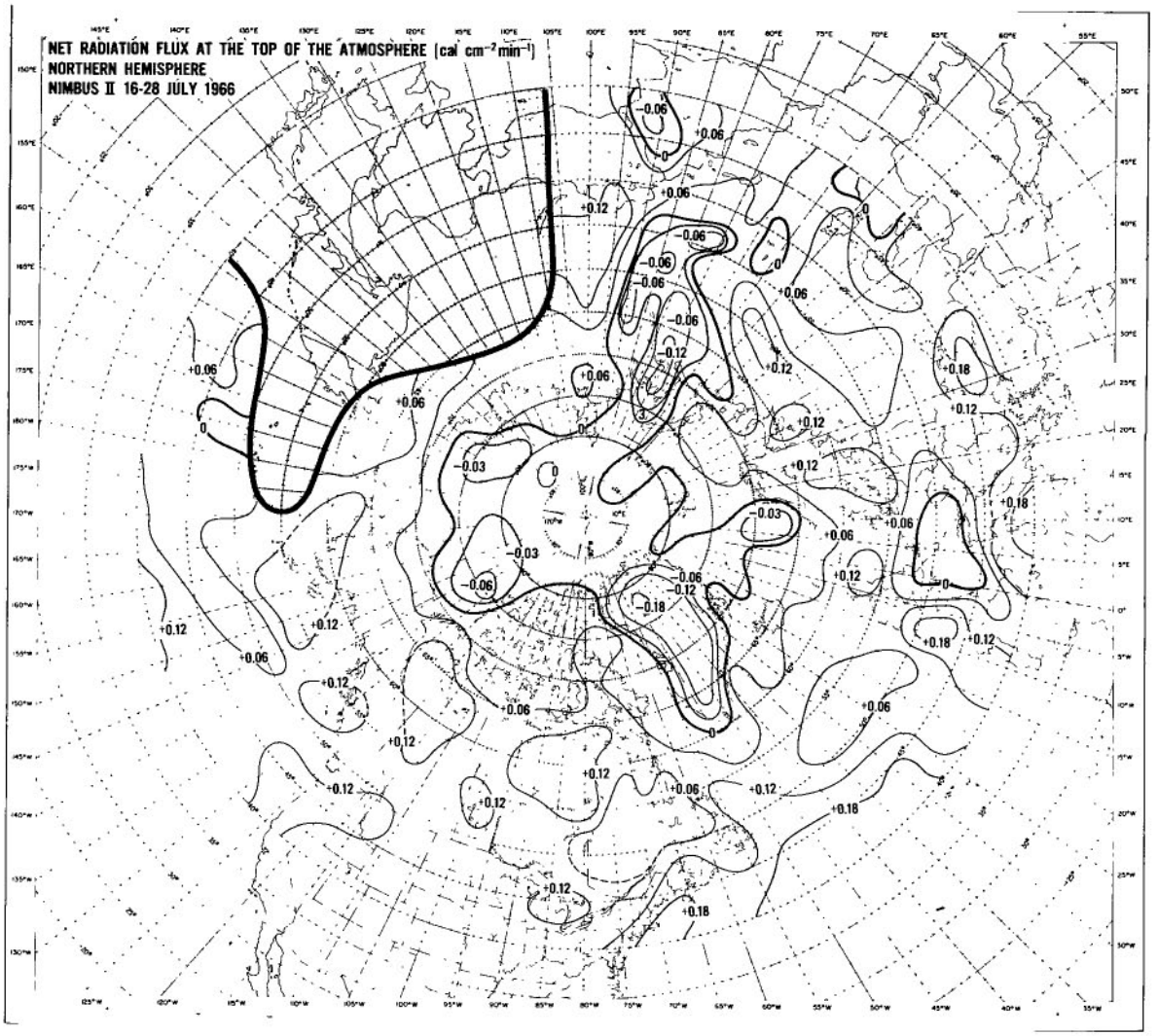

Figure E30—Radiation balance of the earth-atmosphere system over the northern hemisphere during the period 16—28 July 1966.

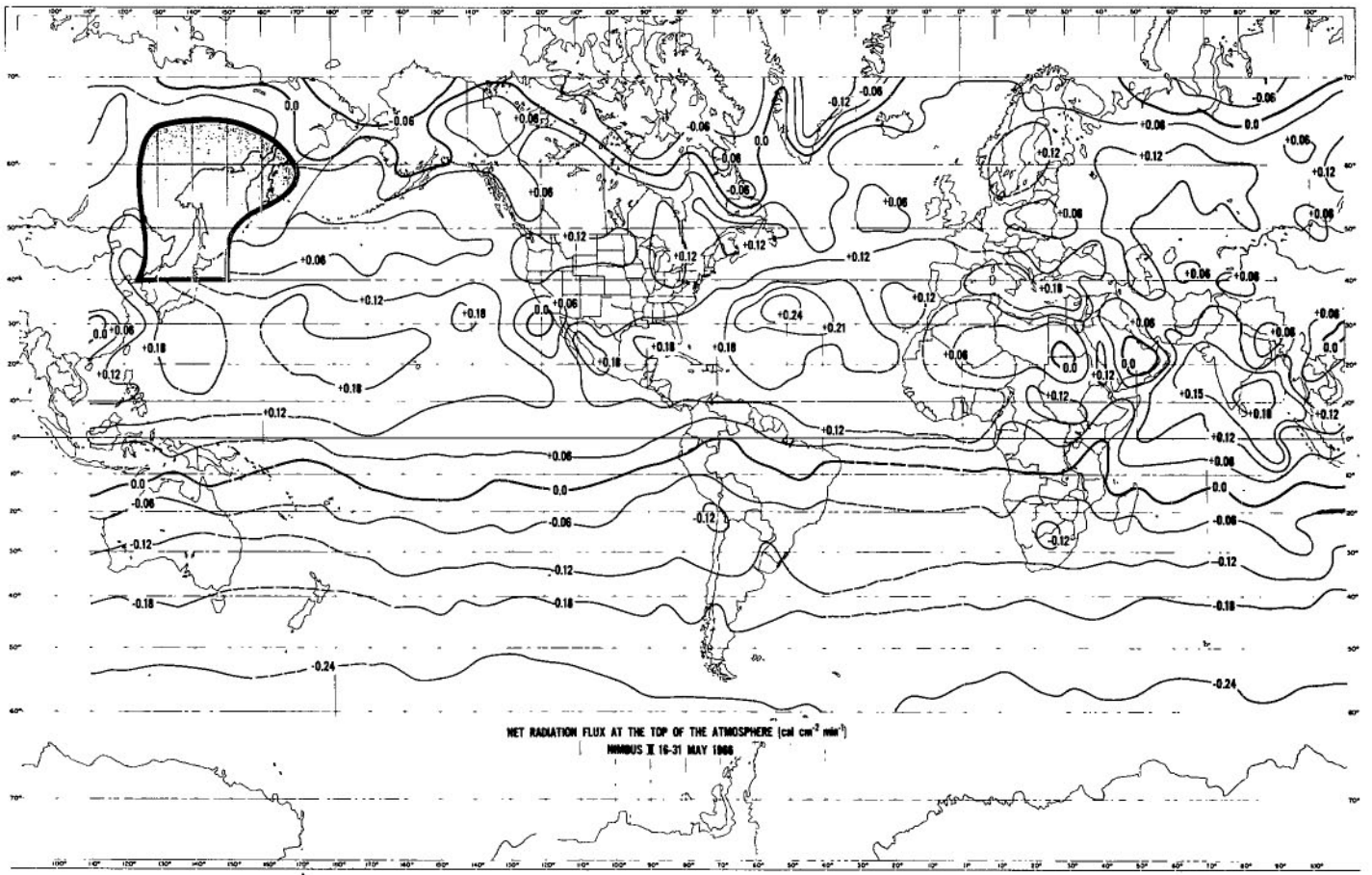

Figure E31—Radiation balance of the earth-atmosphere system between 70°N and 60°S during the period 16—31 May 1966.

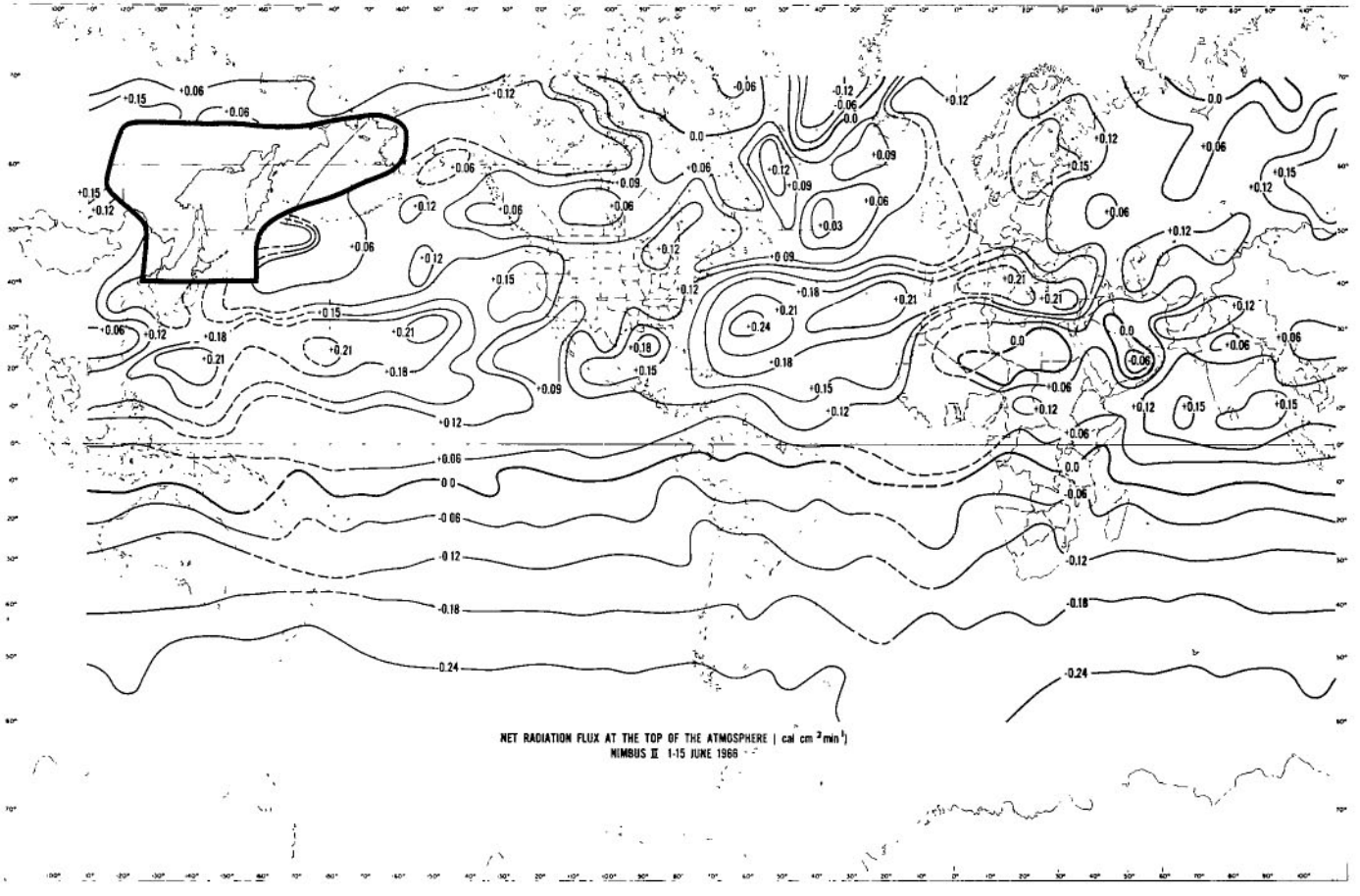

Figure E32—Radiation balance of the earth-atmosphere system between 70°N and 60°S during the period 1—15 June 1966.

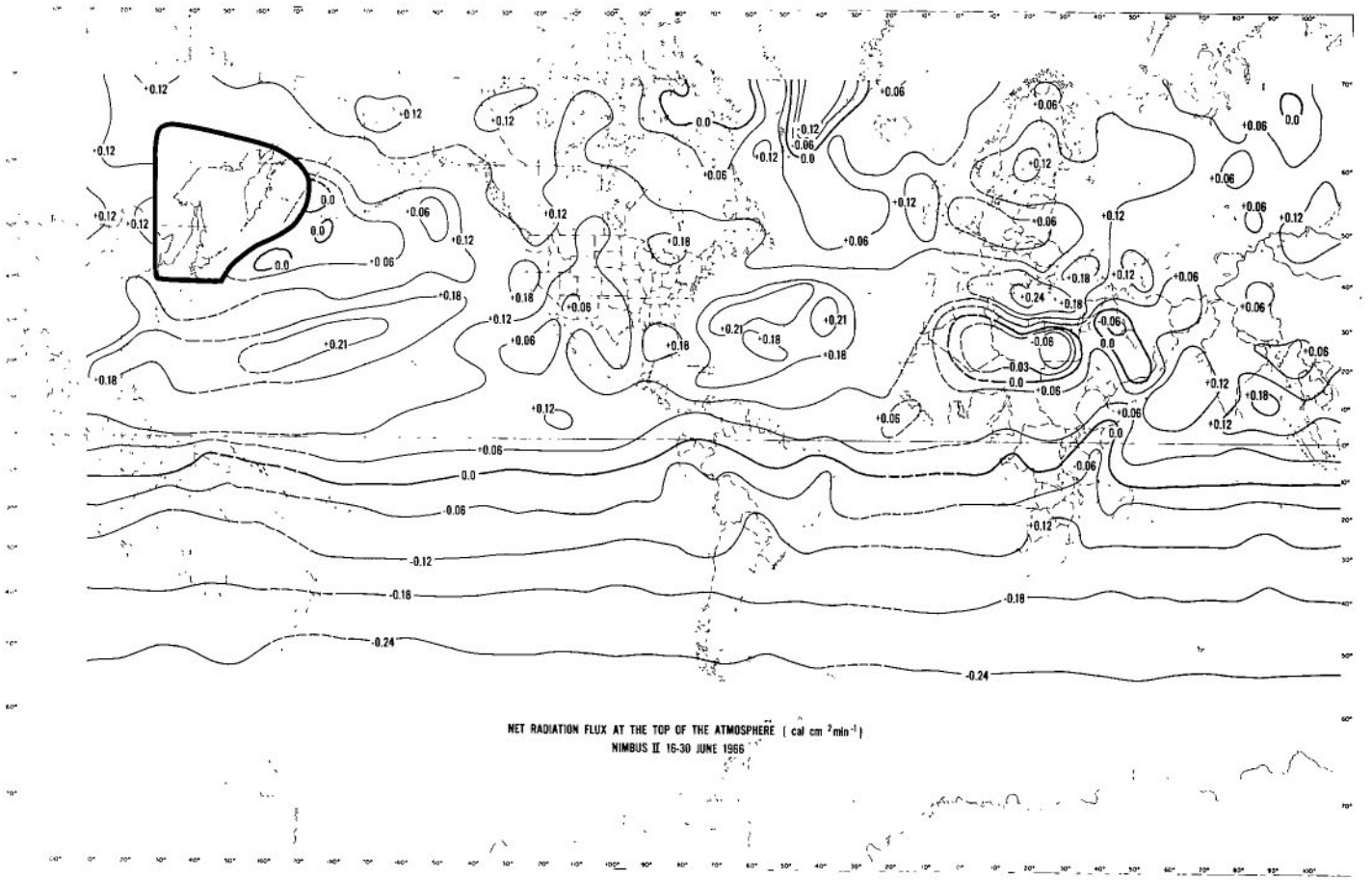

Figure E33—Radiation balance of the earth-atmosphere system between 70°N and 60°S during the period 16—30 June 1966.

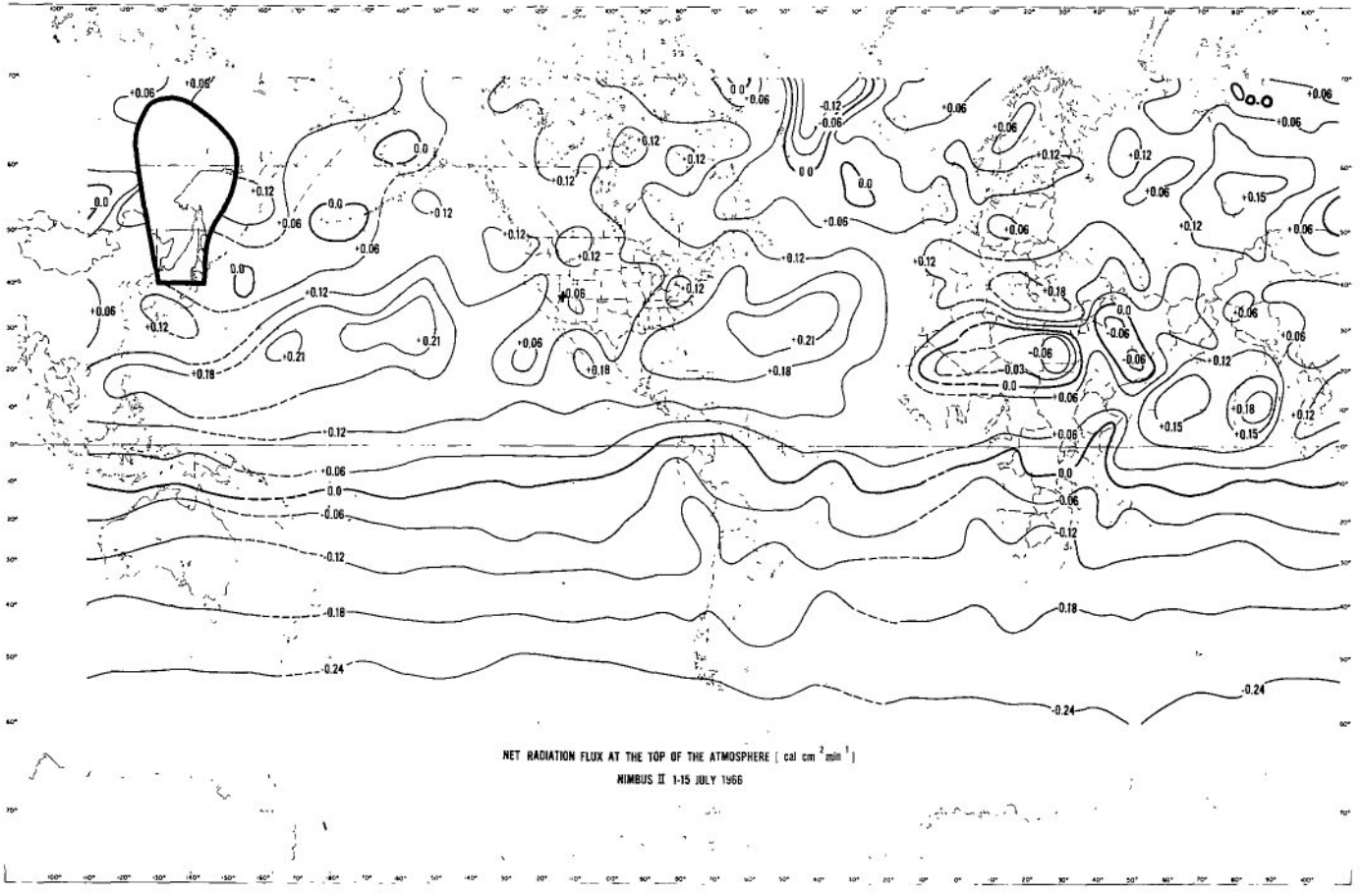

Figure E34—Radiation balance of the earth-atmosphere system between 70°N and 60°S during the period 1—15 July 1966.

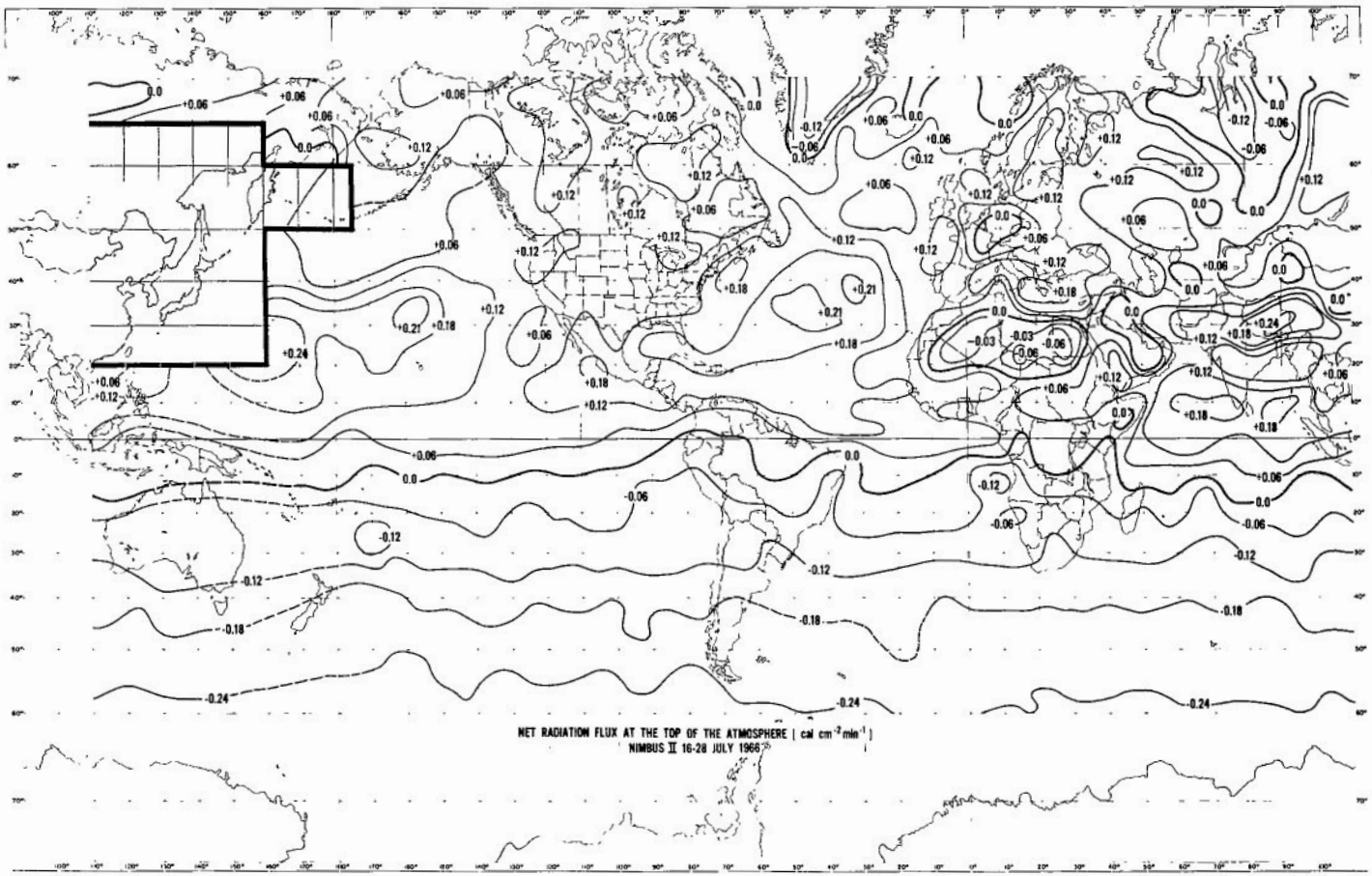

Figure E35—Radiation balance of the earth-atmosphere system between 70°N and 60°S during the period 16—28 July 1966.

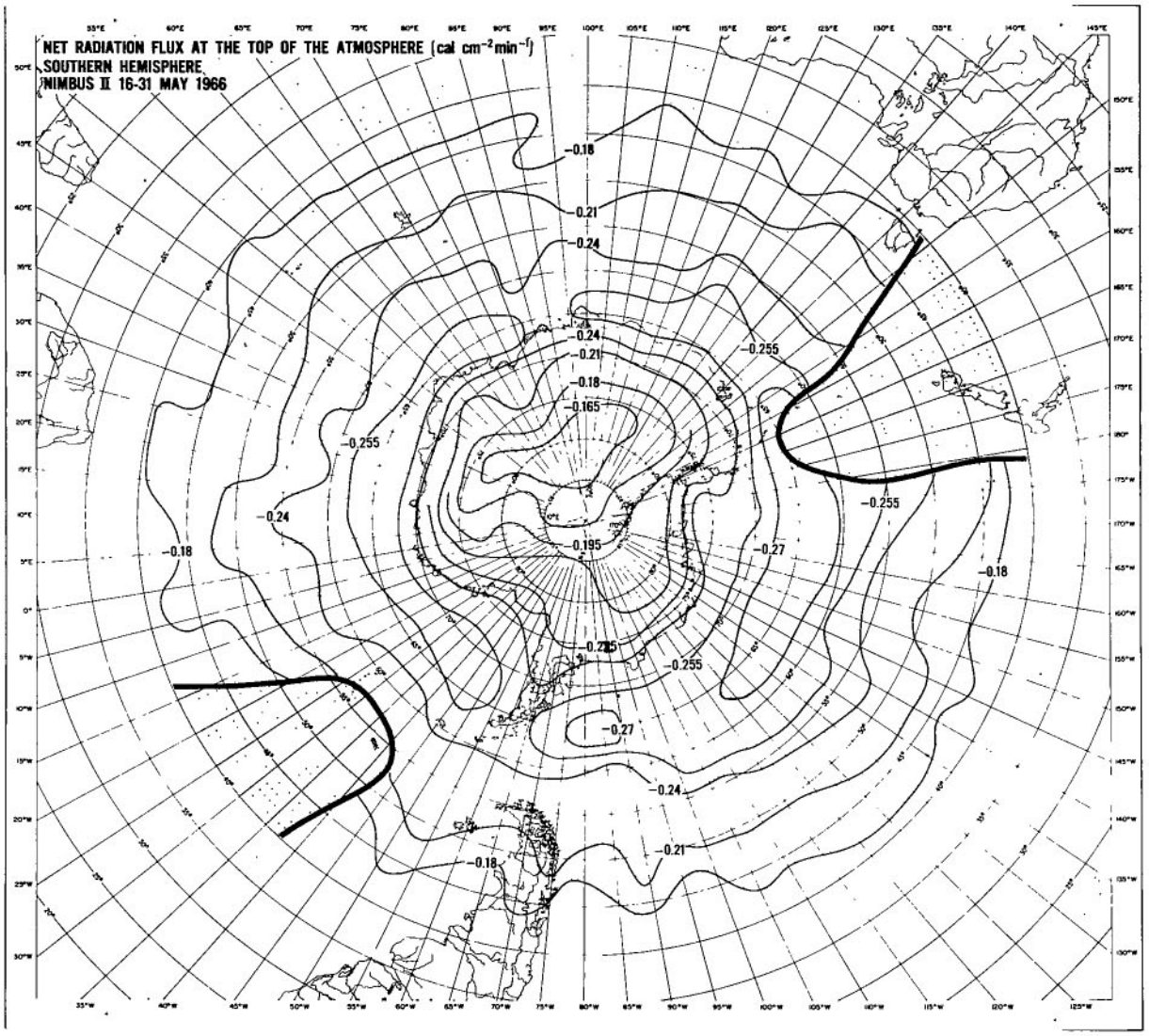

Figure E36—Radiation balance of the earth-atmosphere system over the southern hemisphere during the period 16—31 May 1966.

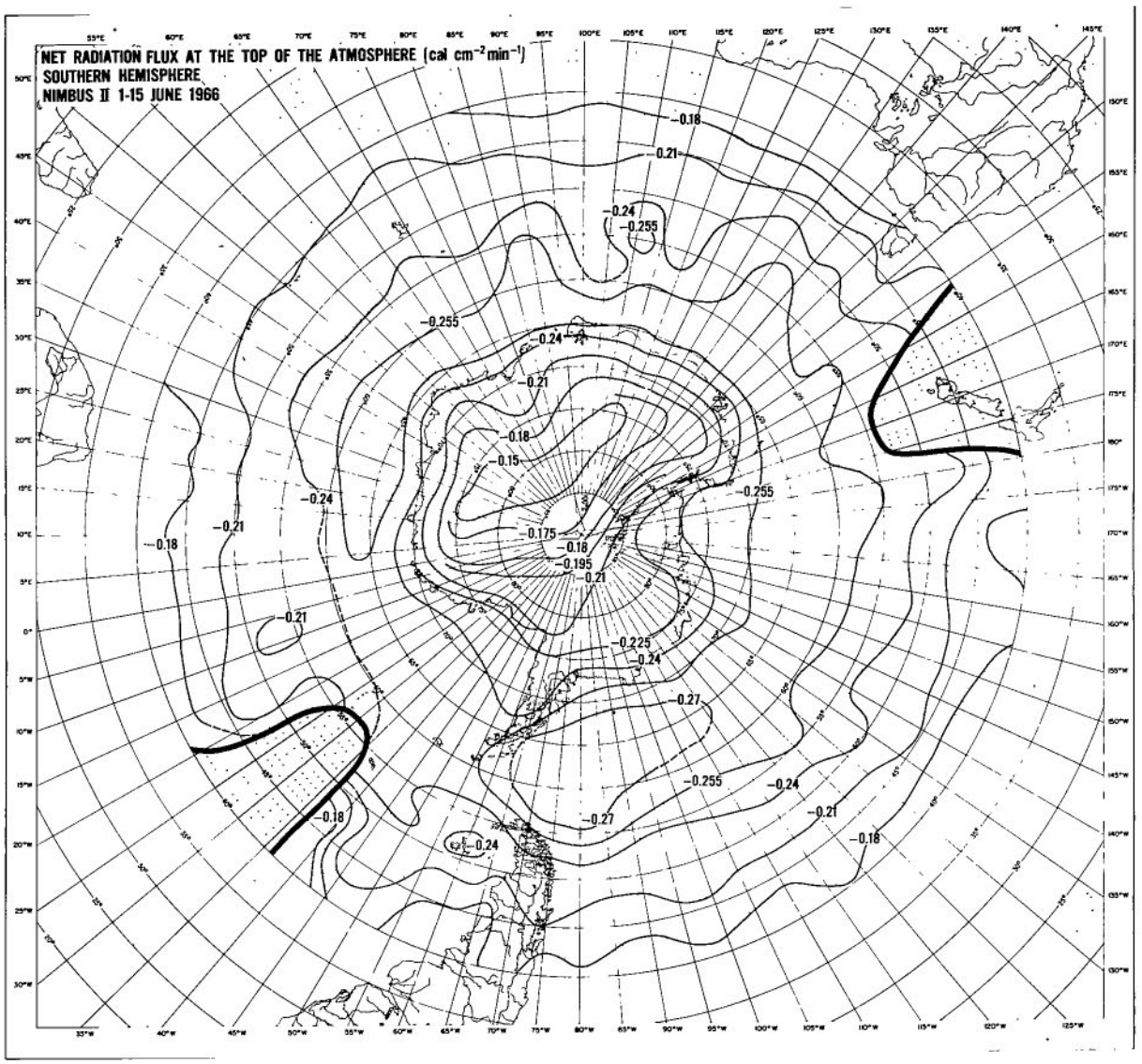

Figure E37—Radiation balance of the earth-atmosphere system over the southern hemisphere during the period 1—15 June 1966.

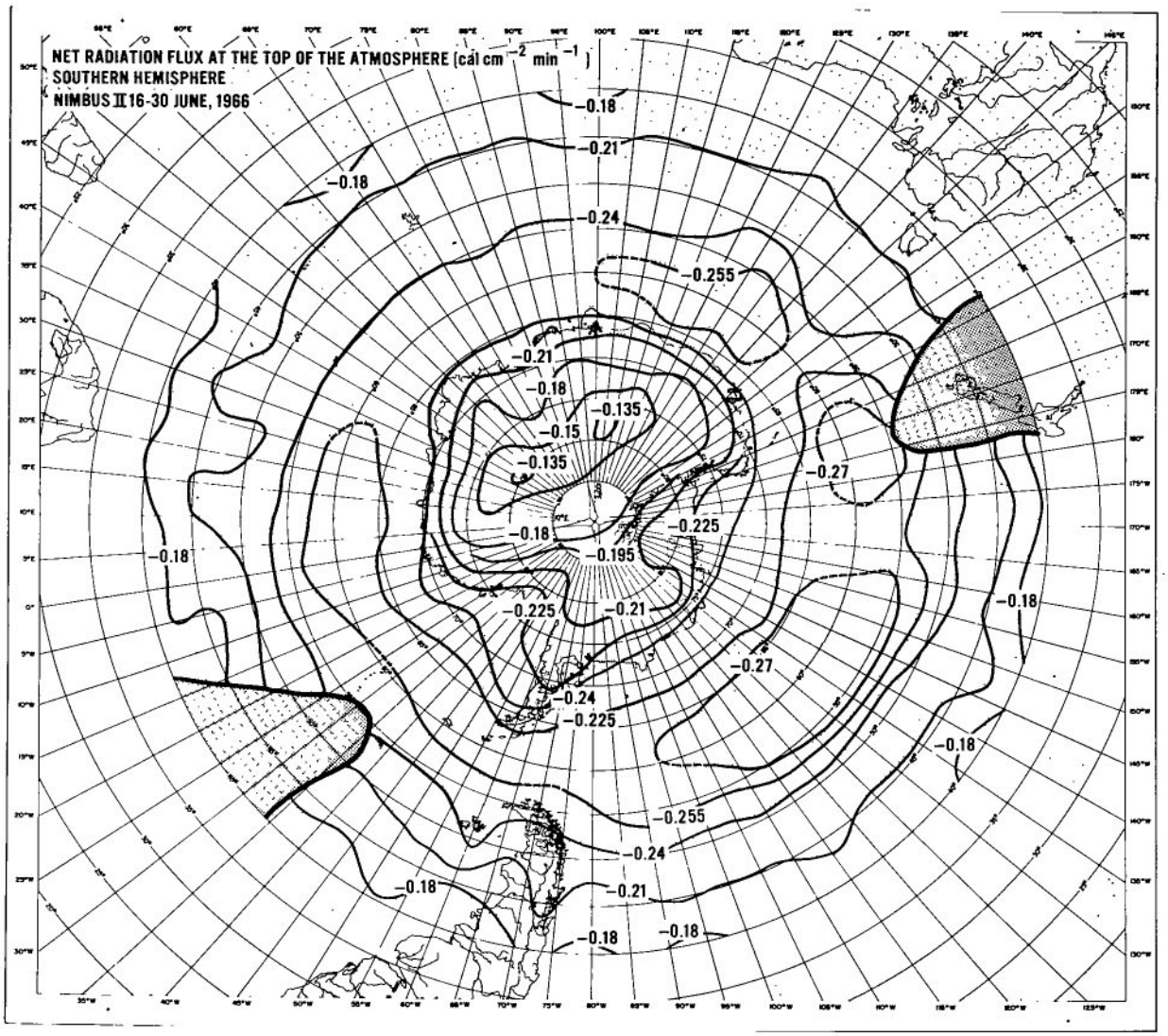

Figure E38—Radiation balance of the earth-atmosphere system over the southern hemisphere during the period 16–30 June 1966.

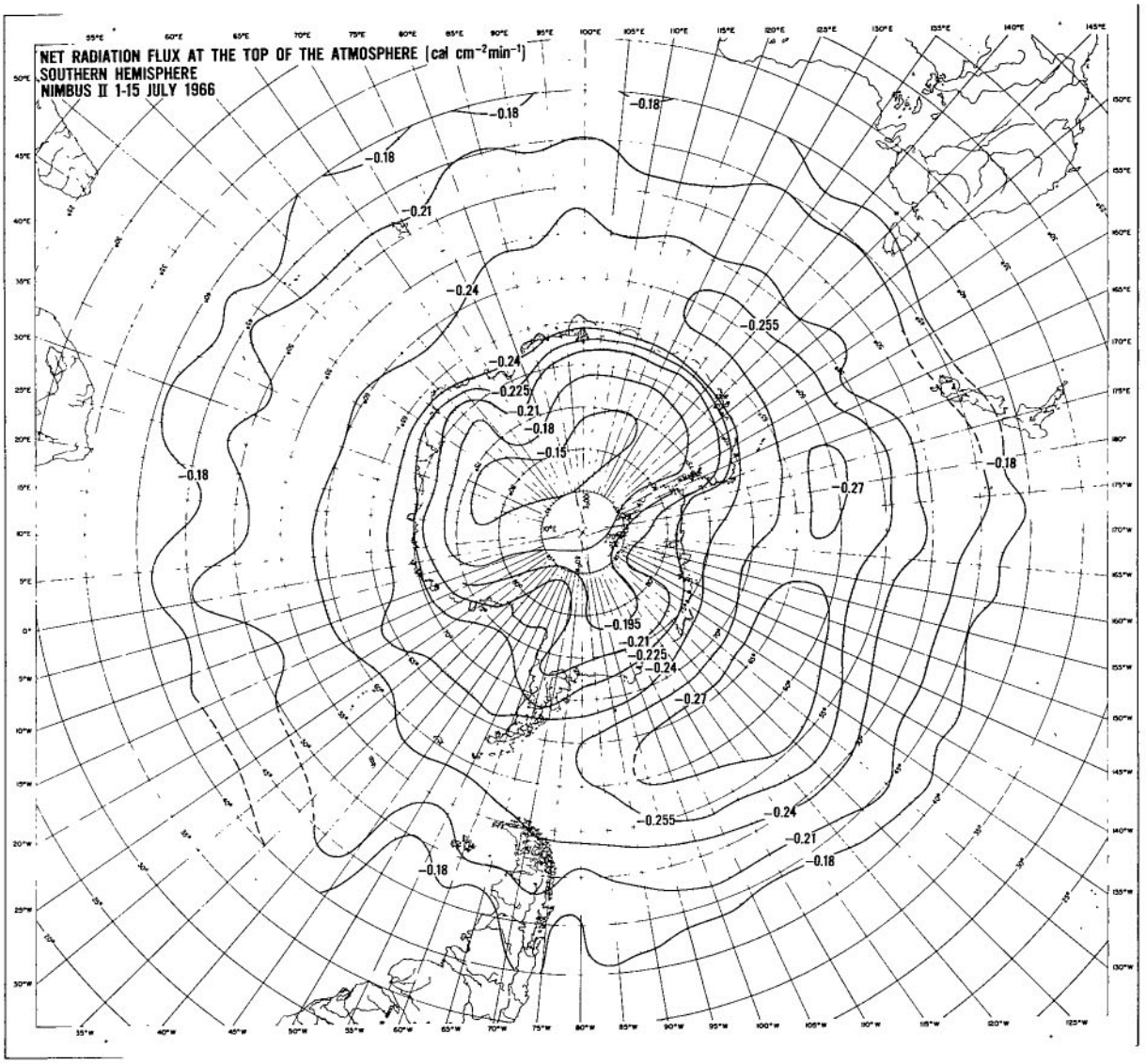

Figure E39—Radiation balance of the earth-atmosphere system over the southern hemisphere during the period 1—15 July 1966.

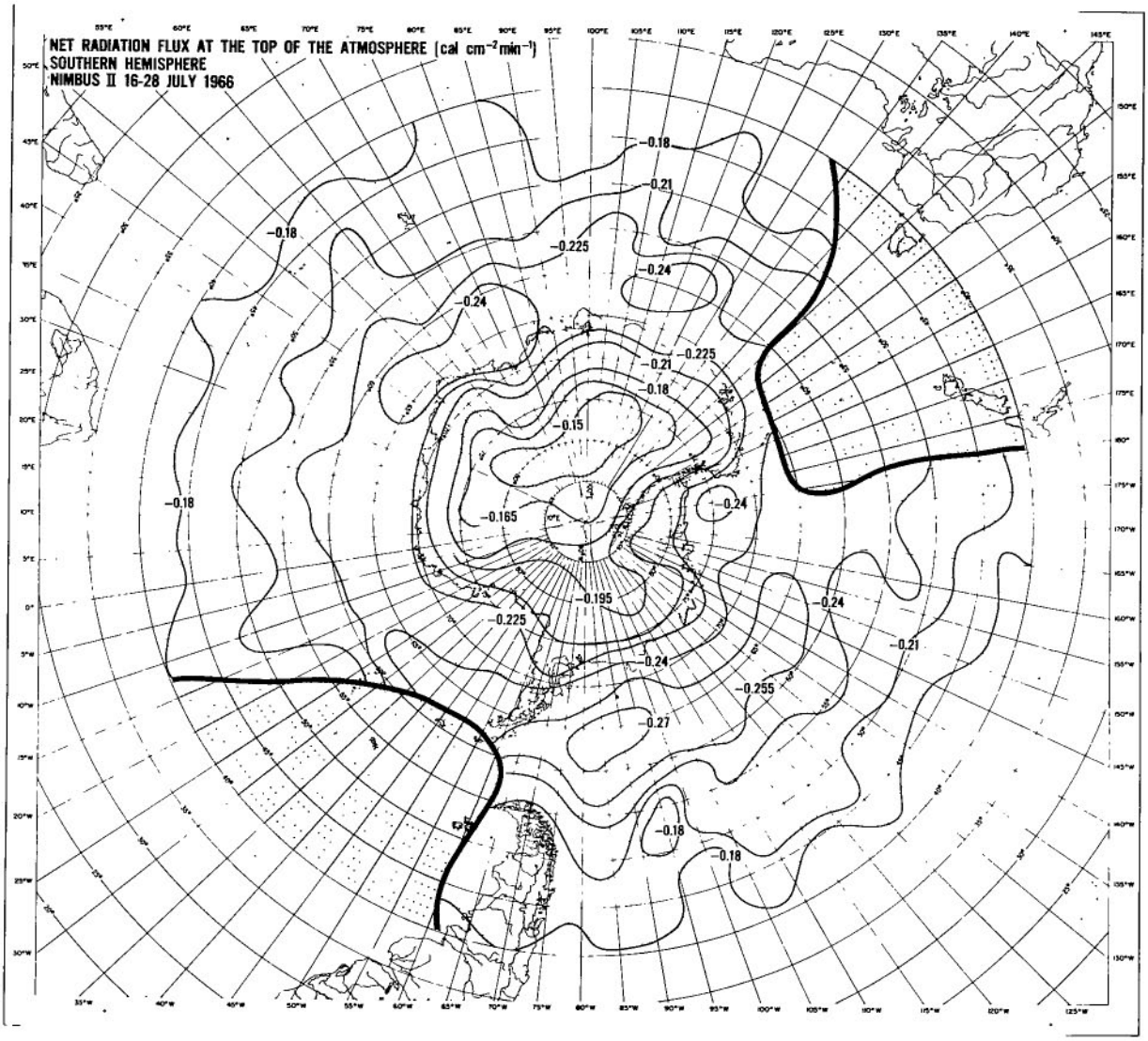

Figure E40—Radiation balance of the earth–atmosphere system over the southern hemisphere during the period 16—28 July 1966.

Appendix F

Mean Cloud Cover Over the Northern Hemisphere

Maps of the mean cloud cover (Figures F1 through F5) over the northern hemisphere are added to this report. They were obtained by the USAF Environmental Technical Applications Center, Washington, D. C.,* from ground observations.

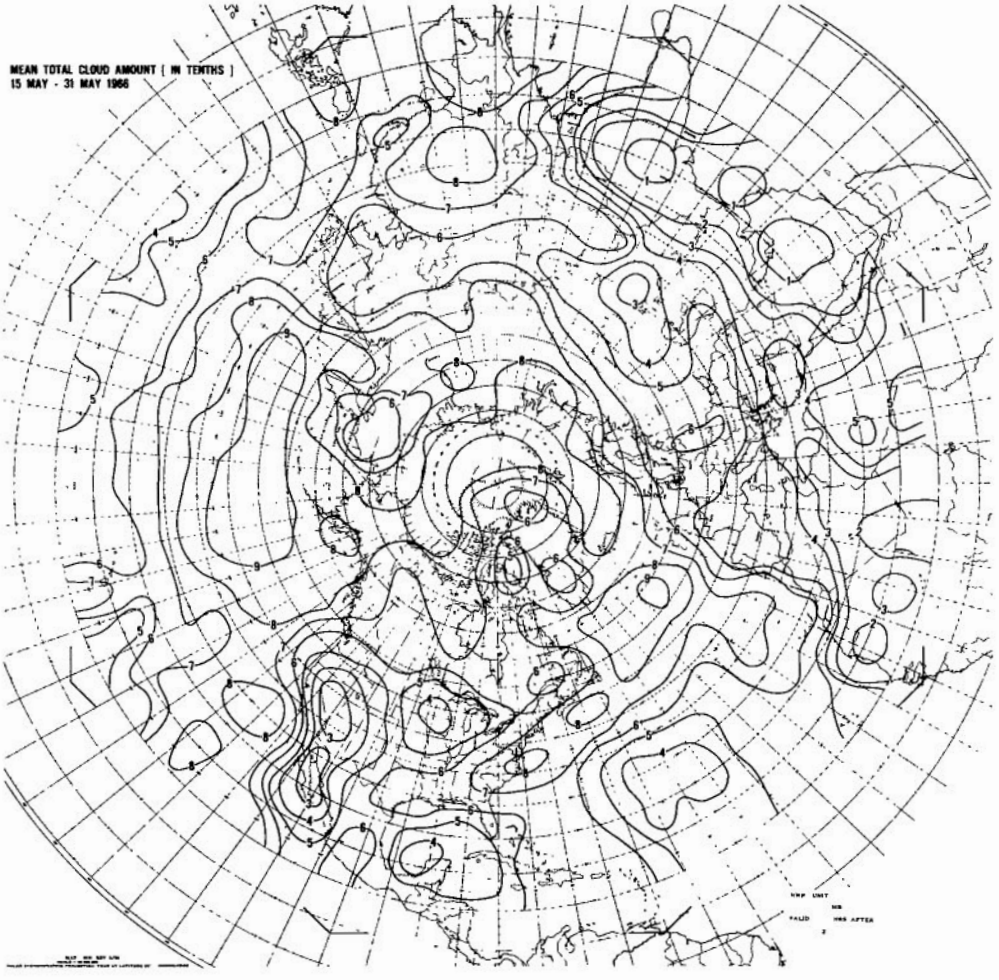

Figure F1—Mean cloud cover over the northern hemisphere during the period 16—31 May 1966 from operational data.

*USAF Environmental Technical Applications Center, Washington, D. C., (private communication through Maj. E. Kreins), 1967.

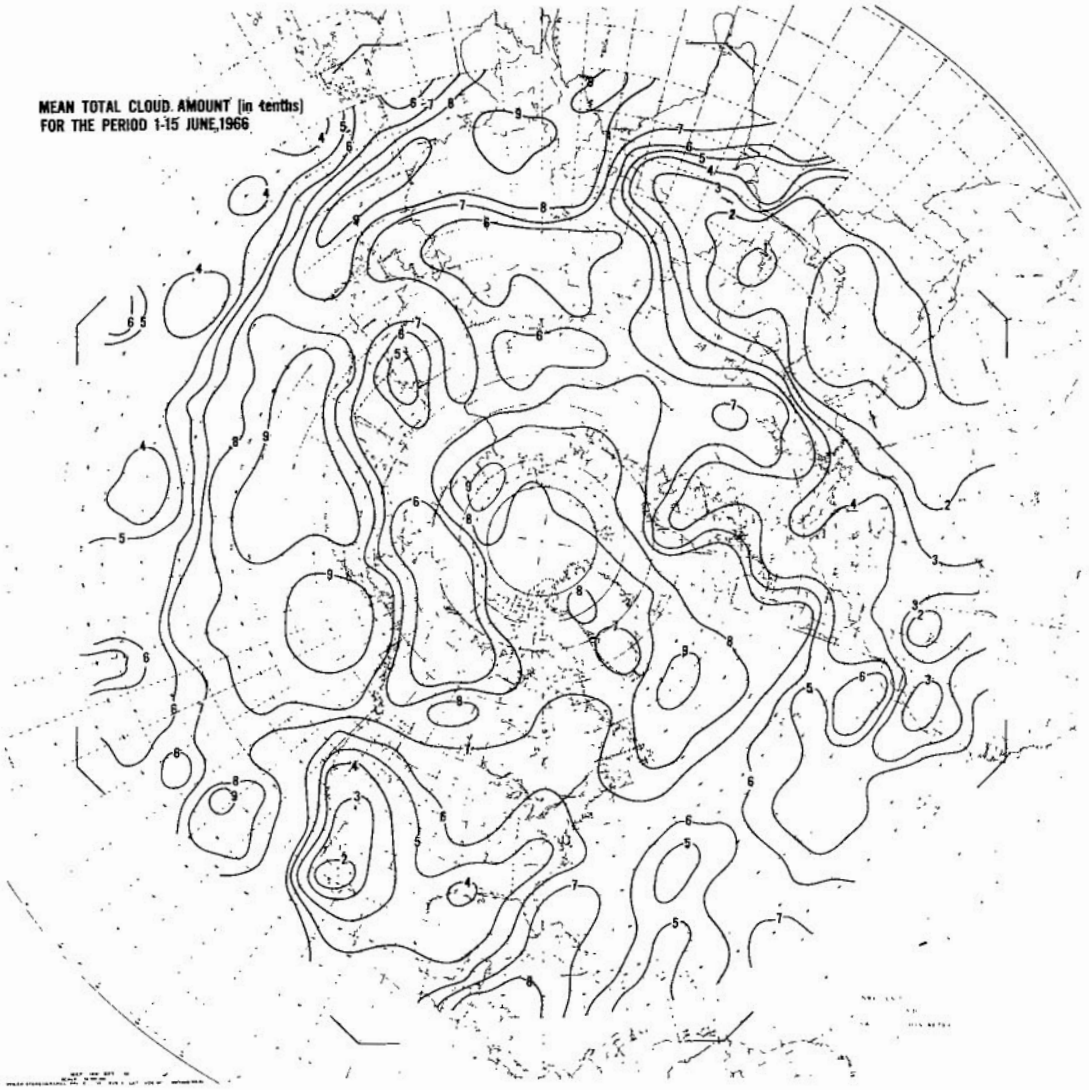

Figure F2—Mean cloud cover over the northern hemisphere during the period 1—15 June 1966 from operational data.

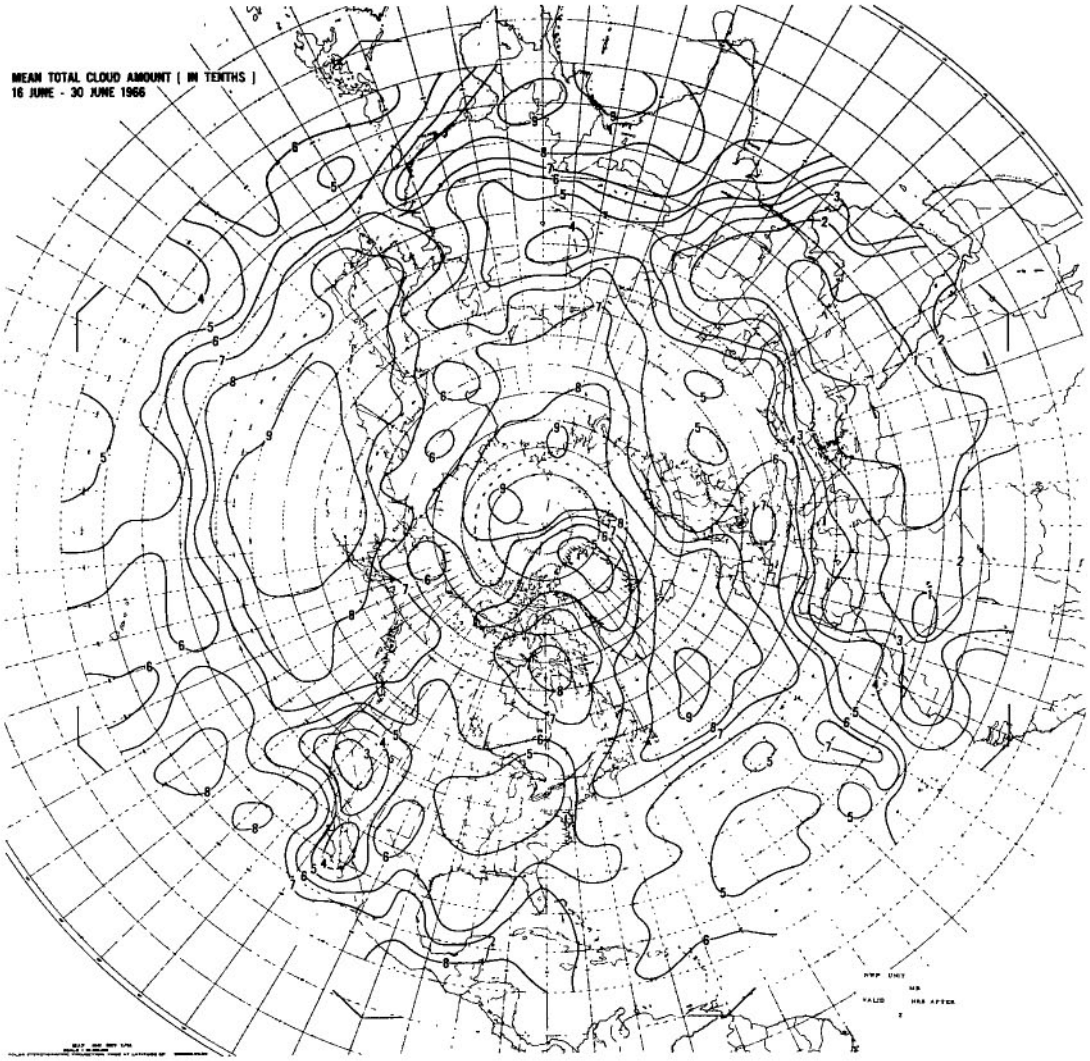

Figure F3—Mean cloud cover over the northern hemisphere during the period 16—30 June 1966 from operational data.

Figure F4—Mean cloud cover over the northern hemisphere during the period 1—15 July 1966.

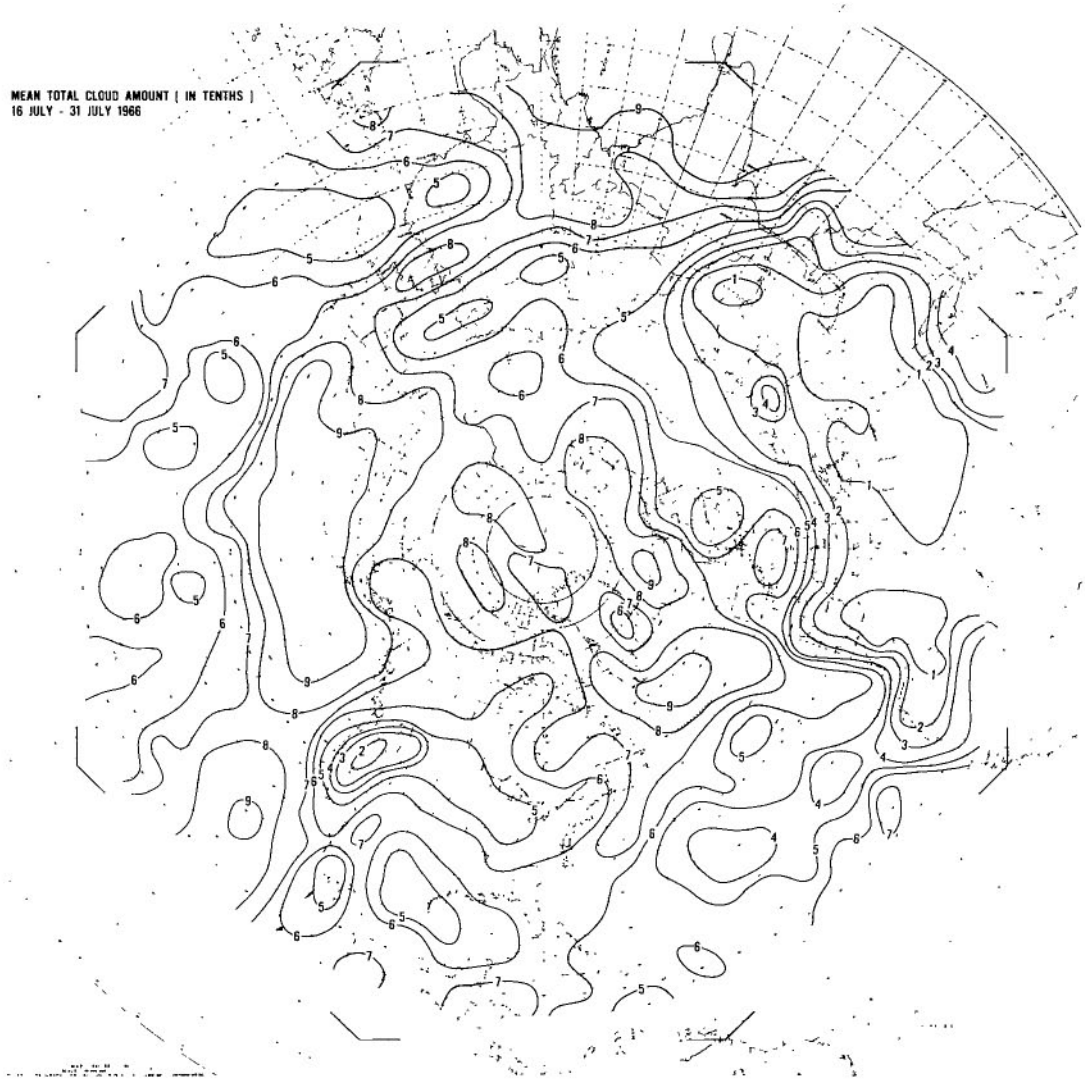

Figure F5—Mean cloud cover over the northern hemisphere during the period 16—31 July 1966.

NATIONAL AERONAUTICS AND SPACE ADMINISTRATION
WASHINGTON, D.C. 20546
OFFICIAL BUSINESS

FIRST CLASS MAIL

POSTAGE AND FEES PAID
NATIONAL AERONAUTICS AN
SPACE ADMINISTRATION

POSTMASTER: If Undeliverable (Section 15:
Postal Manual) Do Not Retu

"The aeronautical and space activities of the United States shall be conducted so as to contribute . . . to the expansion of human knowledge of phenomena in the atmosphere and space. The Administration shall provide for the widest practicable and appropriate dissemination of information concerning its activities and the results thereof."

—NATIONAL AERONAUTICS AND SPACE ACT OF 1958

NASA SCIENTIFIC AND TECHNICAL PUBLICATIONS

TECHNICAL REPORTS: Scientific and technical information considered important, complete, and a lasting contribution to existing knowledge.

TECHNICAL NOTES: Information less broad in scope but nevertheless of importance as a contribution to existing knowledge.

TECHNICAL MEMORANDUMS: Information receiving limited distribution because of preliminary data, security classification, or other reasons.

CONTRACTOR REPORTS: Scientific and technical information generated under a NASA contract or grant and considered an important contribution to existing knowledge.

TECHNICAL TRANSLATIONS: Information published in a foreign language considered to merit NASA distribution in English.

SPECIAL PUBLICATIONS: Information derived from or of value to NASA activities. Publications include conference proceedings, monographs, data compilations, handbooks, sourcebooks, and special bibliographies.

TECHNOLOGY UTILIZATION PUBLICATIONS: Information on technology used by NASA that may be of particular interest in commercial and other non-aerospace applications. Publications include Tech Briefs, Technology Utilization Reports and Notes, and Technology Surveys.

Details on the availability of these publications may be obtained from:

SCIENTIFIC AND TECHNICAL INFORMATION DIVISION

NATIONAL AERONAUTICS AND SPACE ADMINISTRATION

Washington, D.C. 20546